Mechanical characterization of thrombi by studying shear and friction

An in vitro study towards a better comprehension of thrombus biomechanics

Sanne van Kuijk
4555015

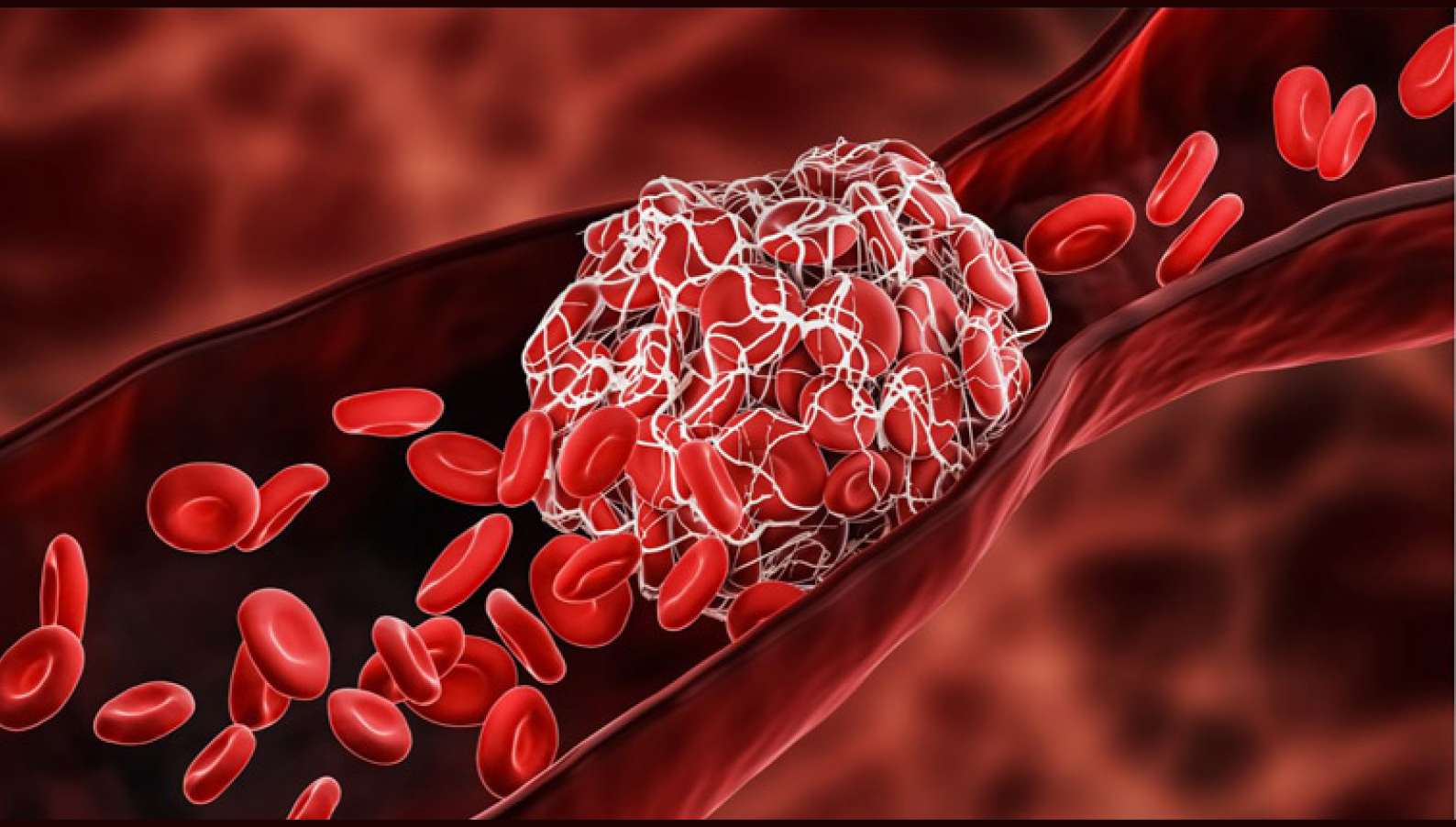

TU Delft

Erasmus MC
Universitair Medisch Centrum Rotterdam

Mechanical characterization of thrombi by studying shear and friction

An in vitro study towards a better comprehension of thrombus biomechanics

by

Sanne van Kuijk
4555015

Supervisors:	Dr. ir. Frank Gijsen, Dr. Behrooz Fereidoonnezhad
Date:	December 23th, 2023
Faculty:	Faculty of Biomechanical Engineering, Delft

Preface

This report has been written for the completion of the Master of Science degree in Biomedical Engineering at the Delft University of Technology. The research was conducted at the department of Cardiovascular Biomechanics within the Erasmus Medical Center. Over the past months, I have thoroughly enjoyed working on my thesis project. Despite encountering occasional challenges, I look back at this period with pride and excitement. As I complete my master's degree, I am excited to embrace new challenges that lie ahead. This academic journey has equipped me with valuable skills and knowledge, and I look forward to applying them in the next phase of my career.

I would like to thank my supervisors, Frank Gijsen and Behrooz Fereidoonnezhad for their guidance over the past couple of months. Your feedback and support has helped me greatly while finishing this project. Furthermore, your enthusiasm about the project was infectious. I would like to thank Michiel Manten for helping me making the shear test setup come to life. Moreover, I would like to thank Robert Beurskens for his assistance throughout the development of the experimental setup. Your door was always open for a question or little chat, which I greatly appreciate. Additionally, I would like to thank everyone at the Cardiovascular Biomechanics department for all the fun and interesting discussions we had. I would like to thank my friends whose company has made my study years very enjoyable, filled with great memories. Lastly, I would like to thank my family who always believe in me.

Sanne van Kuijk
Rotterdam, December 2023

Abstract

Stroke, caused by large vessel occlusions, is the second leading cause of death worldwide. Large vessel occlusions are the result of thrombosis, the undesired coagulation of blood within the vasculature. Due to this coagulation, a vessel can get blocked, prohibiting blood flow to areas distal from the occlusion, with all the serious consequences that may ensue. Since 2015, mechanical thrombectomy procedures have been widely accepted as a successful treatment technique to remove thrombi from the vasculature. However, complete reperfusion is only reached in 50% of acute ischemic stroke cases.

To successfully remove a thrombus from the vasculature, it is necessary to apply a specific retrieval force. This force must exceed the opposing forces, including the impaction force generated by the blood pressure gradient across the thrombus and the interaction forces between the thrombus and the vessel wall. Multiple studies have focused on tensile and compressive properties of thrombi. However, little is known about shear loading of the thrombus and about the interaction properties of the thrombus-vessel wall interface. Therefore, the aim of this study is to gain a better comprehension of thrombus biomechanics by studying the shear behavior of thrombi and the interaction of the thrombus-vessel wall interface *in vitro*.

In order to perform these *in vitro* studies, two custom-made test setups have been designed and developed. The friction test setup contains a plate of which the angle can be inclined slowly. By placing a thrombus-vessel wall sample on top of this plate, it is aimed to determine the static and kinetic coefficient of friction of the thrombus-vessel wall interface. Furthermore, it is aimed to determine the effect of time on this interaction. The thrombus-vessel wall interface was created by obtaining a piece of vein and blood from pigs. To study the shear behavior of thrombi a shear test setup has been developed. Two thrombi types have been utilized for this study, red blood cell- and fibrin-rich. Within the shear test setup it is possible to perform shear experiments under different normal loading conditions. A comprehensive analysis of the data acquired from experiments performed with both test setups has been conducted. Furthermore, a computational model has been developed to fit towards the experimental data obtained from the shear experiments.

The friction experiments suggest that time positively influences the bonds formed between a thrombus and the vessel wall as the coefficients of friction increase with an increased waiting time. Furthermore, a strong positive correlation was found between the static and kinetic coefficient of friction. This result was also found when doing an extensive analysis of the data obtained from the shear experiments. Additionally, the shear experiment showed that the thrombus composition influences its mechanical properties. Higher shear moduli and kinetic coefficients of friction were found for the fibrin samples, compared to the red blood cell samples.

The results obtained from the friction and shear experiments provide valuable insights into thrombus biomechanics. By extending the performed studies a better comprehension on thrombus mechanics and the thrombus-vessel wall interaction can be achieved.

Contents

List of Figures

List of Tables

Nomenclature

Abbreviations

Abbreviation	Definition
AIS	Acute ischemic stroke
FBR	Fibrin
HS	Hemorrhagic stroke
IVT	Intravenous thrombolysis
LVO	Large vessel occlusion
NETs	Neutrophil extracellular traps
RBC	Red blood cell
r-tPA	Recombinant-tissue plasminogen activator
SEM	Scanning Electron Microscopy

Symbols

Symbol	Definition	Unit
A	Top area of sample	[m^2]
a	Acceleration of sample	[m/s^2]
F_g	Gravitational force	[N]
F_N	Normal force	[N]
F_S	Shear force	[N]
g	Gravitational acceleration	[m/s^2]
h	Sample height	[m]
s	Traveled distance	[m]
t	Time	[s]
$v_{actuator}$	Velocity of the actuator	[m/s]
γ	Shear strain	
θ	Angle of inclination	$^\circ$
μ	Coefficient of friction	
τ	Shear stress	[Pa]

1 Introduction

Stroke, the second leading cause of global mortality, accounts for approximately 11% of all deaths worldwide [1]. There are two main types of stroke, acute ischemic stroke (AIS) and hemorrhagic stroke (HS). HS results from the rupture of intracranial blood vessels, causing internal bleeding. In contrast, AIS, constituting 87% of all strokes, occurs due to the obstruction of large blood vessels, hindering blood flow and leading to restricted oxygen supply [2]. This type of obstruction is also known as a large vessel occlusion (LVO). Prolonged oxygen deprivation during AIS can result in brain tissue damage, potentially leading to disability or even death.

1.1. Thrombus formation

The occurrence of a LVO is due to the formation of a thrombus, the coagulation of blood, within a blood vessel. Thrombus formation is an undesired event that could occur through the hemostasis process, which is responsible for restoring a cut or severed blood vessel after injury. The hemostasis process consists of two phases: primary and secondary hemostasis. During primary hemostasis, platelets are activated, and adhesion and aggregation of platelets take place, as a response to injury. Subsequently, during secondary hemostasis, the coagulation cascade is initiated. During this cascade, a fibrin network is formed and matures, ultimately restoring the integrity of the blood vessel [3]. Consequently, a platelet plug is formed and the fibrin network will partially or completely dissolute [4]. As mentioned, besides restoring an injured blood vessel, the hemostasis process can also lead to undesired thrombus formation, occluding a blood vessel. A triad of factors contribute to thrombus formation. As described by Rudolf Virchow in 1856, the stasis of flow, hypercoagulation and endothelial injury are factors contributing to the occurrence of thrombosis [5].

1.2. Endovascular treatment

Since 1996, intravenous thrombolysis (IVT) has been the primary treatment for thrombosis. During an IVT procedure, intravenous recombinant-tissue plasminogen activator (r-tPA) is administered to the occluded vessel within 4.5 hours of stroke onset [6]. The r-tPA activates plasminogen to plasmin, breaking down the fibrin fibers in thrombi, dissolving a thrombus to restore blood flow [7]. However, due to differences in thrombus composition, the success of the intervention is dependent on the type of thrombus [8]. Furthermore, the location of occlusion influences IVT success as well. A study in 2001 [9] showed that recanalization after IVT administration was achieved for 30% of patients with a proximal occlusion of the middle cerebral artery, whereas this was only achieved for less than 10% of patients with a carotid artery occlusion.

Due to the limited success of AIS treatment with IVT, mechanical thrombectomy techniques were developed. These techniques are endovascular treatment techniques that attempt to retrieve a thrombus from the location of occlusion, thereby restoring blood flow. Mechanical thrombectomy devices have been in development since 1999, with the first being FDA approved in August 2004. This first-generation device is the MERCI retriever which is delivered to the place of occlusion via a microcatheter. The MERCI retriever consists of multiple helical loops designed to capture the occluding thrombus to remove it from the vasculature [10]. In 2015, mechanical thrombectomy became widely accepted as a

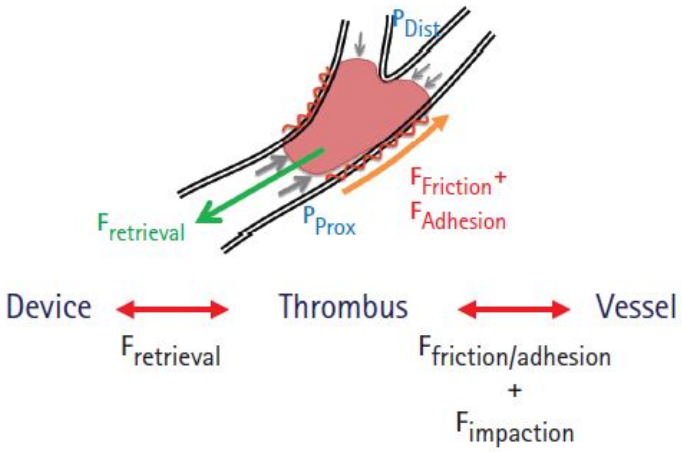

Figure 1.1: Device-thrombus-vessel interaction. Adopted from [12].

successful treatment technique, with or without the administration of IVT priorly. This was due to landmark randomized clinical trials that showed lower disability rates among patients who were treated for LVOs with mechanical thrombectomy [11]. The last few years, many new devices have been developed. The commercially available devices that are currently used are third-generation mechanical thrombectomy devices. There are many variations between the available devices, however, they can be divided into three main classes: stent retrievers or aspiration devices, or a combination of the two techniques. Stent retriever mechanical thrombectomy uses the deployment of a stent to capture a thrombus in the occluded blood vessel in order to remove it. With an aspiration catheter, a thrombus will be removed from the blood vessel through suction. The combined techniques uses both stent deployment and suction to retrieve a thrombus from the vasculature [11].

Even though the success rate of thrombus retrieval has improved since the usage of endovascular treatment techniques, complete reperfusion is only reached in about 50% of AIS cases [12]. Studies have shown that thrombectomy success is influenced by multiple procedural and device design differences. For stent retrievers these procedural differences include the positioning of the stent relative to the thrombus [13], the application of waiting time between stent deployment and retrieval [14, 15], the technique used during the period of stent deployment [15, 16], and how the captured thrombus is retrieved from the body afterward [7, 17]. Similar factors, like the positioning of the catheter tip [18, 19] and application of waiting time [20], are relevant for aspiration thrombectomy procedures. Furthermore, the location of occlusion [21] and the applied aspiration mode [22, 23, 24] seem to impact aspiration thrombectomy success. The stent design plays a role in how a thrombus is captured [25, 26, 27], and the catheter tip design is important for aspiration devices as the catheter tip's inner diameter influences how easy or hard it is to capture a thrombus [28]. Moreover, thrombus biomechanics plays a role in the success of mechanical thrombectomy procedures.

1.3. Thrombus biomechanics

Endovascular treatment techniques need to apply a certain retrieval force on the thrombus in order to be able to remove it from the location of occlusion. This retrieval force needs to transcend the opposing forces acting on the thrombus. The opposing forces include the force of impaction and the frictional and adhesive forces between the thrombus and vessel wall (Fig. 1.1). The force of impaction is determined by the blood pressure gradient across a thrombus which is the difference between systemic blood pressure, proximal to the thrombus, and the retrograde collateral blood flow, distal from the thrombus [12]. About the frictional force between the thrombus and vessel wall is known that it is influenced by the thrombus composition, which affects the coefficient of friction of the thrombus [29, 30].

The main components found within thrombi are fibrin (FBR) fibers, platelets, red blood cells (RBCs), leukocytes, and neutrophil extracellular traps (NETs). The ratio of components in thrombi is unique for each thrombus, with the thrombus location and disease pathology having an effect on the contribution of each component [31, 32, 33]. Due to the thrombus-specific composition and the thrombus-specific

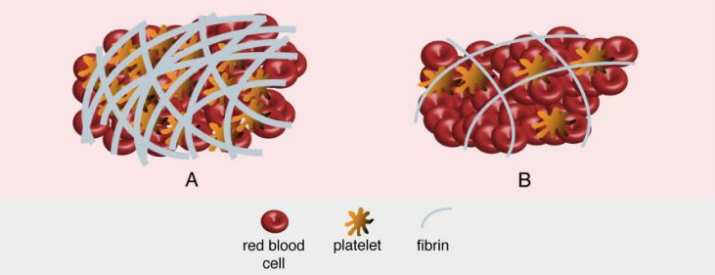

Figure 1.2: Components of (A) fibrin-rich and (B) RBC-rich thrombi (components not drawn to scale). Adopted from [8].

component organization, a thrombus is highly heterogeneous. In literature, thrombi are usually described as soft RBC-rich and hard FBR-rich thrombi, with intermediate thrombi ranging in between these two thrombi types. RBC-rich thrombi predominantly consist of RBCs with thin fibrin fibers. They have a looser, more porous structure compared to the more compact FBR-rich thrombi, who contain platelet-rich zones together with dense fibrin fibers (Fig. 1.2) [8].

As touched upon, the composition influences the coefficient of friction of a thrombus. Gunning et al. [29] studied the static friction between ovine thrombus analogs of different compositions and a low-frictional PTFE-coated stainless steel surface by slowly tilting the surface on which the thrombus analog was placed. The angle of inclination at which the thrombus started to slide was used to determine the static coefficient of friction (μ_s). It was found that the static coefficient of friction decreases with increasing RBC content. A similar relation was found by Elkhayyat et al. [30]. In their *in vitro* study, bovine thrombus analogs were created and placed on pieces of material that are regularly used to recreate the vasculature for *in vitro* experiments. The materials they included were glass, PVC tubing, silicone, and bare nitinol. Besides the static coefficient of friction, the kinetic coefficient of friction (μ_k) was determined by Elkhayyat et al. [30]. The kinetic coefficient of friction was found to be lower than the static coefficient for all surfaces. Besides the experiments performed on the low-frictional surfaces, both studies also placed their thrombus analogs on an arterial surface and performed their experiments again. Gunning et al. [29] and Elkhayyat et al. [30] respectively used bovine aortic and bovine carotid surfaces for their experiments. Both studies again found that thrombus composition significantly influences the static coefficient of friction. Furthermore, they both found that the static coefficient was significantly higher between a thrombus and arterial surface compared to the static coefficient between the thrombus and one of the low-frictional surfaces. Even though the studies found the same trend in their results, the static coefficient of friction of FBR thrombi found by Gunning et al. [29] is around three times larger than the one found by Elkhayyat et al. [30]. Up to this point, no studies have been found that focus on the adhesive aspect of the thrombus-vessel wall interaction, and how this contributes to the opposing forces acting on the thrombus.

1.4. Aim of the study

In order to optimize endovascular treatment techniques, a comprehensive understanding of the biomechanical characteristics of thrombi and the thrombus-vessel wall interaction is required. Previous studies have performed biomechanical tensile and compression tests on clot analogs [34, 35, 36], laying a foundation for studies towards thrombus biomechanics.

To broaden the knowledge, a new layer is added to the understanding of thrombus biomechanics within this study. In order to achieve this, custom-made test setups have been designed, enabling the *in vitro* mechanical testing of thrombi. This study delves into shear properties across different thrombus compositions, concurrently investigating the thrombus-vessel wall interaction through friction experiments. The overall objective of the research is to contribute to the comprehension of thrombus biomechanics.

2

Custom-designed test setups

2.1. Introduction

Two experimental test setups have been developed to study the mechanical response of thrombi under shear deformation and the thrombus-vessel wall interaction in an *in vitro* environment. This has been done by designing and developing a shear and friction test setup. In this chapter the design and working mechanism of both test setups will be explained, starting with the shear test setup. Both devices are controlled in the same manner. Specifics about the control are described after the mechanics of the shear and friction test setups are laid down.

2.2. Shear test setup

2.2.1. Goal of the setup

During mechanical thrombectomy procedures a certain retrieval force needs to be reached in order to extract the thrombus from the vasculature [12] (Section 1.3). Consequently, multiaxial loading is exerted on a thrombus. Although mechanical behavior of thrombi under compression and tension has been studied before [34, 35, 36], their mechanical response under shear deformation is not well understood. As shear forces play a role at the thrombus-vessel wall interface, this is an important aspect to investigate, in order to improve thrombosis treatment in the future.

In order to study this aspect of thrombus biomechanics, a shear test setup was designed and developed. The aim of this test setup is to gain insight into the shear behavior of clot analogs. Within this thesis, the test setup has been used to study the shear response of different thrombus compositions under multiple loading conditions. However, the shear test setup has been designed to study the shear response between a thrombus and vessel wall as well.

2.2.2. Requirements

Before designing the shear test setup, several requirements were established. The primary objective is to apply shear deformation to the thrombus and measure the resulting shear force. Furthermore, it must be possible to apply a normal force on the sample, enabling the realization of shear deformation [37]. This normal force should be controllable, allowing for varying magnitudes to be applied to samples of different heights.

Additionally, it is required that the sample is clearly visualized during the experiment, enabling the continuous observation of the deforming thrombus. In case a thrombus-vessel wall sample is tested, visualization of the interaction between both components is of importance. Therefore, it should be possible to use ultrasound imaging within the test setup.

Lastly, requirements must be made regarding the materials that will be tested during the experiments, which will be human tissue. Firstly, it should be possible to control the physiological conditions of the tested samples by controlling the temperature and by conducting experiments within a fluid medium. Secondly, it is of high importance that the test setup is easy to clean. Therefore, it should be a modular system that can easily be assembled and dissembled.

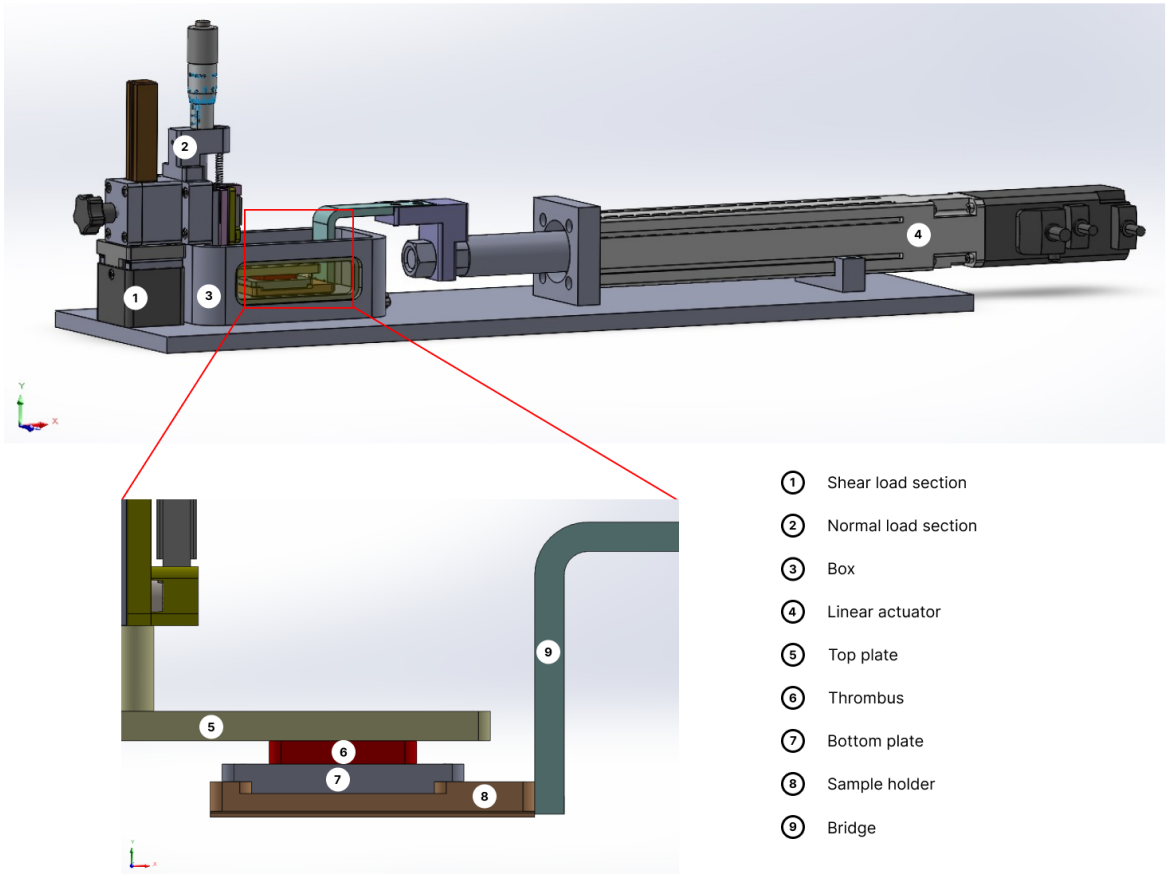

Figure 2.1: A schematic model of the custom-made shear test setup created in Solidworks: mechanical hardware.

2.2.3. Setup design

The different mechanical components of the shear test setup can be found in figure 2.1. The top plate can be replaced roughly and at micrometer level in order to apply a normal force on the sample to be tested. Once the right normal force is set in place, the actuator initiates the shear experiment by retracting at a velocity of 0.5mm/s. A camera is located in front of the test setup to record the entire experiment through the window within the box. As a scale reference, a ruler has been included in the visualized area. In figure 2.2, an electronic connectivity overview of the shear test setup is presented, illustrating how all components are interconnected. This electronic configuration links the setup to the driving components, which are controlled by software. In the following sections, all hardware and software components used within the shear test setup are described.

Hardware

Load cells (FSH03869, FUTEK)

The shear test setup includes two load cells which both have a maximum capacity of 50g. These load cells have been selected due to previous findings done within the Cardiovascular Biomechanics research group and by considering the aspiration force used during mechanical thrombectomy procedures [38]. One of the load cells will be used to measure the shear force during the experiment, and the other is used to determine the amount of normal force that is applied on the sample. They are built into sections of the test setup that will be referred to as the normal load and shear load section in the remainder of this report. Due to the low capacity and high fragility of the load cells, both sections include a locking system such that the load cells are isolated from any kind of accidentally applied force when not in use. Both locking mechanics can be seen in figure 2.3. It is of high importance that these locks are removed before an experiment is started. The shear load cell is unlocked by removing the bottom screw, whereas both screws from the locking mechanism should be removed to unlock the normal load cell. Furthermore, both load cells are mounted on smooth bearings to limit the effect of the weight that

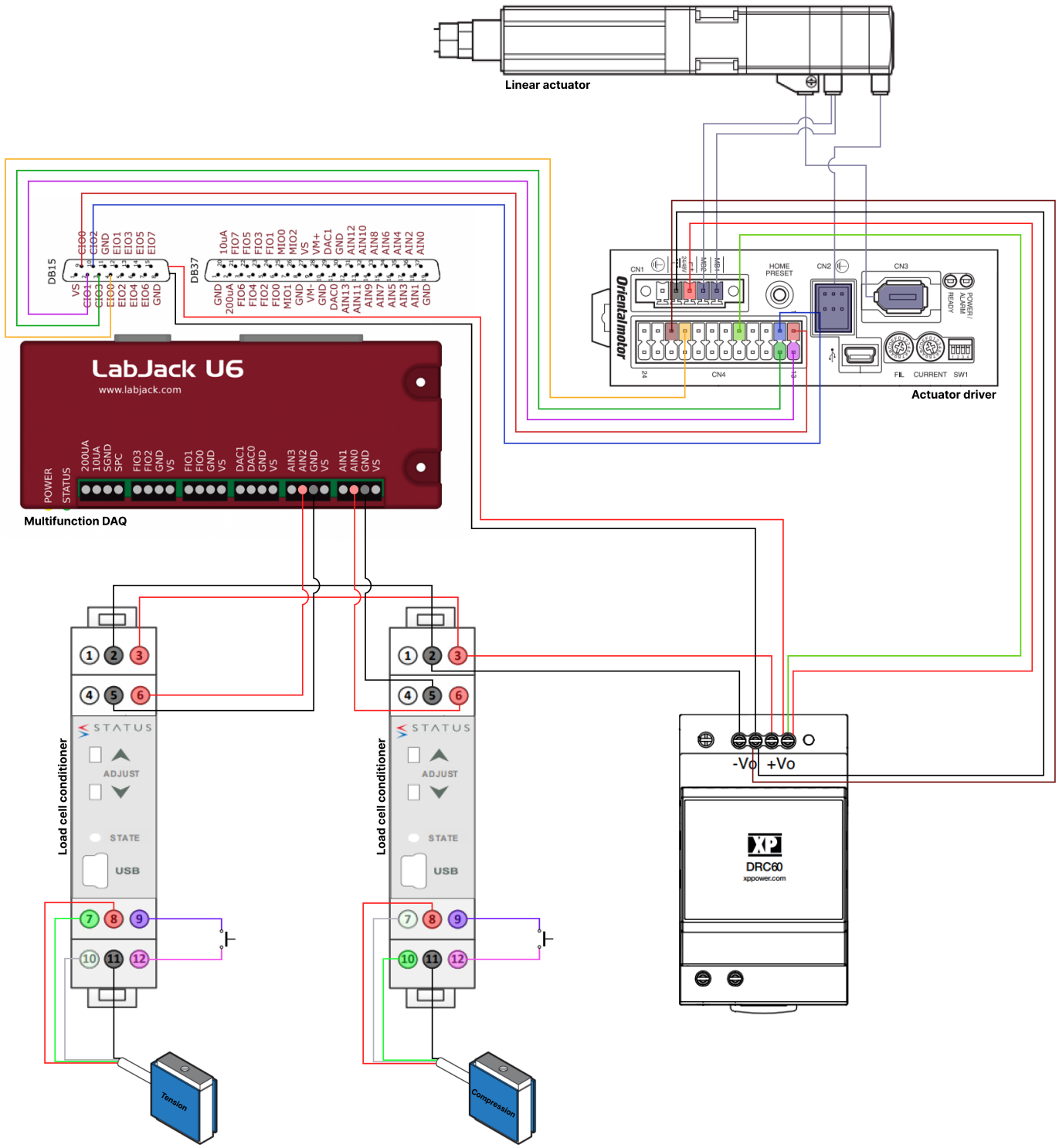

Figure 2.2: Electrical composition of the custom-made shear test setup (components not shown to scale). Not shown in this overview is the optocoupler interface in between the Multifunction DAQ and actuator driver. Furthermore, the Multifunction DAQ is connected to a laptop and the power supply and linear actuator are connected to a power socket.

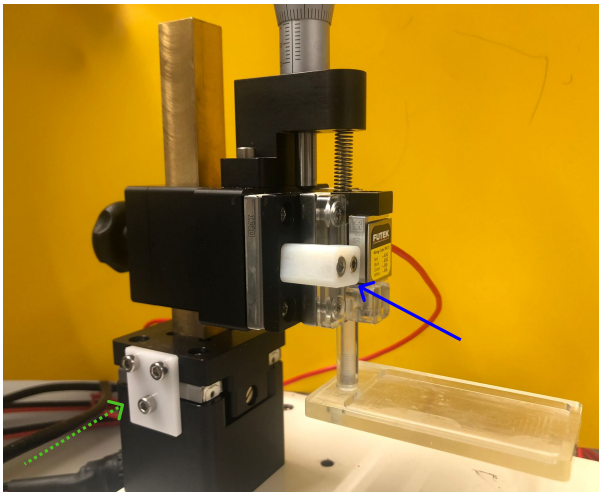

Figure 2.3: Image portraying the shear and normal load cell locking mechanisms. The green dotted arrow points towards the shear load cell lock, and the blue continuous arrows towards the normal load cell lock.

is already placed on the load cells by other test setup components.

The load cells operate on the principle of a Wheatstone bridge. Instead of resistors, strain gauges are arranged in a diamond shape. When tension or compression is applied to these gauges, the resistance increases or decreases, leading to a corresponding change in voltage. A 10V output is equivalent to the maximum load cell capacity of 50g. Since voltage and force are proportional, the applied force can be calculated throughout an experiment. Before utilizing the load cells, they undergo calibration according to the calibration protocol provided in Appendix A.4. The calibration is deemed successful when the load cell measures force within a 5% offset. This implies that when, for instance, 10g is applied, the load cell should register a measurement within the range of 9.5g to 10.5g. Consequently, the load cells are said to have an accuracy rate of 5%.

The shear load section (Fig. 2.4a) consists of a base and a square rod, with the load cell being placed horizontally in between the two. The square rod is used as a guider to roughly replace the normal load section (Fig. 2.4b). The normal load section furthermore contains a micrometer displacer such that displacement of the top plate on a micrometer scale is possible as well. This gives the opportunity to accurately apply a normal force on the sample (Fig. 2.5). The built-in normal load cell does not immediately drop down as it is held up with a spring.

Load cell conditioner (SEM1600B, Status Instruments)
As the output of the load cells is small, they need to be amplified by a load cell conditioner. Besides amplifying the electrical load cell signal, the load cell conditioner facilitates zero balancing of the load cell. This is accomplished through a push button connected to the volt-free contact inputs, specifically contacts 9 and 10 of the load cell conditioner as illustrated in figure 2.2. By pushing the button, the load cell resets to its zero balance position.

Due to the Wheatstone bridge configuration of the load cells, the wiring of the load cell depends on whether it is used for compression or tension. As the shear load cell operates under tension and the normal load cell under compression, they require distinct wiring configurations. Furthermore, the load cell conditioner is used to calibrate the load cells. Therefore, each load cell needs an individual load cell conditioner. The calibration is performed by connecting the load cell conditioner to a laptop with the load cell calibration software USB SpeedLink, via the microUSB connector (Appendix A.4).

Linear actuator (EACM4E15AZMK, Oriental Motor)
A cylindrical motorized linear actuator is used to drive the shear experiment, as it is connected to the sample holder. Due to the ball screw design, driven by a stepper motor, high performance is possible across a broad range of loads, at low and high speeds. The linear actuator furthermore contains a battery-free absolute encoder and is controlled through its corresponding software, MEXE02.

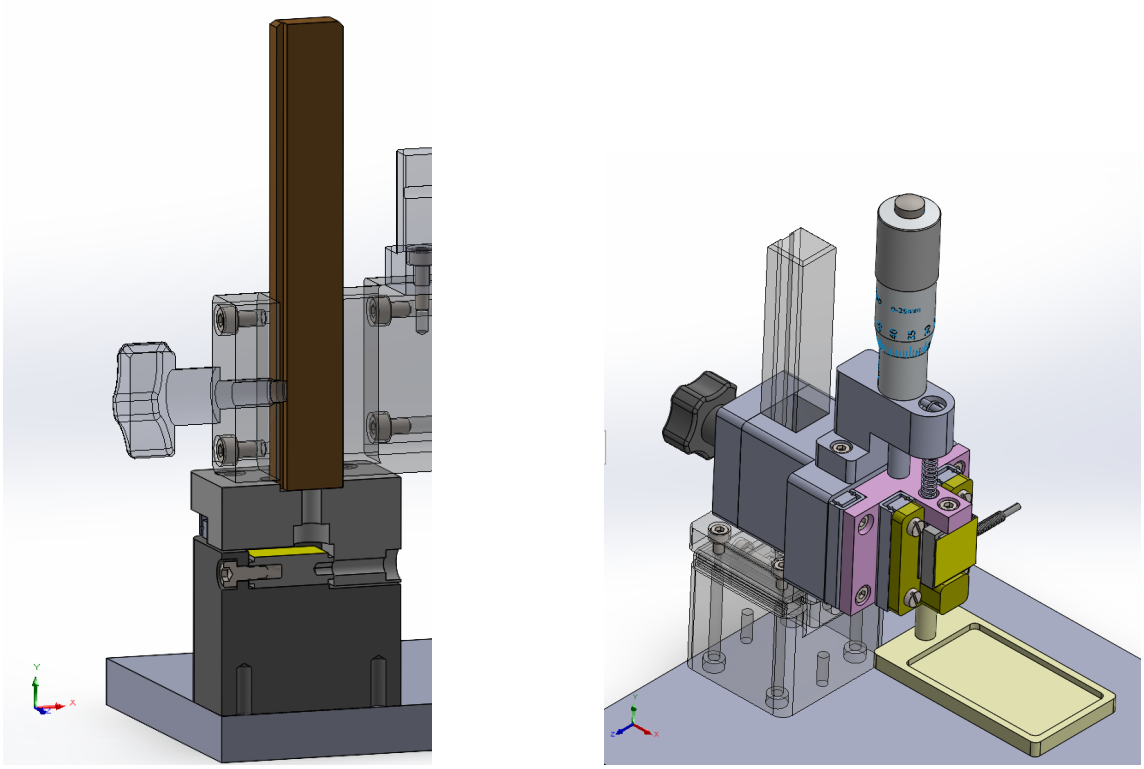

(a) Shear load section (cross-section)

(b) Normal load section

Figure 2.4: A closer look of the two load sections, both holding a FUTEK load cell with a maximum capacity of 50g.

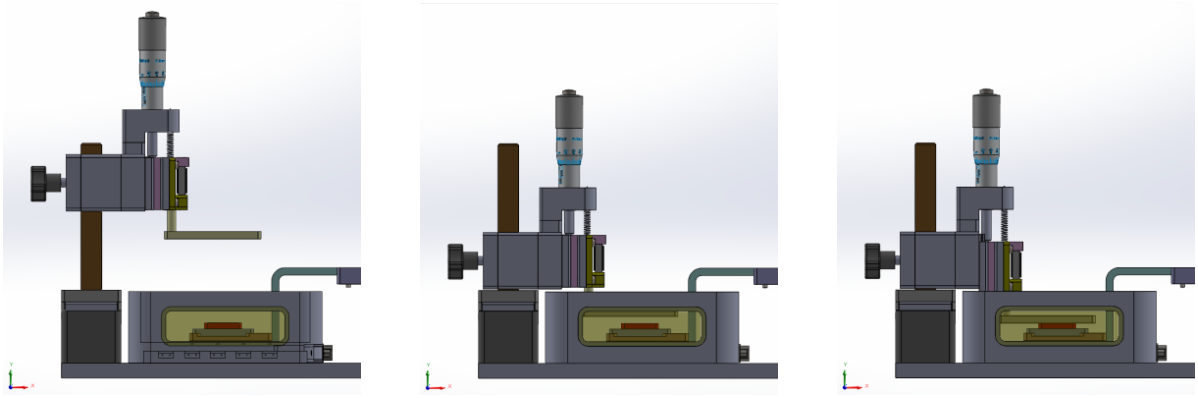

(a) Starting position

(b) Position after rough displacement

(c) Position after micrometer displacement

Figure 2.5: The images show how contact between the top plate and thrombus is established. (a) Shows the starting position after thrombus placement. (b) Shows the situation after the normal load section has been displaced roughly. (c) Shows the position of the top plate after displacement with the micrometer displacer.

Linear actuator's driver (AZD-KD, Oriental Motor)
As the name says, the linear actuator's driver drives the linear actuator. The built-in controller allows for data to be stored on the driver, making it easier to send messages to the actuator. In the shear test setup the controller connections operate via I/O (input/output) control with the USB Multifunction DAQ system (LabJack U6). The I/O pins function as direct inputs, receiving signals to activate various actuator commands. The MEXE02 software is used to connect the pins to the specific commands.

DC power supply unit (DRC60US24, XP Power)
The power supply is required to supply the load cells and linear actuator with a constant voltage of 24V. The power to the linear actuator is supplied through the actuator driver, and the power to the load cells through the load cell conditioner.

USB Multifunction DAQ (LabJack U6-PRO, LabJack)
The LabJack U6-PRO is a data acquisition system that contains three different I/O areas. The connection edge contains an USB type B connector which is used to connect the LabJack to a laptop, providing power to the system. Furthermore, this connection allows the performance of the LabJack to be controlled by a LabVIEW script. The second I/O area is the screw terminal edge. Both load cell conditioners are connected to this edge such that the LabJack obtains analog signals. For the shear and normal load cell this analog signal is obtained through analog inputs AIN0 and AIN1 respectively. Lastly, the LabJack contains a DB edge which has a DB37 and DB15 connector. Within the shear test setup, only the DB15 connector is used which contains 12 digital I/O channels. Through a custom-made optocoupler interface, these channels are used to send digital signals to the actuator driver as a connection between the DB15 connector and actuator driver I/O pins is established.

Optocoupler interface
The optocoupler interface is the component that connects the LabJack, through the DB15 connector, to the actuator driver. It is required as the LabJack operates at a voltage of 5V, whereas the actuator driver uses a voltage of 24V. The optocoupler interface consists of opto-isolators, which are electrical components consisting of LEDs and phototransistors. When a LED is activated by one side of the circuit, the light will be sensed by the phototransistor, which will transfer the signal to the other side. Via this communication it becomes possible for the 5V and 24V systems to communicate with each other safely. The optocoupler interface is not included in the schematic in figure 2.2 to simplify the visualization.

Top plate
The top plate is connected to the normal load cell section and used to apply a normal force on the sample. The top plate is made out of TPX as it needs to be lightweight. Furthermore, the top plate should not substantially interfere with high-frequency sound waves as it should be possible to use the Vevo 3100 Ultrasound imaging system to image the sample underneath the top plate during the shear experiment. The tissue-like acoustic impedance and low attenuation of TPX makes it a suitable material for the top plate [39].

Sample holder
The sample holder is connected to the linear actuator via a bridge such that the actuator can initiate a shear movement during the experiment. Furthermore, the sample holder has two important properties. First, the notch in the sample holder contains tiny magnets such that the bottom plate, on which the samples are created, are easily placed and removed. Second, there are two narrow ridges at the bottom of the sample holder. These are created in order to limit the amount of friction between the sample holder and surrounding box.

Box
The shear experiment takes place within a box. What happens during the experiment can be visualized from the side as windows are included on the long sides of the box. Furthermore, a heating system is built into the bottom of the box, making it possible to create a heated waterbath if required.

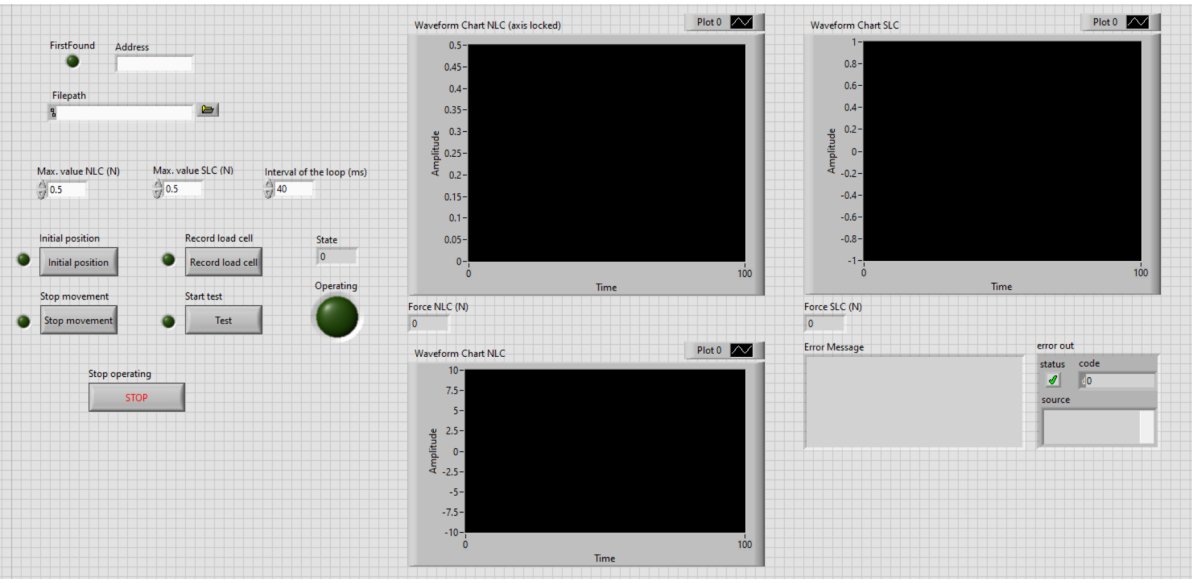

Figure 2.6: Front panel of the custom-made LabVIEW script.

Water level
As the load cells within the test setup are very fragile to any kind of disturbance, it is important that the setup remains stable in the x- and z-plane. Therefore, a level instrument and four set screws are added to the baseplate of the test setup. By adjusting the set screws, the baseplate can be leveled. Before every experiment, it should be checked whether the test setup is leveled or not, and the set screws should be adjusted if required.

Software

Load cell software (USB SpeedLink, Status Instruments)
USB SpeedLink is the load cell software used to calibrate both load cells of the shear test setup. Each load cell is unique and comes with a data sheet with product specific calibration values. As the calibration is performed at 5V excitation, the calibration values from the data sheet must be multiplied times five, before being submitted in USB SpeedLink. For the exact protocol to (re)calibrate load cells, see Appendix A.4.

Linear actuator software (MEXE02, Oriental Motor)
The MEXE02 software is designed to control the linear actuators of Oriental Motor. It allows users to move the actuator to absolute or incremental positions, either directly within the MEXE02 software or through LabVIEW such that the entire test setup is controlled simultaneously. Directly giving tasks to the actuator is done through the ”Teaching, remote operation” window. For integration with LabVIEW, tasks are defined in the ”Operation data” window, and the connection is established by configuring the ”Direct-IN function (DIN)” window. This ensures that different tasks are assigned to different channels. With the LabJack U6-PRO functioning as a bridge between both softwares, effective coordination between MEXE02 and LabVIEW is established.

Programming software (LabVIEW, National Instruments)
LabVIEW is a graphical programming environment that is used to create a custom-made script to control the shear test setup. In addition to sending commands to the test setup, the LabVIEW program allows real-time monitoring of the load cell response. The real-time monitoring can be observed in the ”Front panel” (Fig. 2.6) of the LabVIEW script, which is built up through the ”Block diagram” (Fig. 2.7). The LabVIEW script communicates with the load cells and linear actuator of the shear test setup through the LabJack. LabVIEW works with Virtual Instruments (VIs) that correspond with different functions. The LabJack has its own VIs from the LabJack UD library, provided by the LabJack company. Within the custom-made script, multiple VIs are used, portrayed in the gray blocks in the block diagram.

Communication with the LabJack is initiated through the OpenLabJackS function. If the LabJack

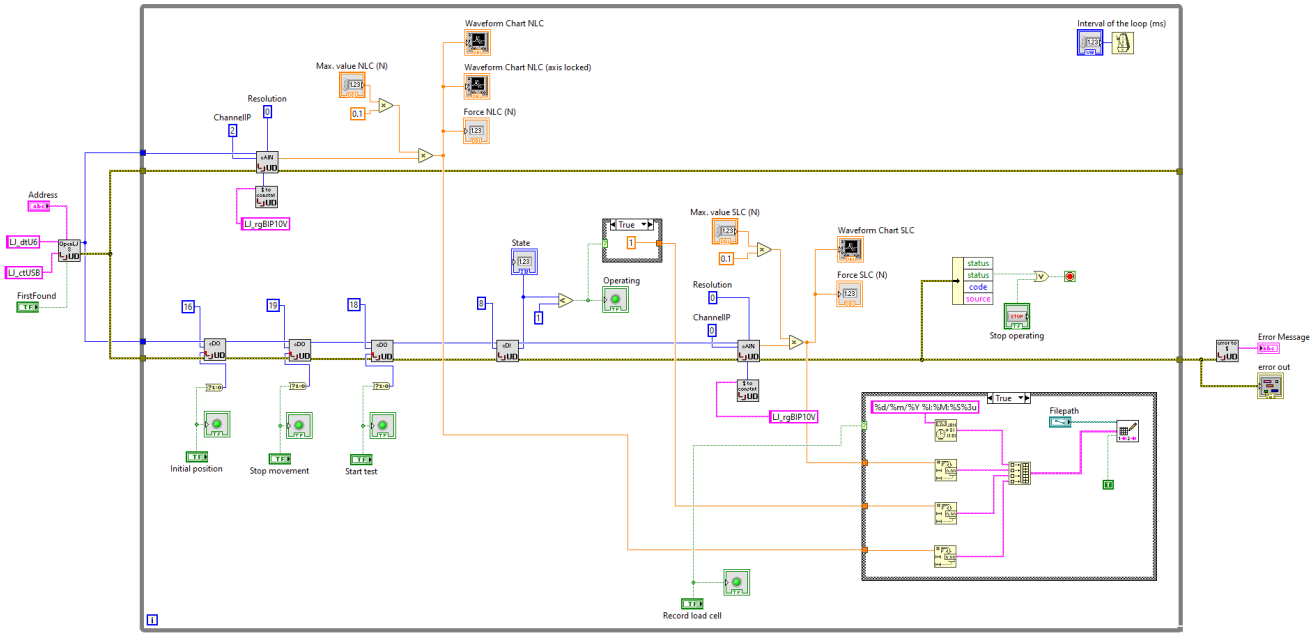

Figure 2.7: Block diagram of the custom-made LabVIEW script.

is not detected, an error message is displayed in the front panel due to the ErrorToString function. Furthermore, eDO functions are used to connect certain tasks to buttons within the front panel. The number connected to an eDO function is the digital channel corresponding with a LabJack DB15 pin.

The eDI function reads the status of a digital input, providing a binary indication of whether the tester is in operation mode. The last used VI is the eAIN function, which returns the reading of an analog input. This reading, in Voltage, is used to determine the output of the load cell in Newton.

When pressing the ”Record load cell” button in the front panel, data recording is initiated and stored in a user-selected text file. The collected data includes a timestamp, the output values from both the shear and normal load cell (in Newton), and the binary operation status. The operation status, denoted by 0 or 1, indicates whether the shear experiment is operating. As the status reverts to 0 as soon as the operation concludes, the status provides an easy way to monitor the experimental run, which is convenient for data post-processing.

2.3. Friction test setup

2.3.1. Goal of the setup

Besides shear forces, the friction between the thrombus and vessel wall is an important aspect of the counteracting forces that need to be overcome in order to retrieve a thrombus during mechanical thrombectomy procedures. To gain more insight into the thrombus-vessel wall interaction, a friction test setup was developed. The aim of the test setup was to determine the static and kinetic coefficient of friction of a thrombus placed on a vessel wall. The coefficient of friction (μ) is the ratio of the frictional (interaction) force between two surfaces (F_i) and the normal force (F_N) pressing on the surfaces (Eq. 2.1).

$$\mu = \frac{F_i}{F_N} \tag{2.1}$$

The static coefficient of friction (μ_s) describes the amount of friction that needs to be overcome in order for motion to appear between two surfaces, whereas the kinetic coefficient of friction (μ_k) describes the friction that occurs between two surfaces during motion.

2.3.2. Requirements

In order to determine both coefficients of friction a few requirements were considered when developing the friction test setup. These requirements are based on the data that needs to be collected in order

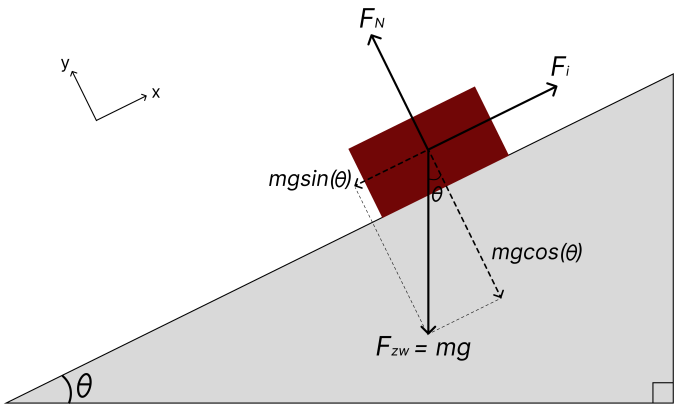

Figure 2.8: A free body diagram of a thrombus on an inclined surface, showing the occurring forces and the angle of inclination. By setting a static or kinetic equilibrium along the x-axis, the interaction force can be derived for either situation, leading to the equations used to calculate the static and kinetic coefficient of friction respectively.

to calculate both coefficients of friction. Furthermore, the requirements concern the sample placement and removal.

In figure 2.8 all forces acting on a thrombus on an inclined surface are shown. The static and kinetic equilibrium of these forces lead to the determination of the static and kinetic coefficient of friction respectively, by substituting the found interaction and normal force in equation 2.1.

Consequently, the static coefficient of friction can be determined by the angle of inclination (θ) according to equation 2.2.

$$\mu_s = tan(\theta) \tag{2.2}$$

Therefore, the setup must include a plate of which the inclination can be adjusted smoothly and slowly, such that the angle of inclination can be determined within an accuracy of 1°. Besides the angle of inclination, the acceleration (a) of the thrombus sliding over the vessel wall is required to calculate the kinetic coefficient of friction, when determined according to equation 2.3, where g represents the gravitational acceleration (9.81m/s^2).

$$\mu_k = \frac{gsin(\theta) - a}{gcos(\theta)} \tag{2.3}$$

In order to determine the acceleration, imaging is required and measurements references within the imaging frame must be available. Consequently, the acceleration can be determined with equation 2.4, where s is the traveled distance and Δt the time period over which the thrombus slides.

$$a = \frac{2s}{\Delta t^2} \tag{2.4}$$

Moreover, it must be possible to pin the vessel wall down on the surface that will be inclined during the experiment. Lastly, as porcine material will be used to perform the friction tests, the developed device should be easy to clean.

2.3.3. Setup design

In figure 2.9 the friction test setup is portrayed. In its initial position, the top plate is located horizontally on top of the framework. The top plate is connected to the actuator by a piece of rope. By driving the actuator, the rope is pulled such that the angle of inclination of the top plate slowly starts to increase, to a maximum of 90°. This is done at a rate of 1 degree per second, meaning that the actuator has to retract at a speed of 0.85mm/s. In order to keep this rate consistent throughout an entire experiment, counter weights were added at the end of the top plate (not shown in the schematic model).

A notch has been created in the top plate such that a piece of foamboard can be easily placed and removed. The foamboard is in turn used to pin the vessel wall down, using insect pins. Furthermore, as the device was made out of MDF, it was coated with liquid-tight lacquer to avoid any fluid absorbance for hygienic purposes.

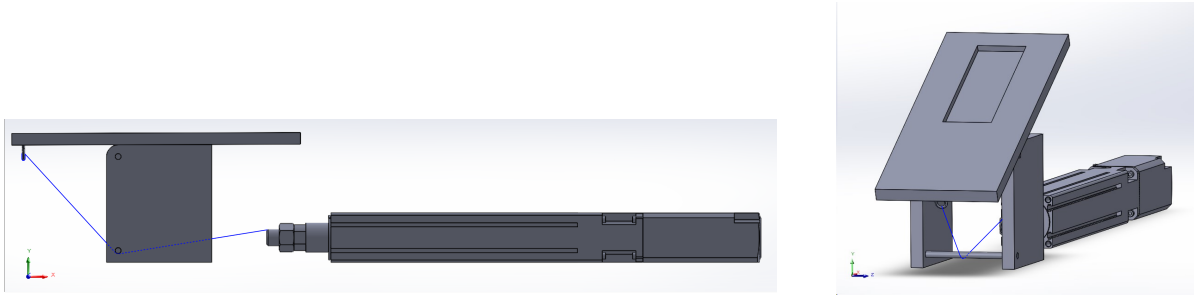

(a) Side view **(b)** Isometric view

Figure 2.9: A schematic model of the custom-made friction test setup, created in Solidworks. (a) Shows a side view of the test setup in its initial position. (b) Shows an isometric view of the setup while the angle of the top plate is inclined, showing the notch within the top plate.

A tripod with camera was placed in front of the test setup to record the entire experiment. A ruler was placed against the test setup, within the imaging frame of the camera, which functions as a measurement reference during post-processing.

The base of the shear test setup, consisting of the baseplate and the linear actuator, was used to finalize the friction test setup. Furthermore, MEXE02 software was used to drive the linear actuator. As no load cell read out was required within the friction test setup, the actuator was controlled through the MEXE02 ”Teaching, remote operation” window.

3 Methods

3.1. Introduction

In this chapter, the methodologies employed to conduct shear and friction experiments are laid down, providing a guide through the taken steps. The methodologies involve the preparation of different sample types and specifics about the individual testing procedures, providing clarity on how the experiments are executed. Furthermore, information is provided about how the acquired data will be handled during post-processing. First, the methodology for the friction experiments will be discussed, followed by the methodology of the shear experiments.

3.2. Friction experiment

3.2.1. Sample preparation

Porcine material was used for the thrombus-vessel wall samples in order to perform the friction experiments. The right jugular vein was retrieved from pigs that were sacrificed for a study performed within the Experimental Cardiology department at the Erasmus Medical Center. During their study, the colorant Evans blue was administered to the pigs, meaning that the jugular vein was blue at the moment of retrieval. Before Evans blue was administered to the pig, blood was drawn which was used to create RBC thrombi with a volume of 1200µL. Furthermore, throughout the day, heparin was administered to the pigs. Heparin is an anti-coagulant that needs to be neutralized in order for thrombi to be formed. Therefore, an alteration to the regular thrombus making protocol has been made in which protamine is used to counter the effect of the administered heparin. The details of this protocol can be found in Appendix A.3. How the amount of protamine that needs to be added was determined is explained in Appendix B.1.

The retrieved jugular vein was cut open longitudinally and pinned down on the piece of foamboard within the friction test setup. Consequently, a RBC thrombus, created in the incubator, was placed on top of the opened up vessel wall to create the thrombus-vessel wall sample. For each performed experiment, one jugular vein was collected and five to six RBC thrombi were created. These thrombi were placed on the vein after one another, while keeping the vein hydrated with HEPES buffer in the meantime.

3.2.2. Friction testing

As described in Section 2.3, a custom-made friction testing setup has been developed. After placing the thrombus on the opened and pinned down vessel wall, the angle inclination is initiated immediately (0 minutes) or after a waiting time of 3 or 5 minutes. These waiting times were applied in order to study the effect of time on the thrombus-vessel wall interaction, quantified by friction within this experiment. For the detailed protocol of the thrombus-vessel wall sample preparation and friction test, see Appendix A.2.

3.2.3. Data analysis

The angle of inclination (θ) at which the thrombus starts to slide and the distance (s) the thrombus slides across the vein is determined for each performed test. In order to determine both, all collected

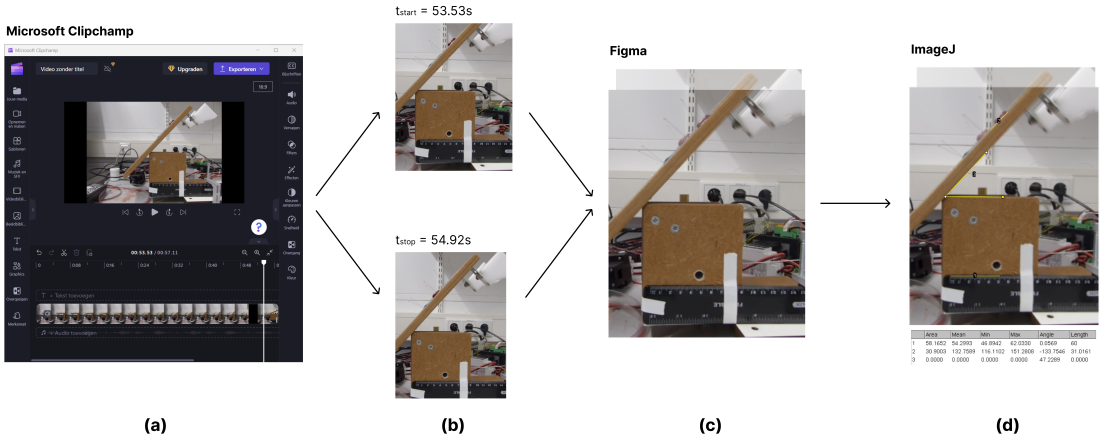

Figure 3.1: Post-processing steps to analyze the videos obtained during friction experiments. During step (a) Microsoft Clipchamp is used to determine (b) the sliding start and end time points. (c) Figma is used to create one image, visualizing the thrombus at two positions. (d) The angle of inclination and sliding distance is determined with ImageJ.

videos were analyzed by Microsoft Clipchamp. The time point at which the thrombus started to slide and the time point at which the sliding stopped were determined and screenshots of these moments were made. The design tool Figma was used to overlay both pictures in order to create one image with the thrombus at different stages. Consequently, the image processing program ImageJ was used to determine the angle of inclination and the traveled distance of the thrombus. The ruler in the image is used to scale the measurements done within ImageJ (Fig. 3.1).

The collected data is used to calculate the static coefficient of friction (Eq. 2.2) and kinetic coefficient of friction (Eq. 2.3), previously described in Section 2.3. Furthermore the interaction force is determined according to equation 3.1, where F_g is the gravitational force.

$$F_i = \mu_s \cdot F_N = F_g \cdot sin(\theta) \tag{3.1}$$

Lastly, similar as for the samples created for the shear experiments, the percentage of contraction was determined for the thrombi for the friction experiments. The calculations were executed with through a python script (Appendix D).

3.3. Shear experiment

3.3.1. Sample preparation

For the shear experiments, two sample types have been tested: RBC and FBR clot analogs. Both thrombus types were generated using blood obtained from healthy human volunteers. RBC clots were produced from whole blood, while FBR clots were created from platelet-rich-plasma, resulting in FBR clots containing 0% RBCs. All thrombus analogs were created with a total volume of 1200µL and were made on top of a piece of Velcro which is stuck to the bottom plate of the mold. The use of Velcro ensured that the samples remained fixed to the bottom plate during the shear experiment. For details on how the samples are created, see the protocol in Appendix A.3.

Multiple weight measurements were performed to determine the amount of clot contraction for each sample, which was calculated according to equation 3.2. The mass of the thrombotic solution in the mold ($m_{V_{mold}}$) is obtained by subtracting the weight of the empty assembled mold from the mold filled with the thrombotic solution. The mass of the formed thrombus (m_{clot}) is determined by subtracting the weight of the bottom plate with Velcro from the weight of the thrombus attached to the bottom plate.

$$Contraction = \frac{m_{V_{mold}} - m_{clot}}{m_{V_{mold}}} \cdot 100\% \tag{3.2}$$

3.3.2. Shear testing

A custom-made shear testing apparatus has been developed as described in Section 2.2. Thrombi exhibit viscoelastic behavior, meaning that they show time-dependent characteristics. Consequently,

the normal stress undergoes relaxation and reaches equilibrium after a certain time period. Therefore, the normal force is applied in two steps, allowing sufficient time for the normal force to reach equilibrium. The waiting time applied in between the normal force application steps and the shear initiation were determined experimentally. This was done per sample type due to the distinct stress relaxation behaviors observed for the FBR and RBC samples. The first waiting period is denoted as the period between normal force application step 1 and 2. The second waiting period is the time period between the second normal force application and shear initiation. For RBC clots, the first and second waiting time were set to 250s and 100s respectively. For the FBR clots these were set to 100s and 50s respectively.

The necessity for a normal force in conducting shear experiments is inherent, as it is required to effectively induce homogeneous shear deformations [37]. Without the application of a normal force, the shear experiment would not be executed successfully. To study the effect of normal force on the shear response, different normal forces have been applied. For the FBR clots a normal force of either 0.10N, 0.15N, or 0.20N was applied. A normal force of 0.15N or 0.20N was applied on the RBC clots.

The shear experiments for the RBC and FBR clots were initially executed according to the same protocol, meaning that the pressure of the top plate was used to establish contact with the sample. However, experimental results showed that the created contact between the sample and top plate was not sufficient for RBC clots as slippage between the sample and top plate occurred for the majority of samples tested (see Appendix B.3 for more information). Consequently, an alteration to the experimental protocol was made for the shear testing of RBC clots. Instead of relying on sufficient frictional contact due to pressure, tissue glue is used to create an adequate connection between the sample and the top plate, meaning that the sample is now fixed on both the bottom and top. The final protocols for the shear experiment on both FBR and RBC samples can be found in Appendix A.1.

3.3.3. Data analysis

The normal and shear force have been recorded throughout the entire experiment using the LabVIEW script. Furthermore, morphological data was collected through images and recordings. These were processed in ImageJ in order to derive the top area (A) and the sample height before ($h_{initial}$) and after normal force application ($h_{compressed}$) for each thrombus.

All collected data was analyzed utilizing custom-made Python scripts (Appendix D). The measured shear force (F_S), together with data collected from imaging, is used to determine the shear stress (τ) and strain (γ) response of the sample (Eq. 3.3, 3.4).

$$\tau = \frac{F_S}{A} \tag{3.3}$$

$$\gamma = \frac{v_{actuator} \cdot t}{h_{compressed}} \tag{3.4}$$

Where $v_{actuator}$ is the velocity of the actuator and t stands for time.

Lastly, the shear force and normal force (F_N) are used to determine the mean kinetic coefficient of friction ($\mu_{k_{mean}}$) of the FBR samples. The kinetic coefficient of friction is determined according to equation 3.5, with *i=1* representing the initial moment in time at which the period of kinetic friction starts.

$$\mu_{k_{mean}} = \frac{1}{N} \sum_{i=1}^{N} \frac{F_S[i]}{F_N[i]} \tag{3.5}$$

Computational models

A computational model has been developed to provide a mechanistic interpretation of the experimentally acquired data. Once calibrated and validated, the computational model can be used for simulations of more complex problems. Specifically, a Finite Element Model was created using Abaqus software to simulate the shear experiment. In this model, the top plate mirrors the dimensions of the plate within the actual test setup and it is used to apply compression on the thrombus. The amount of compression, initiated by a displacement along the y-axis is experiment specific. Furthermore, the dimensions of the modeled thrombus are sample specific. The compressive displacement is applied during the first step, while the bottom of the thrombus is fixed in all directions. During the second step, the shear movement is initiated. This is done by applying a displacement to a reference node at the bottom of the thrombus

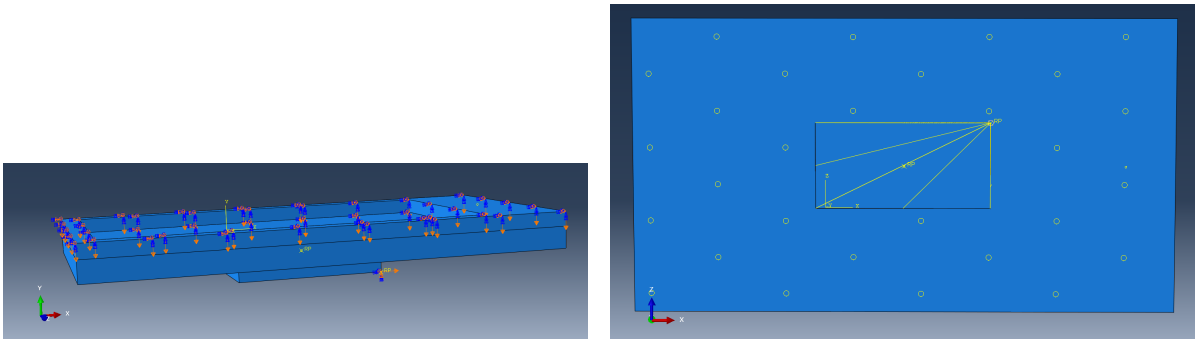

(a) Boundary conditions **(b)** Constraints

Figure 3.2: Abaqus model settings. (a) Shows the applied boundary conditions. The displacement along the y-axis on the top plate is applied during step one. The displacement along the x-axis is applied during step two and initiates the shear movement of the thrombus. (b) The bottom view of the Abaqus model shows how the coupling constraint converges all nodes within the bottom plane of the thrombus to the reference node (RP) at which the displacement in the x-axis is applied. Furthermore, the circles represent the tie constraint between the thrombus and the top plate.

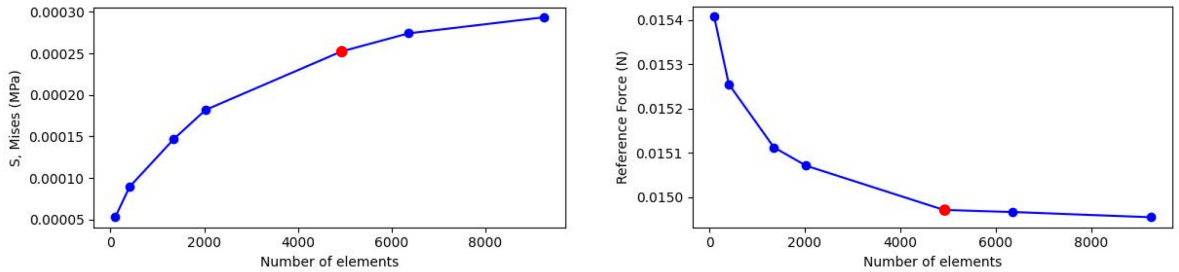

(a) Maximum S. Mises vs the number of elements **(b)** Maximum reference force vs the number of elements

Figure 3.3: Results of the mesh sensitivity study performed on sample RBC33.

sample, to which all nodes within the bottom plane of the thrombus model are coupled. In order to do so, a coupling constraint was used. Furthermore, a tie constraint is used in between the thrombus and top plate, mimicking the experimental conditions of the tissue glue connection (Fig. 3.2).

A mesh sensitivity study was conducted to determine the optimal mesh for the thrombus to run the model of the shear experiment. Both the Von Mises stress and reference force were assessed for different element numbers. Figure 3.3 shows that both quantities converge around 4920 elements, shown by the red dot in the figures. Due to slight differences in dimensions between different samples, the element number varies slightly between the samples. However, as the element size is required to be constant for all samples, a global seed size of 0.5 is used to create a mesh for each modeled sample. The element type used was C3D8H.

Using a MatLab script, a third order hyperelastic Yeoh model is fitted against the experimental data. From the experimental data the shear force and displacement is utilized. For the Yeoh model, the reference force and displacement in the x-direction is extracted from Abaqus.

4

Results

In this chapter, a comprehensive analysis is given of the data derived from the friction and shear experiments. First, the results of the friction experiments will be presented, delving into the relationship between the thrombus-vessel wall interaction and the applied waiting time. Secondly, data from the shear experiments will be analyzed. Various components of the experimental data are dissected to determine multiple mechanical properties, aiming to unveil correlations between the thrombus compositions and these mechanical characteristics. Additionally, the results of the computational model are discussed.

4.1. Friction experiment

4.1.1. Porcine samples

A total of four friction experiments were performed on separate days. For friction experiment 1, 3 and 4, the blood used to create RBC thrombi was drawn from the same pig as the pig the jugular vein was taken from. Unfortunately, this was not the case for experiment 2 as blood was not available the day experiment 2 was performed. Instead, porcine blood from the pig from experiment 1 (24 hours old) was used to create thrombi for experiment 2. In table 4.1, characteristics of the thrombus-vessel wall samples per experiment are depicted. Table 4.2 shows the number of experimental runs per applied waiting time for each experiment.

4.1.2. Static coefficient of friction

In figure 4.2, boxplots for each experiment are given which show the static coefficient of friction per applied waiting time. It is noteworthy that an increased waiting time leads to a higher static friction coefficient. However, another important observation is that these boxplots reveal that no static coefficient of friction could be determined for more than half of the performed experiments. This is due to the angle of inclination reaching an angle of 90°, without the occurrence of any slippage of the thrombus along the vessel wall (Fig. 4.1). This occurred for 17 out of 21 samples within the 3 to 5 minute waiting time group and for 12 out of 22 samples for the 0 minute waiting time group, implying that the interaction between the thrombus and vessel wall is stronger than the gravitational force for these samples. The average static coefficient of friction per experimental condition is shown in table 4.3.

In figure 4.3 the interaction force is set out for each experimental condition. The interaction force for

	Experiment 1	**Experiment 2**	**Experiment 3**	**Experiment 4**
Jugular vein retrieved from	Pig 1	Pig 2	Pig 3	Pig 4
Blood taken from	Pig 1	Pig 1	Pig 3	Pig 4
Number of samples	6	5	6	6
Contraction (%) (SD)	63 (+/- 7)	46 (+/- 7)	68 (+/- 6)	56 (+/- 11)
Sample top area (mm^2) (SD)	131 (+/- 10)	175 (+/- 5)	154 (+/- 12)	181 (+/- 31)

Table 4.1: Thrombus-vessel wall sample characteristics

Experiment 1 Waiting time	Runs	Experiment 2 Waiting time	Runs	Experiment 3 Waiting time	Runs	Experiment 4 Waiting time	Runs
0 min	N = 3	0 min	N = 7	0 min	N = 6	0 min	N = 6
5 min	N = 3	5 min	N = 6	3 min	N = 6	3 min	N = 6

Table 4.2: Number of experiments per experimental condition

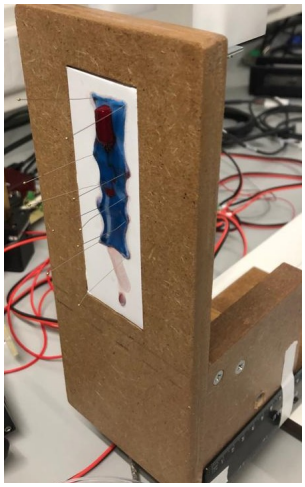

Figure 4.1: Example of an experiment that went to 90° without any slippage of the thrombus along the vessel wall.

all samples is calculated according to equation 3.1. As $sin(\theta) = 1$, this means that the frictional force is equal to the gravitational force for all samples that did not slide at 90°. Therefore, the interaction force for these samples is a minimal interaction force.

4.1.3. Kinetic coefficient of friction

The calculation of the kinetic coefficient of friction involves assessing the acceleration of the thrombus over the venous surface (Eq. 2.3). The performed friction experiments revealed that this acceleration is not constant. As the thrombus moves, it either accelerates or displaces down the vessel wall in multiple phases. To obtain an estimate of the coefficient of friction, the average acceleration was calculated over one movement period with equation 2.4. This means that in cases where a thrombus slipped along the vessel wall in multiple steps, only the acceleration from the first step is considered to determine the kinetic coefficient of friction.

In table 4.3 the mean kinetic coefficient of friction can be found per experimental group. Additionally, the relationship between the kinetic and static friction coefficient is illustrated in figure 4.4a. A highly significant correlation between these characteristics is observed (r=0.999, p=9.969e-25). Furthermore, an exponential relationship is observed between the kinetic coefficient of friction and the angle of inclination at which the thrombus starts to slide (Fig. 4.4b). This relationship aligns with expectations based

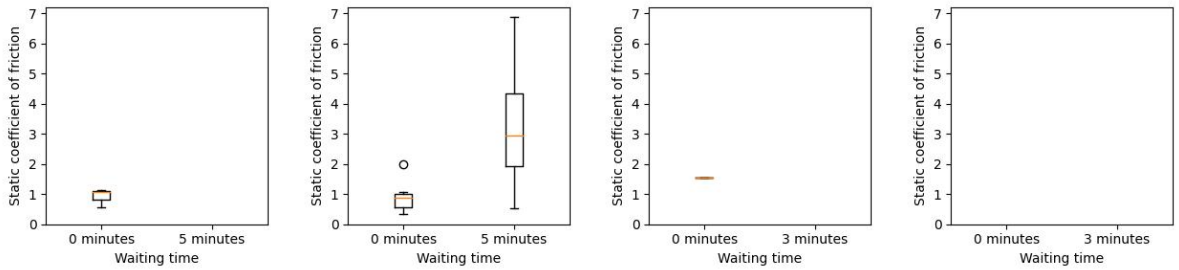

(a) Experiment 1 **(b)** Experiment 2 **(c)** Experiment 3 **(d)** Experiment 4

Figure 4.2: Static coefficient of friction per waiting time for each performed experiment.

	Experiment 1 Waiting time		Experiment 2 Waiting time		Experiment 3 Waiting time		Experiment 4 Waiting time	
	0 min	5 min	0 min	5 min	0 min	3 min	0 min	3 min
Mean static coefficient of friction	0.920	-	0.929	3.324	1.562	-	-	-
Mean kinetic coefficient of friction	0.913	-	0.920	3.258	1.512	-	-	-

Table 4.3: Mean static and kinetic coefficient of friction per waiting time for each performed experiment

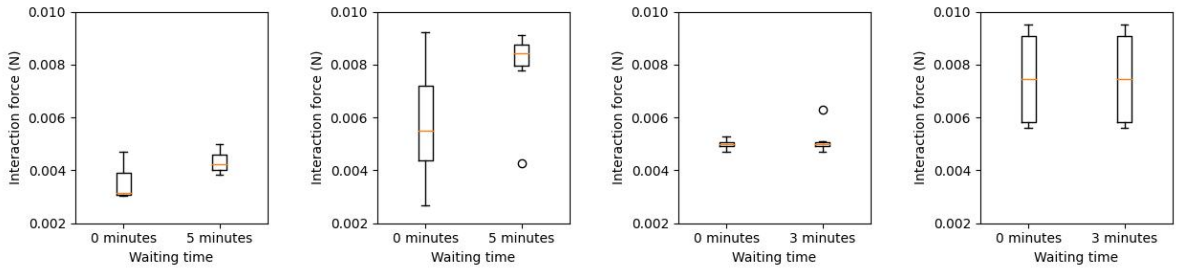

(a) Experiment 1 **(b)** Experiment 2 **(c)** Experiment 3 **(d)** Experiment 4

Figure 4.3: The (minimum) interaction force required to overcome the static coefficient of friction, per waiting time for each performed experiment.

on equation 4.4b. Lastly, it is noteworthy that $\mu_s > \mu_k$ holds for all samples.

4.2. Shear experiment

A total of 28 FBR samples and 22 RBC samples have been created to conduct shear experiments. In tables 4.4 and 4.5 the baseline data of, respectively, all FBR and RBC samples can be found per donor. Noticeable is that the FBR samples have a significant higher percentage of contraction (p=6.119e-13), and consequently smaller surface area and sample height, compared to the RBC samples. In the remainder of this section, the results for the sample types will be discussed separately. The raw data plots of all shear experiments can be found in Appendix C.1.

	Donor 1	Donor 2	Donor 3	Donor 4	Donor 5
Number of samples	5	8	4	8	3
Contraction (%) (SD)	41 (+/- 8)	51 (+/- 9)	47 (+/- 8)	38 (+/- 7)	38 (+/- 4)
Sample top area (mm^2) (SD)	151 (+/- 7)	152 (+/- 26)	148 (+/- 25)	181 (+/- 7)	193 (+/- 3)
Sample height (mm) (SD)	2.1 (+/- 0.2)	2.0 (+/- 0.2)	2.2 (+/- 0.5)	2.4 (+/- 0.3)	2.3 (+/- 0.4)

Table 4.4: Baseline characteristics for the FBR samples created for the shear experiments

	Donor 3	Donor 4	Donor 5	Donor 6
Number of samples	6	5	5	6
Contraction (%) (SD)	20 (+/- 6)	22 (+/- 8)	18 (+/- 4)	24 (+/- 7)
Sample top area (mm^2) (SD)	211 (+/- 11)	209 (+/- 22)	218 (+/- 14)	208 (+/- 18)
Sample height (mm) (SD)	3.2 (+/- 0.3)	3.1 (+/- 0.1)	3.2 (+/- 0.3)	3.3 (+/- 0.2)

Table 4.5: Baseline characteristics for the RBC samples created for the shear experiments

4.2.1. FBR samples

In figure 4.5a the raw data of a shear experiment of two FBR samples can be seen, from normal force application till the end of the shearing part of the experiment. The measured normal force is shown by the dotted lines, and the continuous lines show the shear force over time. The data is plotted for two different samples, FBR18 and FBR19, to show the effect of the normal force on the measured shear force. On the top x-axis, multiple time points are indicated. From t1 till t2, the normal force is applied

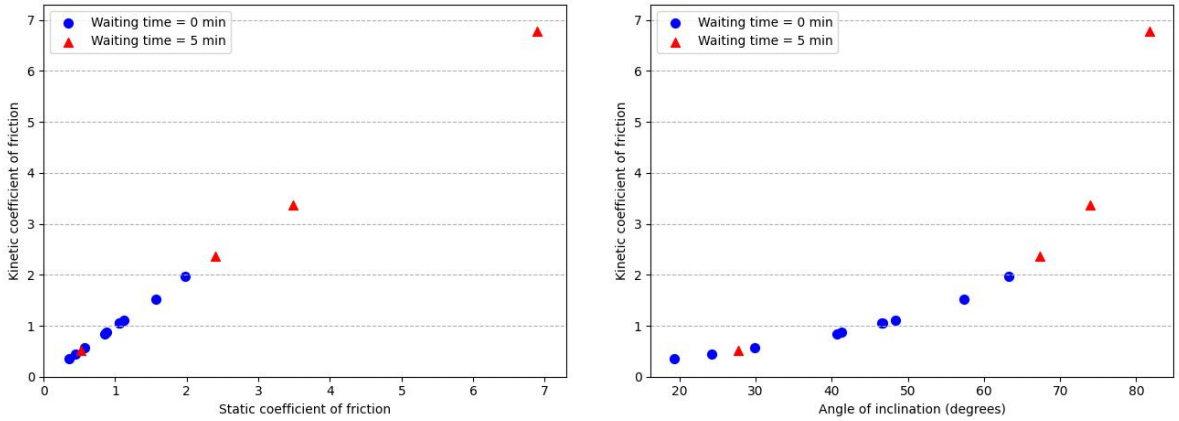

(a) A correlation plot of the static versus kinetic coefficient of friction (r=0.999, p=9.969e-25).

(b) The kinetic coefficient of friction plotted against the angle of inclination at which the thrombus started to slide.

Figure 4.4: The scatter plots show the combined data of the different waiting time groups. Each group is represented by a specific marker, as indicated in the legend. Notable, the experimental groups subjected to a waiting time of 3 minutes are absent from these plots as no coefficients of friction could be determined for the samples within these groups.

for both samples. After a waiting time of approximately 100s, the normal force is re-applied at t3 till t4. During the following waiting time of approximately 50s, the shear load cell is unlocked. The effect of this action can be seen at t5 for sample FBR18 and at t6 for sample FBR19. In both the shear and normal force signal, some disturbance can be seen at these moments. For the shear force measurements, this does not have any consequences as the load cell is still tared after it is unlocked. The disturbance in the normal load cell can not be adjusted, but is usually fairly limited or normalized to its original signal. Following the unlocking of the shear load cell, the shearing part of the experiment is initiated. For sample FBR18 this happens at t6, where a steep rise in the shear force signal is observed. A similar steep rise is seen at t7, which is when the shearing part was initiated for FBR19.

To clarify the results from the shear part of the experiment, an additional plot is shown in figure 4.5b that zooms in on the last part of figure 4.5a for sample FBR19, starting at time point t7. Within figure 4.5b, three regions within the shear load readout can be distinguished. The first period, from t7 till t8, is marked as the shearing period. On average this period takes 1.21s, within the current protocol. A further zoomed in plot of this period is shown in figure 4.5c. This period starts with a toe off region, followed by a rapid increase in the shear force. Afterward a plateau occurs, which indicates the second region, named the slip region (t8). During this period, the thrombus start to slide along the top plate of the test setup. After the thrombus has slipped completely, a horizontal region occurs, from t10 onward, which portrays the period of kinetic friction. Each distinct period is evaluated for different biomechanical characteristics. Detailed explanations are provided in the following sections.

Shearing period

Figure 4.6 shows a shear stress strain curve derived from the raw data, using equations 3.3 and 3.4. Due to the observed non-linearity, low- and high-strain regions are determined to calculate the low- and high-strain shear modulus per sample. To define these strain regions, percentages of the maximum strain are utilized, considering the positive correlation between the applied normal force and the maximum strain (r=0.3808, p=0.0456). An example of the strain regions are depicted in figure 4.6. The low-strain region is defined as 5-15% of the maximum strain, while the high-strain region spans 30-40% of the maximum strain. More information about how these regions are determined can be found in Appendix C.2. Due to noise in the data or due to the strain region occurring in the plateau, four samples had to be excluded when determining the low-strain shear modulus, and three when determining the high-strain shear modulus.

An average low-strain shear modulus of 1713Pa (SD=897Pa) and average high-strain shear modulus of 1310Pa (SD=523Pa) was found. A significant positive correlation between the low- and high-strain shear moduli was established (r=0.8273, p=1.121e-6), showing a relationship between low and high strains. Furthermore, by comparing both shear moduli with a Mann-Whitney U test, no significant difference could be found (p=0.1835).

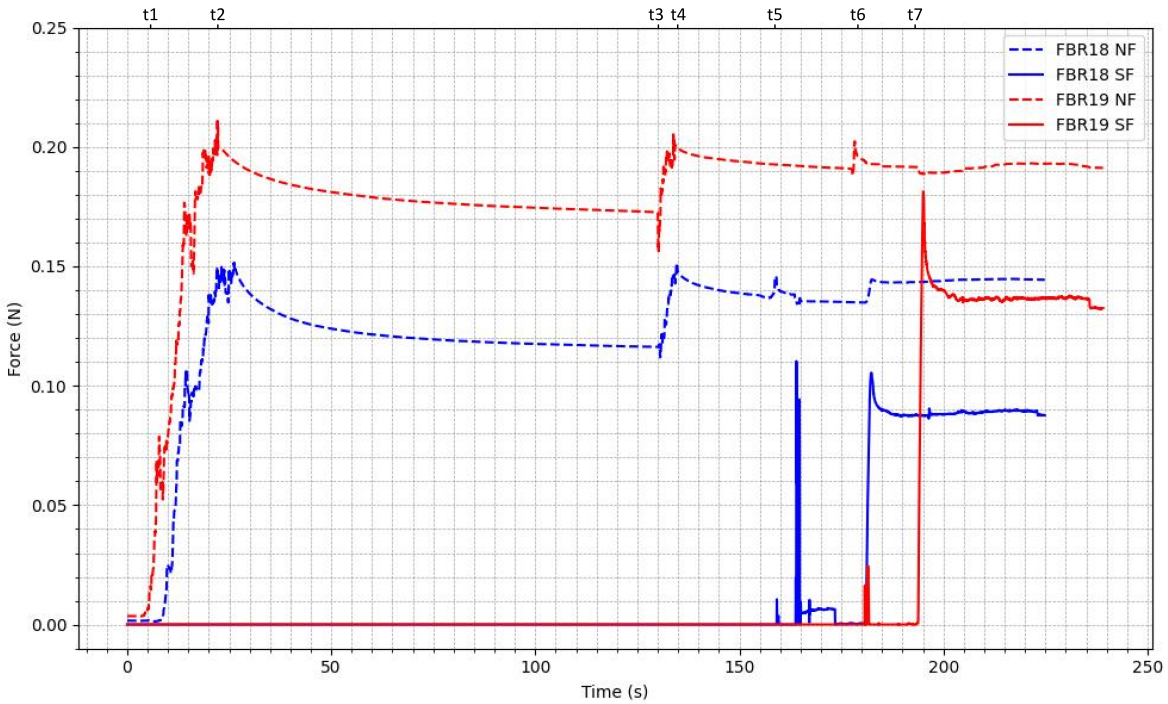

(a) Complete raw data plot of the shear experiment of two FBR samples.

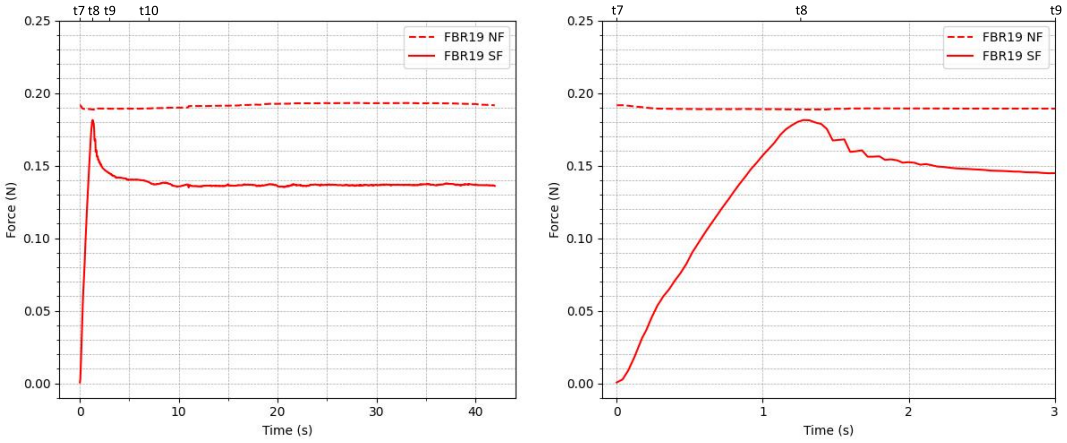

(b) Plot zooming in on the shear part of the experiment of sample FBR19, from t7 onward.

(c) Plot zooming in on the shearing period, observed in the raw data of the shear experiment (t7 till t9) of sample FBR19.

Figure 4.5: (a) Raw data of two FBR samples showing both the normal force and shear force course over time. On the upper x-axis multiple time points are indicated. From t1 till t2, the initial normal force is applied. The normal force is re-applied from t3 till t4. Some disturbance in the signals is found at t5 and t6 for respectively sample FBR18 and FBR19. At t6 the shear part of the experiment is initiated for sample FBR18. This is done for sample FBR19 at t7. (b) This plot shows the shear part of the experiment for sample FBR19, from time point t7 till the end of the experiment. The x-axis starts at t=0s again for analysis purposes of the shear experimental part. The moment of slippage is denoted by t8 and the period of kinetic friction starts at t10. (c) This plot zooms in on time point t7 till t9 for sample FBR19. The shear force starts with a toe off region after which the shear force rapidly increases. The shear force reaches a plateau around t8, which indicates the moment of slippage, after which the force decreases again.

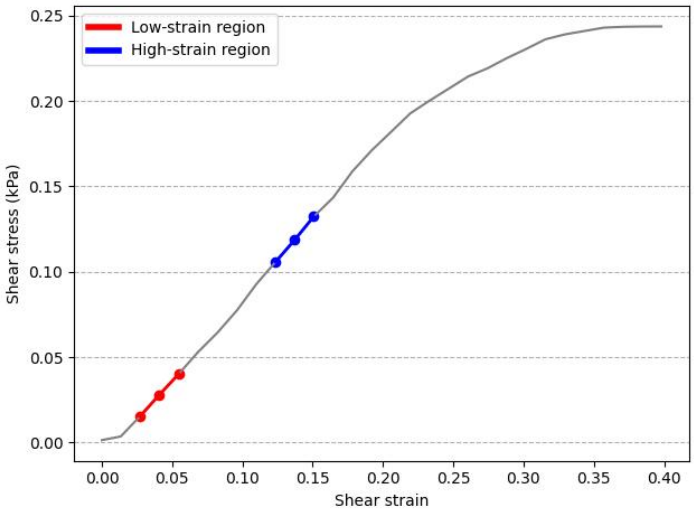

Figure 4.6: Shear stress strain curve of sample FBR32, highlighting the low- and high-strain regions.

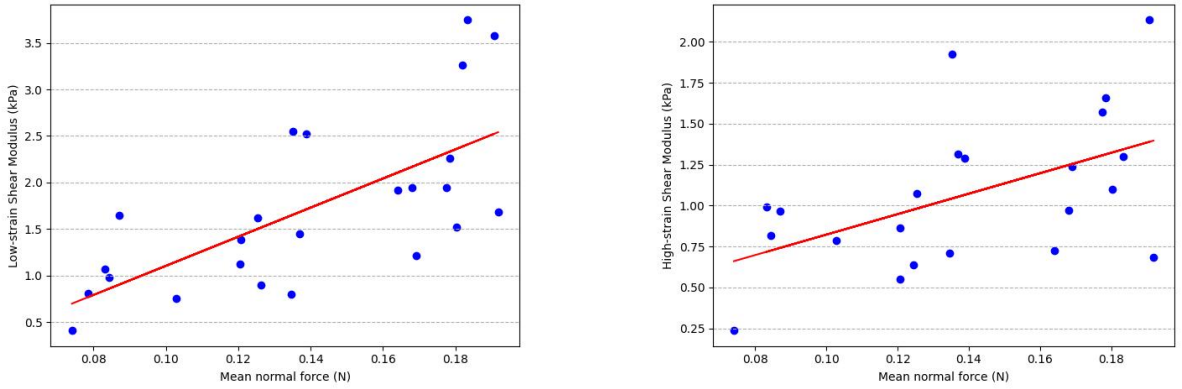

(a) Correlation plot of the low-strain shear modulus against the mean normal force (r=0.6839, p=2.29e-4).

(b) Correlation plot of the high-strain shear modulus against the mean normal force (r=0.5152, p=0.0141).

Figure 4.7: The low- and high-strain shear modulus plotted against the mean normal force for FBR samples.

A positive significant correlation between the low-strain shear modulus and mean normal force (r=0.6839, p=2.29e-4), and between the high-strain shear modulus and mean normal force was observed (r=0.5152, p=0.0141) (Fig. 4.7).

Slippage period

After reaching the maximum shear force, the thrombus starts to slide along the top plate, thereby defining the moment of slippage. The moment the thrombus starts to slide can furthermore be described as the moment the static coefficient of friction is reached. Three samples were excluded from this analysis as no clear slippage moment could be determined. For the remaining 25 samples, the static coefficient of friction is determined according to equation 2.1, in which the interaction force is the maximum shear force and the normal force is assessed at the same time point. The static coefficient of friction positively correlates with the mean normal force (r=0.4388, p=0.0282). Consequently, the average static coefficient of friction is calculated as a weighted average, weighted by the mean normal force. This results in a weighted average of 0.549 (SD_w=0.221). Furthermore, a maximum strain of 0.48 (SD_w=0.19) was found, weighted by the mean normal force due to the positive correlation between both characteristics (r=0.4805, p=0.0150).

Kinetic friction period

The last horizontal area in the raw data, denoted as the period of kinetic friction, is utilized to determine the mean kinetic coefficient of friction per sample. Exclusion criteria have been established, which are

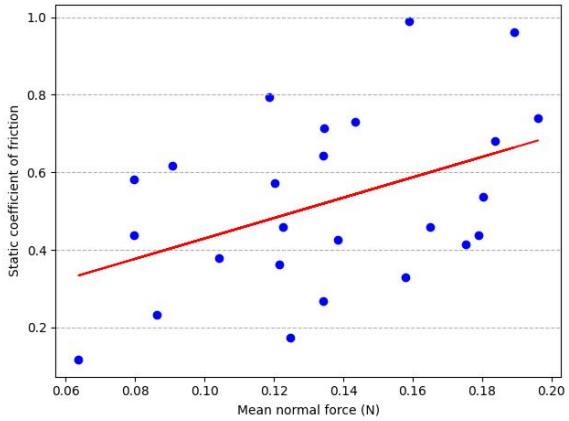

(a) Correlation plot of the static coefficient of friction against the mean normal force (r=0.4388, p=0.0282).

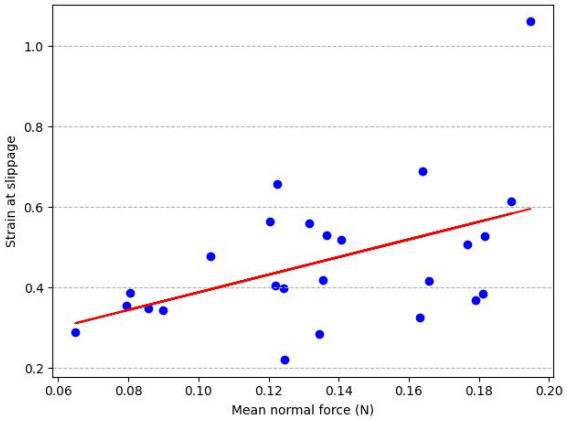

(b) Correlation plot of the strain at slippage against the mean normal force (r=0.4805, p=0.0150).

Figure 4.8: Correlation plots for the slippage region of the FBR samples.

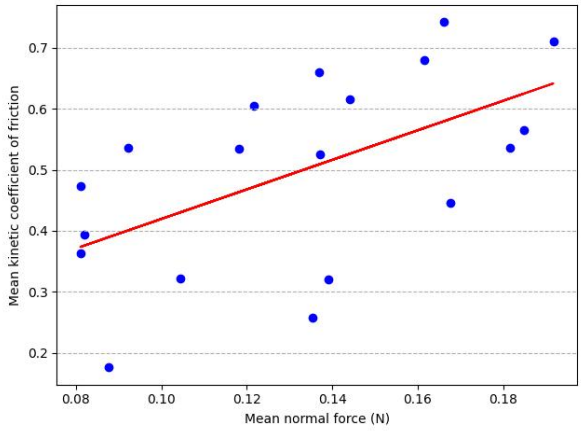

Figure 4.9: Correlation plot of the mean normal force against the mean kinetic coefficient of friction for FBR samples (r=0.5634, p=0.0120).

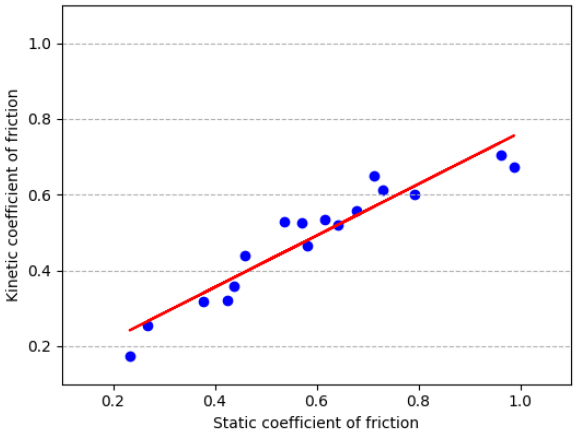

Figure 4.10: A correlation plot of the static and kinetic coefficient of friction of FBR samples, determined from the shear experiment (r=0.9499, p=5.60e-9).

based on the accuracy of the load cell, allowing for a deviation of up to 5%. Therefore, all samples that deviate more than 5% from the mean shear force, during the period of kinetic friction, are excluded from further analysis in this section. By applying this method, nine of the 28 FBR samples were excluded from further analysis for the kinetic coefficient of friction. Details on how the exclusion criterion is determined and applied can be found in Appendix C.3.

As discussed in Section 3.3.3, the mean kinetic coefficient of friction is determined per sample by equation 3.5. The time point at which the period of kinetic friction starts is set at t=7s as each FBR sample has completely passed the moment of slippage at that point. In figure 4.9, the mean kinetic coefficient of friction is plotted against the mean normal force (r=0.5634, p=0.0120). An average of the kinetic coefficient of friction has been determined, weighted by the mean normal force. This weighted average was found to be 0.516 (SD_w=0.151) for the FBR samples.

The static coefficient of friction, found at the moment of slippage, is compared to the kinetic coefficient of friction for the samples that could be included in both determinations, totaling 17 samples. A strong positive correlation was observed between these characteristics (r=0.9478, p=7.64e-9), as depicted in figure 4.10. Furthermore, the kinetic coefficient of friction is smaller than the static coefficient of friction for all samples.

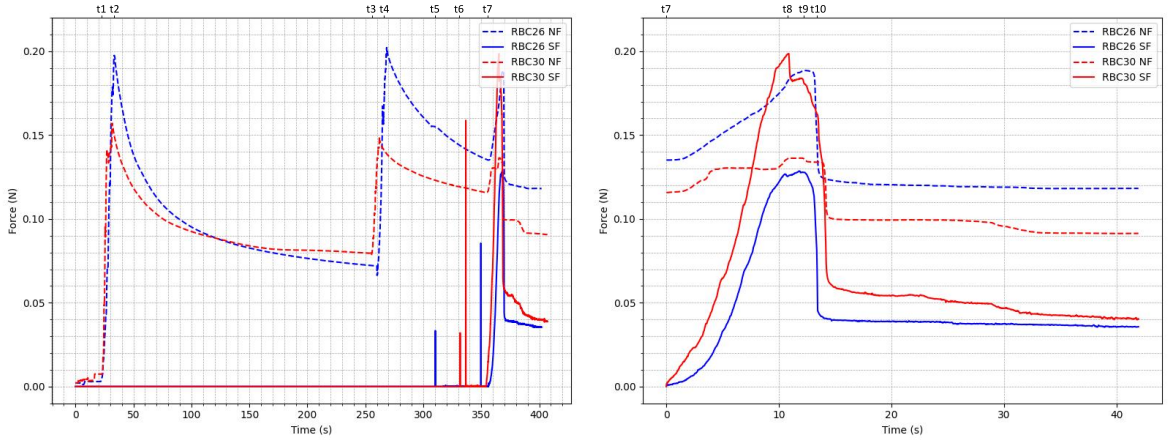

(a) The complete raw data plot of a shear experiment of two RBC samples.

(b) A zoomed plot on the shear part of the experiment, continuing from time point t7.

Figure 4.11: Raw data of two RBC samples showing both the normal force and shear force course over time. On the upper x-axis multiple time points are indicated. (a) From t1 till t2, the initial normal force is applied. The normal force is re-applied from t3 till t4. Due to unlocking of the shear load cell, disturbances in the shear force signal are observed from t5 and t6 until the moment of shear initiation (t7), for sample RBC26 and RBC30 respectively. (b) A zoomed plot of the shear part of the experiment is given, from time point t7 onward. The x-axis starts at t=0s for analysis purposes of the shear experimental part. The shearing period is shown from t7 till t8 and t9, respectively for sample RBC30 and RBC26. It starts with a toe off region, moving towards a plateau after a rapid increase in shear force. The plateau reaches the maximum shear force, at t8 and t9 for RBC30 and RBC26 respectively, indicating the moment of slippage. After the slippage period, a drop in the shear force is observed (t10), followed by the period of kinetic friction.

4.2.2. RBC samples

In figure 4.11 the raw data of an entire performed experiment of two RBC samples is shown. Noticeable is that the forces follow similar curves as in the raw data of the FBR samples (Fig. 4.5). However, there are also some differences noticeable. These are caused by the tissue glue connection created between the sample and the top plate.

First of all, when looking at the shear force, the shearing period takes 9.46s on average, which is more than 8s seconds longer than the shearing period for the FBR samples. The consequent moment of slippage is less immediate due to the tissue glue connection that weakens and breaks during this period. Furthermore, the period of kinetic friction is disturbed more often due to varying amounts of residual glue that is left after the connection breaks. Two samples were completely excluded from analysis as too much tissue glue infiltrated in the samples, causing big chunks of the sample to become hardened and break during the shear experiment (see Appendix B.3). Therefore, 20 RBC samples will be discussed in the remainder of this chapter.

Shearing period

Figure 4.12 shows the shear stress strain curve of a RBC sample in which low- and high-strain areas are portrayed. The low-strain region captures 0.1 to 0.2 strain, and the high-strain region captures 1.5 till 1.6 strain. Specific regions are chosen, instead of percentage of the maximum strain, as the applied normal force does not correlate with the maximum strain, due to the used glue connection between the RBC samples and the top plate. As a consequence of noisy data or the chosen regions being outside the scope of the data of the sample, five of the 20 samples were excluded from the high-strain shear modulus analysis. All samples could be included to determine the low-strain shear modulus (Appendix C.2).

A mean low-strain shear modulus of 69.53Pa (SD=55.33Pa) was found and a mean high-strain shear modulus of 381.65Pa (SD=184.24Pa). The shear moduli are significantly correlated (r=0.6171, p=0.0143), and the difference between both is significant, following from a Mann-Whitney U test (p=5.053e-6).

Slippage period

For the RBC samples, the moment of slippage is identified by the point at which the glue connection between the sample and top plate completely fails. It is expected that the detachment propagation occurs

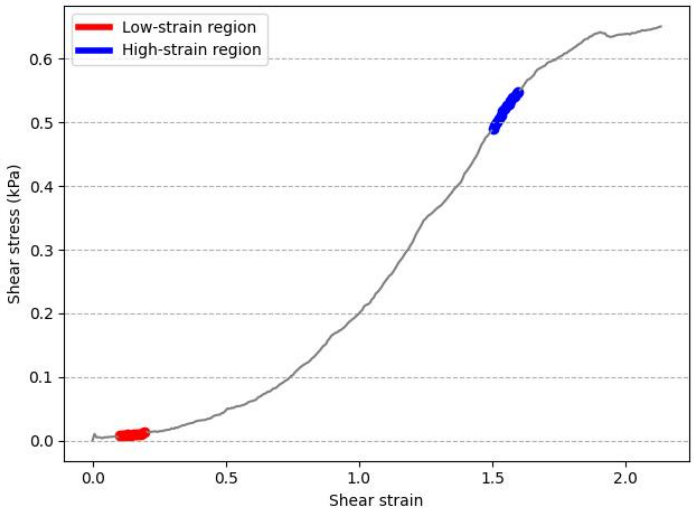

Figure 4.12: Shear stress strain curve of sample RBC26, highlighting the low- and high-strain regions.

Sample	C10 (MPa)	C20 (MPa)	C30 (MPa)	D1	D2	D3
RBC26	7e-6	5.65e-5	-4.476e-7	20	20	20
RBC27	3.5e-5	4.4e-5	-4.476e-7	20	20	20
RBC29	5e-6	2.5e-5	-4.476e-7	20	20	20
RBC30	9.5e-5	2.8e-5	-4.476e-7	20	20	20
RBC31	9e-6	2.8e-5	-4.476e-7	20	20	20
RBC33	4.75e-5	2.8e-5	-4.476e-7	20	20	20
RBC35	5e-6	3e-5	-4.476e-7	20	20	20
RBC39	2e-5	3e-5	-4.476e-7	20	20	20
RBC44	1e-6	7e-5	-4.476e-7	20	20	20

Table 4.6: Material parameters for the Yeoh models to fit the Abaqus model against the experimental data

as the increasing shear force diminishes, but the exact development of this detachment propagation is unknown. Therefore, the moment of slippage is defined as the point where the maximum shear force is observed. Due to the tissue glue connection, no static coefficient of friction can be determined for the RBC samples. An average strain of 1.901 (SD=0.295) was found at the moment of slippage. No correlations were found with the applied normal force.

Kinetic friction period

Based on the same criterion as used for the FBR samples, only two samples can be included for the RBC samples to determine the kinetic coefficient of friction (Appendix C.3). These samples are RBC26 and RBC34, which have a mean kinetic coefficient of friction of 0.037 and 0.051, respectively.

Computational model

In table 4.6 the material parameters are given that were used to fit the Yeoh model to the experimental data. The fit was made for nine RBC samples which are shown in figure 4.13. Parameters C30, D1, D2 and D3 were kept constant for each sample. For parameters C10 and C20, the median and interquartile range is determined, shown in table 4.7. This analysis could not successfully be performed for the FBR samples.

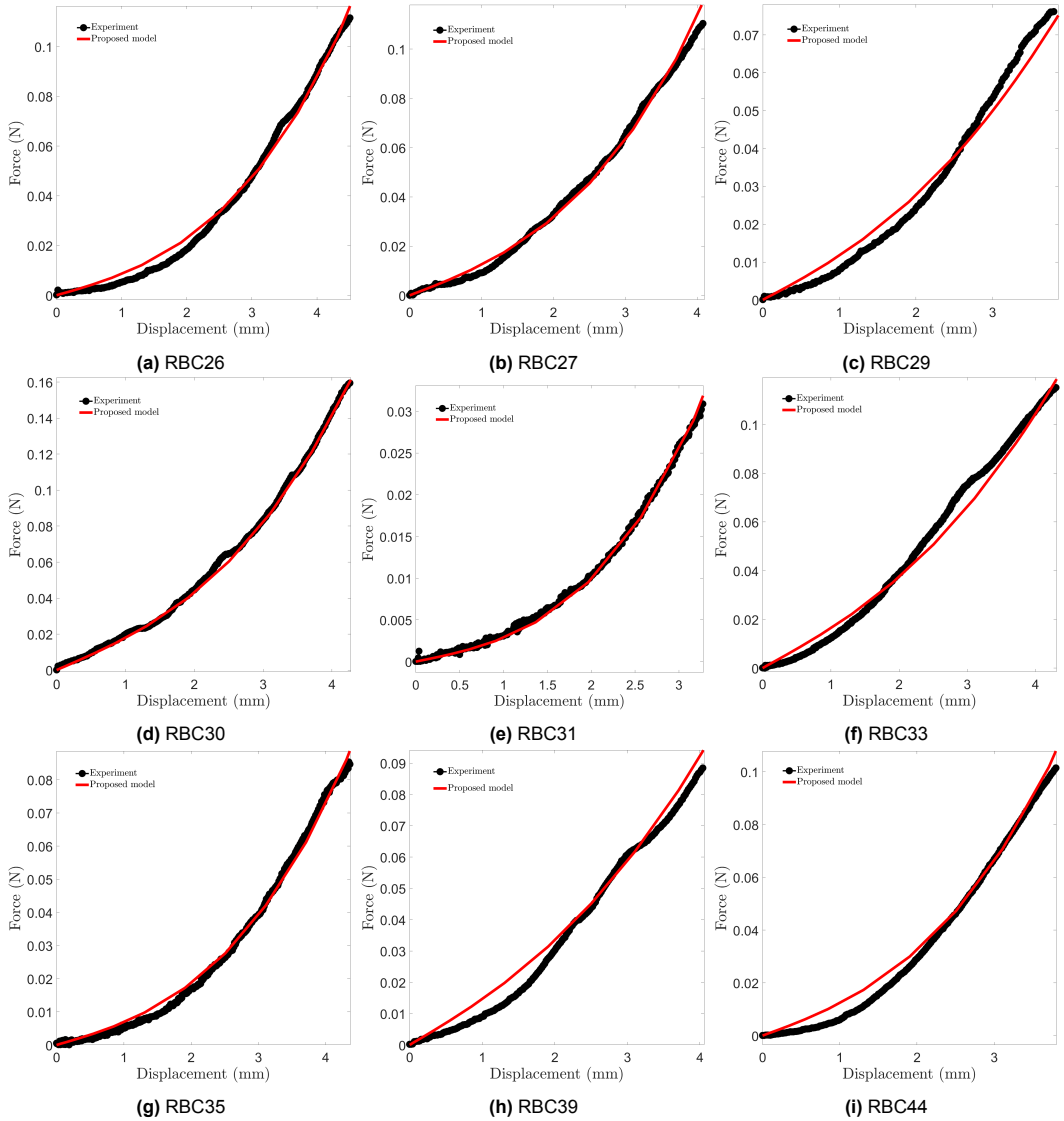

Figure 4.13: The proposed Yeoh model fitted against the experimental data for nine RBC samples.

	C10	C20
Median	9e-06	3e-05
Interquartile range	3e-05	1.6e-05

Table 4.7: The median and interquartile range for Yeoh parameters C10 and C20 used to fit nine different RBC samples

5 Discussion

5.1. Custom-made test setups

For this thesis, two experimental test setups were successfully designed and developed to conduct shear and friction experiments. The shear test setup is designed to investigate the shear behavior of thrombi, as well as the thrombus-vessel wall interaction. Within this thesis, shear experiments have been performed on *in vitro* created thrombi of two different compositions, RBC and FBR thrombi. The shear experimental test setup consists of three main components: the shear load section, normal load section, and actuator connected to the sample holder. The actuator displaces the sample holder at a speed of 0.5mm/s with an accuracy of $\pm$ 0.02mm. The sample holder secures the sample through a magnetic connection with the bottom plate. A 50g load cell is included in both load sections, measuring force with an accuracy of 5%. The normal load section allows adjustment of the force placed on the sample. The amount of compression can either be determined by looking at the normal force response in LabVIEW or by accurately setting a specific strain on the sample via the micrometer displacement. The micrometer displacer allows the strain to be set with an accuracy of $\pm$ 0.1mm, enabling precise control over the applied strain on the sample. The shear load section measures the shear response during a performed experiment.

As stated previously, the shear test setup has been used to study the shear behavior of thrombi within this thesis. With a few advancements, this test setup can be used to study the shear thrombus-vessel wall interaction as well. First of all, an effective method needs to be established to mount the opened-up vessel wall on the top plate, without exceeding the maximum force handled by the load cell. A potential solution might be to create tiny notches in the top plate in which foamboard or a silicone elastomer is inserted such that the vessel wall can be pinned down. Another method that could work is the application of tissue glue to the edges of the vessel wall and sticking it to the top plate. Experimental work conducted during this thesis has demonstrated that tissue glue serves as a suitable technique for adhering thrombi to the top plate. These results indicated that establishing a connection was feasible without substantially affecting the thrombus. A similar method could potentially be employed for fixing the vessel wall to the top plate as well. As only the material in direct contact with the tissue glue hardens, the surface area used within the experiment will remain unaffected. Additionally, by solely gluing the edges, the thrombus-vessel wall interaction remains observable for ultrasound imaging.

It would be a great addition to the experimental results if the thrombus-vessel wall interaction was imaged throughout the shear experiment by ultrasound imaging. The necessary components to conduct ultrasound imaging during a shear experiment are already available. A probe holder has been made to steadily place and relocate the ultrasound probe over the experimental surface during an experiment. Furthermore, the top plate has been created out of TPX because of its low acoustic impedance properties, making it possible to image through the top plate with ultrasound. However, detailed specification on how to optimize the visualization need to be investigated. Additionally, an effective method must be developed such that the ultrasound probe maintains the correct distance from the sample without making contact with the top plate. Contact between the probe and the top plate could exert force on the normal load cell, potentially causing damage. A practical adjustment would involve modifying the probe holder to facilitate the gentle displacement of the probe's height, eliminating the need for the current

setup involving the unlocking and locking of multiple screws. Furthermore, visualization of the experiment from the side, and therefore also the probe-sample distance, could be enhanced by increasing the size of the window within the box. Moreover, if the waterbath is deemed unnecessary for the performed experiment, it could be removed completely, provided that the sample holder is still displaced along a smooth surface.

Another component of the shear test setup that is worth improving is the shear load cell locking mechanism. Currently, the shear load cell is unlocked after the normal force has been applied. This approach is taken as a safety measure in order to avoid applying too much load on the shear load cell while applying the normal force via the micrometer displacer. The unlocking of the shear load cell results in a peak in the shear force signal and a slight disturbance within the signal of the normal load cell. Due to the shear load cell being zero balanced after unlocking, the peak does not influence the shear results. However, the disturbance seen in the normal load cell signal cannot be adjusted as the normal load is already set. The amount of disturbance that occurs depends on how gently the screw from the shear load cell lock is removed. To limit the influence of unlocking, the locking mechanism should be adjusted to make it simpler to unlock the shear load cell. A potential solution might be to replace the screw connection with a pin that is more easily removed, limiting disturbance.

The friction test setup is used to study the interaction between the thrombus and the vessel wall. This is realised by slowly tilting a plate of which the angle of inclination can be determined. The actuator moves at a speed of 0.85mm/s, causing the angle of inclination to increase with 1° per second. Consequently, the angle of inclination at which the thrombus starts to slide can be determined with an accuracy of 1° as the entire experiment is recorded visually.

During this thesis, the friction test setup has been used to study the interaction between RBC thrombi and a venous surface. However, the setup's design allows for easy surface replacement. Therefore, experiments with different thrombus compositions on different venous or arterial surfaces can easily be performed. This would provide useful insight into the differences between the friction between different surfaces. To extend the comprehension of these experiments, it would be a valuable addition if both the shear and friction test setups are used to perform experiments on samples from the same donor. As a result, a more complete understanding of the thrombus-vessel wall interaction will be achieved, as data on shear properties and the static and kinetic coefficient of friction will be available.

5.2. Friction experiment

The friction experiments provided initial insight into the effect of waiting time on the interaction properties between *in vitro* created whole blood thrombi and the jugular vein retrieved from pigs. The findings suggest that an extended waiting time correlates with increased coefficients of friction, suggesting an enhancement in the connection between a thrombus and the vessel wall over time. Furthermore, among the 43 samples, 29 showed that the interaction between the thrombus and vessel wall surpasses the gravitational force of the thrombus, preventing slippage even at 90° inclination. This observation implies the potential formation of active bonds at the thrombus-vessel wall interface, potentially involving platelets, RBCs, Von Willebrand factor, NETs, fibronectin and fibrinogen [40, 41]. However, these active bonds require further investigation. An approach to study this interaction could be to use Scanning Electron Microscopy (SEM), previously used to study the interaction between thrombi and stent retrievers [42, 43]. Conducting such a study could provide a more detailed understanding of the bonds formed over time between a thrombus and the vessel wall. Integrating the findings with a more comprehensive friction study will provide useful insight in the thrombus-vessel wall interaction.

The observations that the angle of inclination reached 90° without the occurrence of any slippage were primarily done during two of the four experiments, even in instances where no waiting time was applied. As there were no differences in the protocol between all performed experiments, there are no direct actions that account for the differences observed in the experimental outcomes of the different experiments. A wide variety of factors could be of influence. For instance, the diet or stress levels of the pigs may contribute to alterations in hormonal levels, influencing blood clotting [44, 45]. Additional, even though all thrombi are created from whole blood, each pig has its own unique blood. Consequently, different components can be more or less present in the samples created per experiment, influencing the bonds formed between the thrombus and vessel wall. Therefore, a valuable contribution would be to study the thrombus composition of the samples used during the experiments. Investigating whether

variations in thrombus composition correlate with the differences observed in the results - reaching an angle of inclination of 90° or not - would provide valuable insights. Furthermore, the condition of the endothelium of the jugular veins could be of influence on the interaction between a thrombus and the vessel. Endothelial injury is one of the factors attributing to thrombus formation [46]. The presence of potential endothelial injury might impact the bonds formed between the thrombus and vessel wall, consequently influencing the interaction between both.

For the 14 samples that did slip before reaching 90° of inclination, a static coefficient of friction could be determined. A mean static coefficient of friction of 0.99 was found for the experiments performed with a 0-minute waiting time. This is slightly lower than the mean coefficient of friction of 1.38 that was found by Gunning et al. [29]. However, Gunning et al. used an arterial surface – bovine aortic tissue - whereas venous tissue was used during the experiments performed within this thesis. The tunica intima of arteries appear to have a wavier structure compared to the smooth structure found in veins [47]. This difference in surface structure could contribute to the higher coefficients of friction found by Gunning et al. [29]. It would be of great interest to conduct a comparative study in which the difference between arteries and veins is studied when it comes to the interaction with thrombi.

Besides the static coefficient of friction, the kinetic coefficient of friction was determined. The kinetic friction coefficient was lower for all samples compared to the static coefficient of friction, confirming findings done by Elkhayyat et al. [30]. A strong significant correlation was found between both characteristics, suggesting a nearly perfect linear relationship between the friction coefficients. However, it should be kept in mind that the calculated kinetic coefficient of friction is an estimation as the acceleration of the thrombus was not constant. Furthermore, the acceleration was calculated after the displacement was determined manually in ImageJ. This approach introduces inaccuracies. Future improvements of the experiments could involve the use of an accelerometer and inclinometer, to respectively determine the acceleration and angle of inclination more accurately. The observed correlation sparks interest to explore this in more detail. A more extensive study, employing a more precise methodology is warranted.

The number of platelets present in whole blood positively correlate with the percentage of clot contraction [48]. Moreover, the platelet count decreases over time in stored blood [49]. Therefore, the clot contraction is expected to be lower for thrombus analogs created from older blood. This explains the lower percentage of contraction for thrombi created for experiment 2 of the friction experiments, as blood from the previous day was used. Another interesting aspect of all thrombi created for these experiments is that they were created by first countering the effect of heparin with protamine. To the best of my knowledge, it is unknown what the effect of these substances is on the clot contraction of *in vitro* created thrombi. Previous experimental research within our research group found that the average clot contraction for whole blood samples from porcine blood is 33%. As the average for the samples used in the friction study is 56%, the heparin and protamine seem to positively influence the amount of contraction. Studies [34, 50] show that the thrombus composition, and therefore percentage of clot contraction, correlates with mechanical properties of thrombi. Therefore, the difference found in clot contraction could indicate that the heparin and protamine influence the mechanical properties of the thrombus as well by influencing the contraction. A comparative study should be executed in which the coefficient of friction of thrombi created from regular whole blood are compared to thrombi with heparin and protamine. This will give insight in whether the added substances indeed influence the mechanical properties of thrombi. Consequently, it would be of interest to determine a more optimal heparin-protamine ratio, with the goal to find a ratio that results in thrombi that mimic the properties of thrombus analogs with regular whole blood as good as possible. The findings from such a research could be used for other studies in which heparin is administered to the donor as well. Additionally, it would be an interesting improvement for the interaction experiments if the thrombus could be created directly on the endothelium of the vessels instead of placing it after formation.

5.3. Shear experiment

The shear experiments have yielded three sets of information, including the low- and high-strain shear modulus, the period of slippage, and the period of kinetic friction. These results were obtained for FBR and RBC samples. The FBR samples, created with platelet rich plasma (0% RBCs), have a significantly

higher percentage of contraction than the RBC samples created with whole blood. This trend aligns with previous research by Cahalane et al. [34], who furthermore found that the clot composition influences its mechanical properties. This correlation is further substantiated by the findings of the shear experiments.

The shear stress strain plots, from shear initiation till the moment of slippage, for both FBR and RBC samples exhibit non-linear behavior. Consequently, low- and high shear strain regions were chosen to determine shear moduli. The approach to determining these regions varied between the two sample types due to protocol differences. While the FBR samples' strain regions were defined as a percentage of the maximum strain, specific strain regions were chosen for RBC samples. This was chosen due to the lack of correlation between the applied normal force and maximum strain for the RBC samples, attributed to the tissue glue connection used during their experiments.

Riha et al. [51] observed that the shear modulus tends to increase with decreasing RBC content, a trend also observed in our shear experiments. Furthermore, Riha et al. [51] noted strain stiffening behavior, indicating increased stiffness under deformation. This behavior is commonly found in biological tissues [52]. However, a strain stiffening response was not directly observed in the FBR samples, as the high-strain shear modulus (1310Pa, SD=523Pa) was lower than the low-strain shear modulus (1713Pa, SD=897Pa). The Mann-Whitney U test indicated this difference was not statistically significant ($p=0.1835$), suggesting an approximate linear response. Prior research by Cahalane et al. [34] also observed linear behavior in thrombi under tension.

The higher contraction percentage of FBR samples is the result of a higher percentage of platelets that are shown to contribute greatly to clot contraction [48]. Platelet-rich areas contain more dense fibrin structures [53]. Fibrin's high elasticity [48] could contribute to the initial linear response in FBR samples. Furthermore, the FBR samples in this study had an average height of 1.5mm when the shear experiment was initiated. Due to the small sample height, only small strains can be reached, possibly contributing to the absence of strain hardening. Stiffening of individual fibrin fibers typically occurs at strains exceeding 110% [48]. The chosen strain range of 30-40% in this study to determine the high-strain shear modulus precedes fiber stiffening, potentially explaining the absence of observed strain stiffening behavior. This strain range was selected due to slippage initiation shortly after reaching these strains for most FBR samples. Expanding the study with FBR samples of larger dimensions could enable reaching higher strains and possibly revealing strain stiffening behavior.

In contrast, RBC thrombi did exhibit strain stiffening behavior, with a significantly higher high-strain shear modulus (382Pa, SD=184Pa) compared to the low-strain shear modulus (70Pa, SD=55Pa). This aligns with findings in literature [54]. The stiffening of RBC thrombi under shear loading can be attributed to RBCs losing their deformability under strain [55], causing the cells to harden and consequently leading to increased stiffness in the thrombus under deformation.

For both sample types, the moment of slippage is defined as the moment at which the maximum shear force is reached. In the case of FBR samples, this marks the point at which the sample completely slips, while for RBC samples, it indicates the point at which the glue connection fails entirely. Although the slippage and breaking of the glue layer initiates before the maximum shear force is reached, the moment of maximum shear force is chosen as it signifies complete slippage. This can be observed in the raw data plots where a sudden decrease in shear force occurs after reaching the maximum shear force. The period during which the slippage and breaking of the glue layer is initiated is denoted as the plateau region. It is hypothesized that during this period, the connection between the sample and the top plate slowly starts to deteriorate, although it is currently unknown how this exactly transpires. Future studies could explore this by using imaging techniques such as ultrasound. This would be especially interesting when the shear experiments are executed with samples containing a thrombus-vessel wall interface.

At the currently used strain rate of 0.5mm/s, it takes an average of 1.2s before the moment of slippage is reached for the FBR samples, whereas it takes an average of 9.5s for the RBC samples. This difference is attributed to the tissue glue connection used, creating a more secure contact between the sample and top plate. Consequently, the average maximum strain reached is approximately four times higher for the RBC samples compared to the FBR samples.

For the FBR samples, both the static and kinetic coefficient of friction could be determined for the

majority of the samples. The determination of these properties was limited for the RBC samples due to the tissue glue connection that was used in order to perform the shear experiments successfully. An average static coefficient of friction for the FBR samples, weighted by the mean normal force, was found to be 0.549 (SD_w=0.221). The weighted average kinetic coefficient of friction was determined as 0.516 (SD_w=0.151). It was opted to determine the averages as weighted averages due to the positive correlation that was found between the applied normal force and the coefficients of friction.

Similar to the results from the friction experiments, the coefficients of friction obtained from the shear experiments validate the findings of Elkhayyat et al. [30], suggesting that the static coefficient of friction is higher than the kinetic coefficient of friction. Furthermore, Gunning et al. [29] reported a static coefficient of friction for FBR clots on a PTFE-coated surface of 0.507 (SD=0.189), which is comparable to our results. It is noteworthy that the experiments performed within this thesis did not utilize PTFE, but the low-frictional material TPX. This difference could potentially influence the determined coefficients of friction. However, as both TPX and PTFE are low-friction surfaces, this influence is expected to be limited.

A strong positive correlation was found between the static and kinetic coefficients of friction for the FBR samples. This corresponds to what was found during the friction experiments, performed with RBC thrombi on a venous surface. It would be interesting to explore the correlation between the friction coefficients further as it indicates a highly predictable relationship. A larger sample size including different thrombus compositions and interaction surfaces will give valuable insight into the friction mechanics of thrombi.

A preliminary glimpse into the influence of thrombus composition can be obtained by examining the kinetic coefficient of friction in RBC samples. Due to the tissue glue connection used in the experiments, no static coefficients of friction could be determined and only two kinetic coefficient of friction. These kinetic coefficients, 0.037 and 0.051, give an estimation of what could be expected when studying the kinetic coefficient of friction of RBC samples sliding along a TPX plate. Consistent with other studies [29, 30], the friction coefficient is smaller for RBC samples compared to the FBR samples, further highlighting the impact of clot composition on mechanical properties. To validate the coefficients of friction obtained with the shear test setup, conducting additional experiments with the friction test setup under the same surface interactions would be a valuable addition.

Lastly, a computational model has been made to fit the experimental data of nine RBC samples. A good fit could be made for most samples by varying parameters of the Yeoh model. Unfortunately, attempts to run the model for the FBR samples were unsuccessful. Aside from sample-specific dimensions and material properties, no other changes were made to create a model of the FBR samples, compared to the model made for the RBC samples. Therefore, the failure to run the model effectively is likely due to the stiffer material properties of the FBR samples. The current computational model for the RBC samples demonstrates promising competence in modeling the shear response of thrombi. It would be of great interest to calibrate the model to experimental data of tension, compression, and shear tests at the same time. This will allow a more comprehensive mechanical characterization of thrombi. To this end, tensile, compressive, and shear tests on the thrombus samples created from blood from the same volunteer is required, which could be the topic of a future study. This approach would allow for a more comprehensive analysis, providing a better understanding of thrombus biomechanics.

6

Conclusion

Within the scope of this thesis, two custom-made experimental test setups have successfully been designed and implemented to study multiple biomechanical characteristics of thrombi and of the thrombus-vessel wall interaction. Both test setups have proven to be valuable in acquiring data on thrombus biomechanics. The shear test setup, used to investigate the shear behavior of thrombi, has the potential to be used for the shear characterization of the thrombus-vessel wall interaction as well. Proposed enhancements, including effective methods for mounting the vessel wall and incorporating ultrasound imaging, could further enhance the setup's capabilities.

The friction test setup, designed to explore the interaction between thrombi and vessel walls, provided valuable insights into the effect of waiting time on interaction properties. The experiments suggested a correlation between extended waiting time and increased coefficients of friction, hinting at the potential formation of active bonds at the thrombus-vessel wall interface. Further investigation, potentially using SEM, is proposed to study these active bonds in detail.

The experiments conducted with the shear test setup yielded diverse results, extending beyond the scope of merely examining shear behavior of thrombi. Besides the low- and high-strain shear moduli, insight was gathered in the moment of slippage, and on both static and kinetic frictional properties for RBC and FBR thrombi. From all obtained results, it is evident that the thrombus composition correlates with the mechanical properties.

From both the friction and shear experiments, the static and kinetic coefficient of friction could be determined. A strong significant correlation was observed between both coefficients of friction. This result requires for more extensive studies to be performed, focusing on the thrombus composition and surface interactions.

Lastly, the established computational model for RBC samples shows promise for modeling shear responses. A valuable addition would be to calibrate the model with experimental data from tension, compression and shear tests such that more complex problems can be tackled *in silico* in the future.

In conclusion, this master thesis contributes valuable insights and lays a foundation for future experimental studies on thrombus biomechanics and quantifying the thrombus-vessel wall interaction. The proposed enhancements on the current test setups and ideas for research areas provide guidelines for researchers aiming to contribute to the field of the biomechanical characterization of thrombi and the thrombus-vessel wall interaction.

References

[1] World Health Organization. *The top 10 causes of death*. Dec. 2020. URL: https://www.who.int/news-room/fact-sheets/detail/the-top-10-causes-of-death.

[2] Salim S. Virani et al. “Heart Disease and Stroke Statistics—2020 Update: A Report From the American Heart Association”. In: *Circulation* 141.9 (Mar. 2020). ISSN: 0009-7322. DOI: 10.1161/CIR.0000000000000757.

[3] Ombretta Repetto and Valli De Re. “Coagulation and fibrinolysis in gastric cancer”. In: *Annals of the New York Academy of Sciences* 1404.1 (Sept. 2017), pp. 27–48. ISSN: 00778923. DOI: 10.1111/nyas.13454.

[4] Peter. L. Gross et al. “Chapter 55: Hemostasis & Thrombosis”. In: *Harper’s Illustrated Biochemistry, 30e*. Ed. by Victor W. Rodwell et al. New York: McGraw Hill Education, 2016. Chap. 55. URL: accessmedicine.mhmedical.com/content.aspx?aid=1106060797.

[5] William E Winter, Sherri D Flax, and Neil S Harris. “Coagulation Testing in the Core Laboratory”. In: *Laboratory Medicine* 48.4 (Nov. 2017), pp. 295–313. ISSN: 0007-5027. DOI: 10.1093/labmed/lmx050.

[6] Anushree Dwivedi et al. “Measuring the effect of thrombosis, thrombus maturation and thrombolysis on clot mechanical properties in an in-vitro model”. In: *Journal of Biomechanics* 129 (Dec. 2021), p. 110731. ISSN: 00219290. DOI: 10.1016/j.jbiomech.2021.110731.

[7] Ray McCarthy et al. “Aspects of ischemic stroke biomechanics derived using ex-vivo and in-vitro methods relating to mechanical thrombectomy”. In: *Journal of Biomechanics* 131 (Jan. 2022), p. 110900. ISSN: 00219290. DOI: 10.1016/j.jbiomech.2021.110900.

[8] Precious Jolugbo and Robert A.S. Ariëns. “Thrombus Composition and Efficacy of Thrombolysis and Thrombectomy in Acute Ischemic Stroke”. In: *Stroke* 52.3 (Mar. 2021), pp. 1131–1142. ISSN: 0039-2499. DOI: 10.1161/STROKEAHA.120.032810.

[9] I Christou et al. “Arterial status after intravenous TPA therapy for ischaemic stroke. A need for further interventions”. In: *International Angiology* 20.3 (Sept. 2001), pp. 208–213.

[10] Jeffrey M Katz and Y Pierre Gobin. “Merci Retriever in acute stroke treatment”. In: *Expert Review of Medical Devices* 3.3 (May 2006), pp. 273–280. ISSN: 1743-4440. DOI: 10.1586/17434440.3.3.273.

[11] Anna Luisa Kühn et al. “Biomechanics and hemodynamics of stent-retrievers”. In: *Journal of Cerebral Blood Flow & Metabolism* 40.12 (Mar. 2020), pp. 2350–2365.

[12] Albert J. Yoo and Tommy Andersson. “Thrombectomy in Acute Ischemic Stroke: Challenges to Procedural Success”. In: *Journal of Stroke* 19.2 (May 2017), pp. 121–130. ISSN: 2287-6391. DOI: 10.5853/jos.2017.00752.

[13] Nihat Sengeze and Semih Gıray. “Does the Stent Retriever Placement in the Division of Middle Cerebral Artery Affect the Recanalization Success in M1 Occlusions?” In: *Eurasian Journal of Medicine* 54.1 (2022). ISSN: 13088742. DOI: 10.5152/eurasianjmed.2022.20281.

[14] Ho Jun Yi, Dong Hoon Lee, and Jae Hoon Sung. “Clinical Usefulness of Waiting after Stent Deployment in Mechanical Thrombectomy: Effect of the Clot Integration”. In: *World Neurosurgery* 119 (Nov. 2018), e87–e93. ISSN: 18788750. DOI: 10.1016/j.wneu.2018.07.040.

[15] Kajo van der Marel et al. “Quantitative assessment of device–clot interaction for stent retriever thrombectomy”. In: *Journal of NeuroInterventional Surgery* 8.12 (Dec. 2016), pp. 1278–1282. ISSN: 1759-8478. DOI: 10.1136/neurintsurg-2015-012209.

[16] Diogo C. Haussen, Leticia C. Rebello, and Raul G. Nogueira. “Optimizating Clot Retrieval in Acute Stroke”. In: *Stroke* 46.10 (Oct. 2015), pp. 2838–2842. ISSN: 0039-2499. DOI: 10.1161/STROKEAHA.115.010044.

[17] Sebastien Soize et al. “Fast Stent Retrieval Improves Recanalization Rates of Thrombectomy: Experimental Study on Different Thrombi”. In: *American Journal of Neuroradiology* 41.6 (June 2020), pp. 1049–1053. ISSN: 0195-6108. DOI: 10.3174/ajnr.A6559.

[18] Frank Lally et al. “In vitro experiments of cerebral blood flow during aspiration thrombectomy: potential effects on cerebral perfusion pressure and collateral flow”. In: *Journal of NeuroInterventional Surgery* 8.9 (Sept. 2016), pp. 969–972. ISSN: 1759-8478. DOI: 10.1136/neurintsurg-2015-011909.

[19] Yubing Shi et al. “Suction force-suction distance relation during aspiration thrombectomy for ischemic stroke: A computational fluid dynamics study”. In: *Physics in Medicine* 3 (June 2017), pp. 1–8. ISSN: 23524510. DOI: 10.1016/j.phmed.2016.11.001.

[20] Cyril Chivot et al. “Direct aspiration for thrombectomy in ischemic stroke: Impact of dwell time”. In: *Interventional Neuroradiology* 26.2 (Apr. 2020), pp. 211–215. ISSN: 1591-0199. DOI: 10.1177/1591019919886410.

[21] Gianmarco Bernava et al. “Experimental evaluation of direct thromboaspiration efficacy according to the angle of interaction between the aspiration catheter and the clot”. In: *Journal of NeuroInterventional Surgery* 13.12 (Dec. 2021), pp. 1152–1156. ISSN: 1759-8478. DOI: 10.1136/neurintsurg-2020-016889.

[22] Scott Simon et al. “Exploring the efficacy of cyclic vs static aspiration in a cerebral thrombectomy model: an initial proof of concept study”. In: *Journal of NeuroInterventional Surgery* 6.9 (Nov. 2014), pp. 677–683. ISSN: 1759-8478. DOI: 10.1136/neurintsurg-2013-010941.

[23] Vladimir Kalousek et al. “Cyclical aspiration using a novel mechanical thrombectomy device is associated with a high TICI 3 first pass effect in large□vessel strokes”. In: *Journal of Neuroimaging* 31.5 (Sept. 2021), pp. 912–924. ISSN: 1051-2284. DOI: 10.1111/jon.12889.

[24] Bryan C. Good et al. “Development of a computational model for acute ischemic stroke recanalization through cyclic aspiration”. In: *Biomechanics and Modeling in Mechanobiology* 19.2 (Apr. 2020), pp. 761–778. ISSN: 1617-7959. DOI: 10.1007/s10237-019-01247-w.

[25] Jiahui Li et al. “Impact of stent-retriever tip design on distal embolization during mechanical thrombectomy: a randomized in vitro evaluation”. In: *Journal of NeuroInterventional Surgery* (May 2023), pp. 2023–020382. ISSN: 1759-8478. DOI: 10.1136/jnis-2023-020382.

[26] Naoki Kaneko et al. “Stent retrievers with segmented design improve the efficacy of thrombectomy in tortuous vessels”. In: *Journal of NeuroInterventional Surgery* 11.2 (Feb. 2019), pp. 119–122. ISSN: 1759-8478. DOI: 10.1136/neurintsurg-2018-014061.

[27] Carmen Serna Candel et al. “First-Pass Reperfusion by Mechanical Thrombectomy in Acute M1 Occlusion: The Size of Retriever Matters”. In: *Frontiers in Neurology* 12 (2021). ISSN: 16642295. DOI: 10.3389/fneur.2021.679402.

[28] Rose A. Arslanian et al. “Complete clot ingestion with cyclical ADAPT increases first-pass recanalization and reduces distal embolization”. In: *Journal of NeuroInterventional Surgery* 11.9 (2019). ISSN: 17598486. DOI: 10.1136/neurintsurg-2018-014625.

[29] Gillian M Gunning et al. “Clot friction variation with fibrin content; implications for resistance to thrombectomy”. In: *Journal of NeuroInterventional Surgery* 10.1 (Jan. 2018), pp. 34–38. ISSN: 1759-8478. DOI: 10.1136/neurintsurg-2016-012721.

[30] Omar Elkhayyat and Bryan C. Good. *Analysis of frictional forces during blood clot removal in experimental models of acute ischemic stroke*. Poster presentation at *SB3C*, Colorado, USA. 2023.

[31] Ghadir Alkarithi et al. “Thrombus Structural Composition in Cardiovascular Disease”. In: *Arteriosclerosis, Thrombosis, and Vascular Biology* 41.9 (Sept. 2021), pp. 2370–2383. ISSN: 1079-5642. DOI: 10.1161/ATVBAHA.120.315754.

[32] Senna Staessens et al. “Structural analysis of ischemic stroke thrombi: histological indications for therapy resistance”. In: *Haematologica* 105.2 (Feb. 2020), pp. 498–507. ISSN: 0390-6078. DOI: 10.3324/haematol.2019.219881.

[33] Hajo Hund et al. “Quantitative thrombus characteristics on thin-slice computed tomography improve prediction of thrombus histopathology: results of the MR CLEAN Registry”. In: *European Radiology* 32.11 (Apr. 2022), pp. 7811–7823. ISSN: 1432-1084. DOI: 10.1007/s00330-022-08762-y.

[34] Rachel M. E. Cahalane et al. “Tensile and Compressive Mechanical Behaviour of Human Blood Clot Analogues”. In: *Annals of Biomedical Engineering* 51.8 (Aug. 2023), pp. 1759–1768. ISSN: 0090-6964. DOI: 10.1007/s10439-023-03181-6.

[35] J. Y. Chueh et al. “Mechanical characterization of thromboemboli in acute ischemic stroke and laboratory embolus analogs”. In: *American Journal of Neuroradiology* 32.7 (2011). ISSN: 01956108. DOI: 10.3174/ajnr.A2485.

[36] John H. Ashton et al. “Compressive mechanical properties of the intraluminal thrombus in abdominal aortic aneurysms and fibrin-based thrombus mimics”. In: *Journal of Biomechanics* 42.3 (2009). ISSN: 00219290. DOI: 10.1016/j.jbiomech.2008.10.024.

[37] M. Destrade, J. G. Murphy, and G. Saccomandi. “Simple shear is not so simple”. In: *International Journal of Non-Linear Mechanics* 47.2 (2012). ISSN: 00207462. DOI: 10.1016/j.ijnonlinmec.2011.05.008.

[38] Jiahui Li et al. “Catheter tip distensibility substantially influences the aspiration force of thrombectomy devices”. In: *Journal of NeuroInterventional Surgery* (Apr. 2021), pp. 2021–017487. ISSN: 1759-8478. DOI: 10.1136/neurintsurg-2021-017487.

[39] Ernest L. Madsen, Meagan E. Deaner, and James Mehi. “Properties of Phantom Tissuelike Polymethylpentene in the Frequency Range 20-70 MHZ”. In: *Ultrasound in Medicine and Biology* 37.8 (2011). ISSN: 03015629. DOI: 10.1016/j.ultrasmedbio.2011.05.023.

[40] Jessica Lin et al. “Physical forces regulating hemostasis and thrombosis: Vessels, cells, and molecules in illustrated review”. In: *Research and Practice in Thrombosis and Haemostasis* 5.5 (July 2021), e12548. ISSN: 24750379. DOI: 10.1002/rth2.12548.

[41] Christopher O. Audu et al. “Inflammatory biomarkers in deep venous thrombosis organization, resolution, and post-thrombotic syndrome”. In: *Journal of Vascular Surgery: Venous and Lymphatic Disorders* 8.2 (2020). ISSN: 22133348. DOI: 10.1016/j.jvsv.2019.09.008.

[42] Anouchska S. A. Autar et al. “High-Resolution Imaging of Interaction Between Thrombus and Stent-Retriever in Patients With Acute Ischemic Stroke”. In: *Journal of the American Heart Association* 7.13 (July 2018). ISSN: 2047-9980. DOI: 10.1161/JAHA.118.008563.

[43] Daniela Dumitriu LaGrange et al. “A high resolution scanning electron microscopy analysis of intracranial thrombi embedded along the stent retrievers”. In: *Scientific Reports* 12.1 (May 2022), p. 8027. ISSN: 2045-2322. DOI: 10.1038/s41598-022-11830-4.

[44] K. C. Chan, P. P. Lou, and J. L. Hargrove. “High casein-lactalbumin diet accelerates blood coagulation in rats”. In: *Journal of Nutrition* 123.6 (1993). ISSN: 00223166.

[45] Petra H. Wirtz et al. “The role of stress hormones in the relationship between resting blood pressure and coagulation activity”. In: *Journal of Hypertension* 24.12 (2006). ISSN: 02636352. DOI: 10.1097/HJH.0b013e32801098e5.

[46] Abigail Kushner et al. *Virchow Triad*. Treasure Island (FL): StatPearls Publishing, Jan. 2022. URL: https://www.ncbi.nlm.nih.gov/books/NBK539697/.

[47] Elaine Nicpon Marieb and Katja Hoehn. *Human anatomy & physiology*. 10th ed. Pearson Education Limited, 2016.

[48] Rustem I. Litvinov and John W. Weisel. “Blood clot contraction: Mechanisms, pathophysiology, and disease”. In: *Research and Practice in Thrombosis and Haemostasis* 7.1 (2023). ISSN: 24750379. DOI: 10.1016/j.rpth.2022.100023.

[49] Ryan J. Keneally et al. “In Vitro Analysis of Platelet Adhesion, Aggregation, and Surface GP1bα Expression in Stored Refrigerated Whole Blood: A Pilot Study”. In: *Anesthesia & Analgesia* 136.5 (May 2023), pp. 920–926. ISSN: 0003-2999. DOI: 10.1213/ANE.0000000000006277.

[50] Nikki Boodt et al. “Mechanical Characterization of Thrombi Retrieved With Endovascular Thrombectomy in Patients With Acute Ischemic Stroke”. In: *Stroke* 52.8 (Aug. 2021), pp. 2510–2517. ISSN: 0039-2499. DOI: 10.1161/STROKEAHA.120.033527.

[51] P. Riha et al. “Elasticity and fracture strain of whole blood clots”. In: *Clinical Hemorheology and Microcirculation* 21 (Mar. 199), pp. 45–49.

[52] R. Q. Erkamp et al. “Exploiting strain-hardening of tissue to increase contrast in elasticity imaging”. In: *Proceedings of the IEEE Ultrasonics Symposium*. Vol. 2. 2000. DOI: 10.1109/ULTSYM.2000.921680.

[53] Rui Gang Xu and Robert A.S. Ariëns. *Insights into the composition of stroke thrombi: Heterogeneity and distinct clot areas impact treatment*. 2020. DOI: 10.3324/haematol.2019.238816.

[54] Gabriella P. Sugerman et al. “A Whole Blood Thrombus Mimic: Constitutive Behavior Under Simple Shear”. In: *Journal of the Mechanical Behavior of Biomedical Materials* (July 2020). DOI: 10.1101/2020.07.19.210732.

[55] Sung S. Lee et al. “Strain Hardening of Red Blood Cells by Accumulated Cyclic Supraphysiological Stress”. In: *Artificial Organs* 31.1 (Jan. 2007), pp. 80–86. ISSN: 0160-564X. DOI: 10.1111/j.1525-1594.2007.00344.x.

[56] Laken B. Warnock and Davis Huang. *Heparin*. Treasure Island (FL): StatPearls Publishing, Jan. 2023.

[57] D. Smittarello et al. “Characterizing the physical properties of gelatin, a classic analog for the brittle elastic crust, insight from numerical modeling”. In: *Tectonophysics* 812 (Aug. 2021), p. 228901. ISSN: 00401951. DOI: 10.1016/j.tecto.2021.228901.

[58] Andrew D. Doyle and Juliet Lee. “Simultaneous, Real-Time Imaging of Intracellular Calcium and Cellular Traction Force Production”. In: *BioTechniques* 33.2 (Aug. 2002), pp. 358–364. ISSN: 0736-6205. DOI: 10.2144/02332rr02.

A

Protocols

A.1. Protocol: Shear experiment

Performing shear experiments with the shear tester requires careful handling in order to avoid disturbances that could affect the load cell readouts. The test setup is very sensitive, and any interruptions, such as bumping against the table or turning on the tap, should be avoided during the experiment.

It is important to note that there is a difference between the protocol for performing shear experiments with RBC samples and FBR samples. If a step is sample specific, this is denoted by placing *RBC* or *FBR* in front of the step.

A.1.1. Required equipment

- Thrombus samples from the incubator
- Absorbent pad
- Thin tweezers
- Weighing scale
- Ruler
- Shear test setup
- Ruler attached to the shear setup
- Laptop with the right MEXE02 and LabVIEW files
- Camera (with additional memory card)
- Set of hex keys
- Tissue
- Fill-in sheet
- *RBC:* Tissue glue (histoacryl) and acetone

A.1.2. Prepare experimental setup

Hardware

1. Connect the components of the shear setup to the baseplate:
   (a) Screw the shear load section into place.
   (b) Place the normal load section on the shear load section. Lock the normal load section at the top.
   (c) Place the waterbath into position on the baseplate.
   (d) Connect the bridge to the actuator.
2. Check whether the setup is leveled. If not, adjust the set screws of the baseplate to level the tester.
3. Plug in the shear tester and laptop. Connect the USB cables to the laptop.
4. Make sure the micro-USB cable is connected to the actuator driver.

Operation data

	Name	Operation type	Position [mm]	Operating speed [mm/s]
#0	initial position	Absolute positioning	63.00	1.00
#1	test	Absolute positioning	42.00	0.50

Figure A.1: Operation data window of MEXE02 to drive the actuator during the shear experiment.

MEXE02

1. Open the MEXE02 file: shear_lab.mx2c
2. Check whether the values correspond to the values shown in figure A.1.
3. Write the file to the actuator driver.
4. In MEXE02, open the 'Remote teaching operation'.
5. Perform operation 0 and 1, respectively initial position and testing, to see whether the sample holder runs smoothly over the bottom of the waterbath. Pay attention to any weird noises. Noise might indicate that the bridge is screwed down to tight, causing the sample holder to scrape along the bottom of the waterbath.
6. Close the remote teaching operation.

LabVIEW

1. Create empty .txt files for all samples that will be tested.
2. Open the LabVIEW file: shear_experiment.exe (Folders: Sanne > shear)
3. Make sure the maximum value of the shear and normal load cell is set to 0.5N.
4. Set the interval of the loop to 40ms.
5. Test the 'Initial position' and 'Start testing' buttons.
6. Remove the lock from the normal load cell and press the tare button. Check whether the load cell reads out by gently pressing against the bottom of the top plate.
7. Move the normal load cell section down along the rod.
8. Remove the lock from the shear load cell and press the tare button. Check whether the load cell reads out by gently pressing against the normal load cell section in the direction of the actuator.
9. Lock both load cells again.

Camera setup

1. Make sure the camera has enough battery and memory.
2. Use glass petri dishes to level the camera to the right height such that the ruler reference and entire window is visualized clearly.

A.1.3. Sample preparation

1. Weigh the sample while still within the mold.
2. Remove the mold from the bottom plate.
   (a) Gently move the tweezers around the edges within the mold.
   (b) Untighten the screws.
   (c) Remove the mold from the bottom plate.
3. Weigh the sample while attached to the bottom plate.
4. Photograph the sample from the top with a ruler placed within the picture.

A.1.4. Start testing

The following steps must be completed per sample, before moving onto the next. In this section, x is a variable for the normal force that is applied during each experiment.

1. Make sure the normal load section is located high on the rod such that there is enough room for sample placement.

2. Place the bottom plate with thrombus within the sample holder. Make sure the magnets are connected.
3. In LabVIEW, press the 'Initial position' button.
4. Open the correct file to write the data to.
5. Unlock the normal load cell and tare it.
6. *RBC:* Apply some histoacryl to the top plate section that will come into contact with the sample. Take care that the maximum load of 0.5N will not be exceeded while applying the glue.
7. With the rough displacer, move the normal load section down such that it does not touch the thrombus sample yet.
8. Tare the normal load cell again.
9. With the micrometer displacer, lower the normal load cell until it touches the sample.
   (a) Photograph the micrometer displacement.
   (b) In LabVIEW, press 'Start recording'.
   (c) Start recording with the camera.
10. With the micrometer displacer, lower the normal load cell until it measures a force of *x* N.
    (a) Start the timer.
    (b) Photograph the micrometer displacement.
    (c) *RBC:* When the timer reaches 200s, go to the next step.
    FBR: When the timer reaches 100s, go to the next step.
11. With the micrometer displacer, lower the normal load cell until it measures a force of *x* N.
    (a) Start the timer.
    (b) Photograph the micrometer displacement.
    (c) Unlock the shear load cell and tare it.
    (d) *RBC:* When the timer reaches 100s, go to the next step.
    FBR: When the timer reaches 50s, go to the next step.
12. In LabVIEW, press the 'Start test' button.
13. Keep a close eye on the sample. If anything extraordinary occurs, select the 'Stop movement' button in LabVIEW.
14. Once the shear tester has stopped operating:
    (a) Unpress 'Start test'.
    (b) Unpress 'Start recording'.
    (c) Stop the camera from recording.
    (d) Lock the shear load cell.
    (e) Use the micrometer displacer to move the normal load section such that it does not touch the sample anymore.
    (f) Use the rough displacer to move the normal load section to the top of the rod.
15. Remove the sample with the bottom plate from the shear tester.
16. If there is any fluid or other residue present on the top plate, clean this gently. Make sure to lock the normal load cell when more than 0.5N force is required to clean the top plate.
    RBC: Due to the histoacryl connection more residue will be left on the top plate. This can be removed with acetone. In order to do so, the top plate has to be taken of the normal load section. Make sure the normal load cell is locked before the top plate is taken off.
17. Remove the thrombus (including Velcro) from the bottom plate.
18. Remove the fluids from the bottom plate.
19. Weight the plate and fill in the data sheet.

A.1.5. End of testing

1. Make sure both load cells are locked.
2. Unscrew the bridge from the actuator and remove the waterbath from the baseplate.
3. Plug everything out.
4. Clean everything and throw away disposable items.
5. Transfer all collected data (videos and .txt files) to an USB stick.

A.2. Protocol: Friction experiment

A.2.1. Required equipment

- Thrombus samples from the incubator
- Vein in HEPES buffer
- Absorbent pad
- Large petri dish
- ± 20 insect pins
- 4x12cm foamboard
- 2x thin tweezers
- Surgical scissors
- Doublesided spoon
- HEPES buffer
- Plastic pipet
- Weighing scale
- Ruler
- Friction setup
- Clamp
- 2x counterweight
- Ruler attached to the friction setup
- Laptop with the right LabVIEW and MEXE02 files
- Camera with tripod (with additional memory card)
- Sticky notes and a marker
- Fill-in sheet

A.2.2. Prepare experimental setup

1. Make sure the camera has enough battery and memory to record all experiments (at least two minutes per experiment). Have an additional (empty) memory card close by.
2. Remove the components of the shear test setup (red shaped parts in Fig. A.2) from the baseplate such that only the actuator remains connected to the plate.
3. Clamp the friction setup into place.
4. Place the piece of foamboard within the notch of the plate of the friction setup. Make sure the foamboard does not slide when the angle of the plate increases.
5. Connect the counterweights to the friction setup and connect the rope from the friction setup to the actuator (Fig. A.3).
6. Plug in the tester to turn it on (hear a 'click' sound).
7. Open the friction_lab.mx2c file in MEXE02. Check that the values in the operation data tab correspond to the values in figure A.4.
8. Write the data to the motor driver (select the button: 'Data writing' or press Ctrl+W).
9. Use the 'Test operation' window within MEXE02 to check whether the given positions allow the plate to move over its entire range.
   (a) If right, continue to the next step.
   (b) If not, alter the position values within the friction_lab.mx2c file such that the entire range is reached and write the data to the motor driver.
10. Place a piece of kneaded eraser on top of the foamboard. The piece should have approximately the same height as the thrombus sample that will be placed later.
11. Alter the position of the camera such that the kneaded eraser is visualized during an entire experimental run by letting the plate move to 90°.
12. Open the friction.exe file in LabVIEW.
13. Press the white arrow in LabVIEW to start the programme.
14. Select the button 'Initial position'.

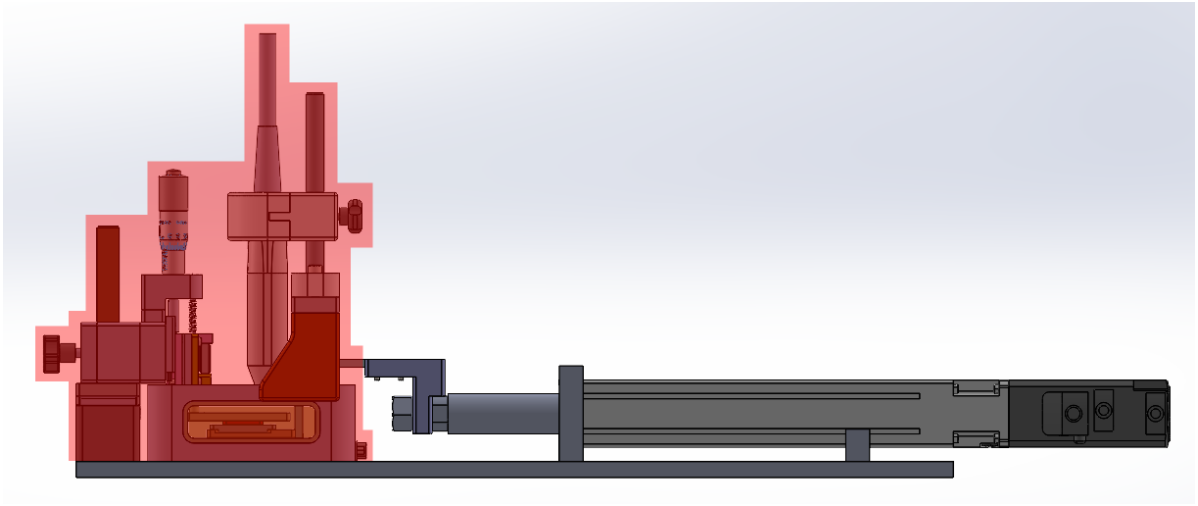

Figure A.2: The red shaded shear test setup parts need to be removed in order to install the friction test setup.

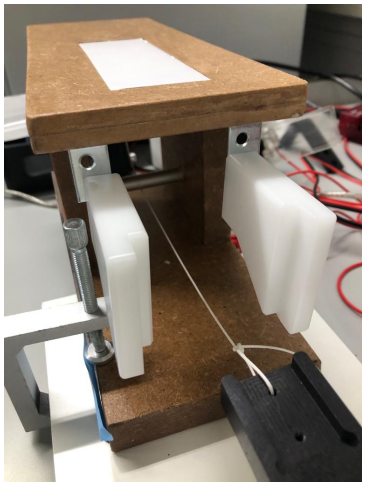

Figure A.3: Friction test setup showing how the rope is connected to the actuator and where the counterweights are placed.

Operation data

	Name	Operation type	Position [mm]	Operating speed [mm/s]
#0	initial position	Absolute positioning	105.00	5.00
#1	start testing	Absolute positioning	23.00	0.85

Figure A.4: Operation data window of MEXE02 to drive the actuator during the friction experiment.

A.2.3. Sample preparation

Vein placement

Start to prepare the vein approximately 10 minutes before the thrombus can be removed from the incubator.

1. Remove excess tissue around the vein as much as possible.
2. Cut the vein open longitudinally.
3. Pin the vein down with insect pins on the foamboard. Start with the corners and continue by placing some pins at the sides of the vein as well.

    (a) Only pin the vein down once the thrombi are taken from the incubator.

Thrombus placement

1. Remove the thrombus from the mold.

    (a) Gently move the tweezers around the edges within the mold.
    (b) Untighten the screws.
    (c) Remove the mold from the baseplate.

2. Pick up the thrombus with the spoon.
3. Remove any latent moisture by gently pressing an absorbent tissue against the edges of the thrombus.
4. Weigh the thrombus and note down the weight on the fill-in sheet.
5. Place a small ruler next to the thrombus and photograph from above.
6. Place the thrombus on the vein.
7. Start the timer.

    (a) The amount of waiting time that needs to be applied is dependent on the experimental schedule. The waiting time will be either 0, 3 or 5 minutes.

A.2.4. Start testing

1. Place a note with the sample number within the imaging frame.
2. Click record on the camera.
3. In the LabVIEW file, press the ‘Start test’ button once the timer goes off.
4. Keep a close eye on the sample. Once it starts to slide, press the ‘Stop movement’ button.
5. Stop the camera from recording once the sample stopped sliding.
6. Move the actuator back to its initial position by pressing the ‘Initial position’ button in LabVIEW.
7. Remove the thrombus from the vein with tweezers, without touching the vein.
8. Hydrate the vein with some HEPES.
9. Check whether the plate is completely horizontal again. If so, continue the experiment by placing the next thrombus on top of the vein by repeating the protocol from step A.2.3 (Thrombus placement) onward.

A.2.5. End of testing

1. Collect the videos from the camera.
2. Clean everything.
3. Replace the piece of foamboard in the top plate.

A.3. Protocol: Thrombus creation

This protocol describes the steps that need to be taken to create thrombus analogs for *in vitro* tests. There are slight differences between the thrombi used for the friction and shear experiments, which are mentioned within the protocol. All blood drawn must be collected in 4.5mL citrated tubes to prevent immediate coagulation of the blood.

A.3.1. Required equipment

The amount (#) that is required is dependent on the amount of samples that need to be made. A maximum of six samples can be made during one session as currently six molds are available.

- Absorbent pad
- #x rectangular molds
- #x Velcro pieces
- #x large glass petri dishes
- Pipettes (1000µL - blue, 200µL - red, 100µL - green, 20µL - yellow)
- Pipette tips (check stocks – rerack if needed)
- Ice in the ice box
- Thrombin aliquots
- $CaCl_2$ stock vial
- Pink rack
- # vials to create samples in
- Disposal beaker
- Thin tweezers
- Scale
- HEPES buffer
- Plastic dropper or syringe
- Alcohol resistant marker (“KP marker plus”)
- Falcon tubes

A.3.2. mold preparation

1. Place the Teflon mold on top of the bottom plate and screw down tightly such that leakage will not occur. Pay attention that the screws are not tightened too much, as this will deform the Teflon mold (Fig. A.5).
2. Weigh the empty (completed) mold and fill in the data sheet.
3. Follow the next step only if samples for shear experiments are created:
   (a) Use tweezers to place a piece of Velcro on the bottom of the mold. Make sure to press it down across the entire area.
   (b) Weigh the mold and fill in the data sheet.
4. Place the molds into the large glass petri dishes.

A.3.3. Sample creation

Different steps need to be taken, depending on the type of sample to be created. When both RBC and FBR samples need to be made from the same batch of blood, it is important that first the right amount of whole blood is set aside for the RBC thrombi. This is required as the blood needs to be centrifuged to generate FBR thrombi. In the section below, the steps for three thrombus types can be found: RBC and FBR thrombi created from regular whole blood, and RBC thrombi created from whole blood with heparin.

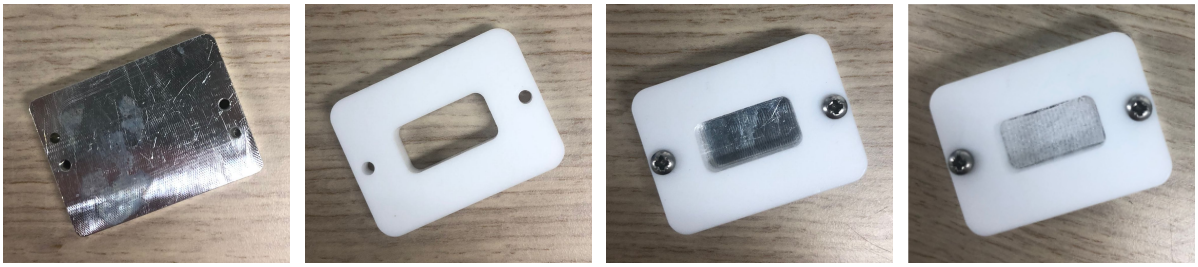

(a) Bottom plate **(b)** Teflon mold **(c)** Assembled mold **(d)** Assembled mold with Velcro

Figure A.5: Components of the custom-made thrombus mold shown (a, b) separately and (c, d) assembled.

Whole blood thrombi (RBC-rich)

1. Invert the blood blood tube four times before use.
2. Follow the following steps for each sample you want to create:
   (a) Add 1164µL of whole blood to the sample vial.
   (b) Add 24µL of $CaCl_2$ to the sample vial below the level of the liquid. Pre-mix the solution by pipetting multiple times. Make sure nothing is left in the tip when you discard.
   (c) Prepare a 1000µL pipette and have the mold ready in close proximity.
   (d) Add 12µL of thrombin to the sample vial below the level of the liquid.
   (e) The next step should only be performed for samples created from blood that contains heparin. If not, step 2f should be performed immediately after adding thrombin to the sample vial.
      i. Add 20µL of protamine to the sample vial below the level of the liquid. Pre-mix the solution by pipetting multiple times. Make sure nothing is left in the tip when you discard.
   (f) Immediately mix the solution one time with the 1000µL pipette and transfer the entire solution to the mold by going to the second stop of the pipette.
   (g) If there are any bubbles, try to remove them.
   (h) Weigh the full mold and fill in the data sheet.
   (i) Substitute some HEPES buffer in the glass petri dish besides the full mold. Make sure there is enough HEPES buffer in the petri dish such that it will not completely evaporate during incubation.
3. Incubate the samples for one hour in lab Ee2316.
4. Start setting up the friction or shear experiment while the samples are maturing.

Fibrin-rich thrombi (0% RBCs)

1. Invert the whole blood tube four times before use.
2. Transfer the whole citrated blood to falcon tubes for the centrifuge. The division of blood should be equal in all tubes for the balance within the centrifuge.
3. Place the falcon tubes symmetrically within the centrifuge in lab Ee2373.
4. Centrifuge the whole blood at 120g for 20 minutes (acceleration 5, brake 5) at RT.
5. Take of the platelet-rich plasma (do not include any RBCs!).
6. Follow the following steps for each sample you want to create:
   (a) Add 1164µL of platelet-rich plasma to the sample vial.
   (b) Add 24µL of $CaCl_2$ to the sample vial below the level of the liquid. Pre-mix the solution by pipetting multiple times. Make sure nothing is left in the tip when you discard.
   (c) Prepare a 1000µL pipette and have the mold ready in close proximity.
   (d) Add 12µL of thrombin to the sample vial below the level of the liquid.
   (e) Immediately mix the solution one time with the 1000µL pipette and transfer the entire solution to the mold by going to the second stop on the pipette.
   (f) If there are any bubbles, try to remove them.
   (g) Weigh the full mold and fill in the data sheet.

(h) Substitute some HEPES buffer in the glass petri dish besides the full mold. Make sure there is enough HEPES buffer in the petri dish such that it will not completely evaporate during incubation.

7. Incubate the samples for one hour in lab Ee2316.
8. Start setting up the friction or shear experiment while the samples are maturing.

A.4. Protocol: Load cell (re)calibration

Both the normal and shear load cell need to be calibrated before being used in the test setup. The calibration of the load cells is done with the USB SpeedLink programme. Hereafter, the calibration is checked by placing high precision weights on the load cell.

A.4.1. Connecting the load cell

The way in which the load cell wires are connected is dependent on how the load cell will be loaded. If loaded under tension, the output is positive, whereas compression loading results in a negative output (Fig. A.6a). To ensure a positive readout under both tension and compression, it is necessary to position the green and white signal wires in opposite orientations when connecting them. In the shear test setup, the shear load cell undergoes tension loading, and the normal load cell experiences compression loading. Figure A.6c illustrates the wiring configurations for both load cell applications.

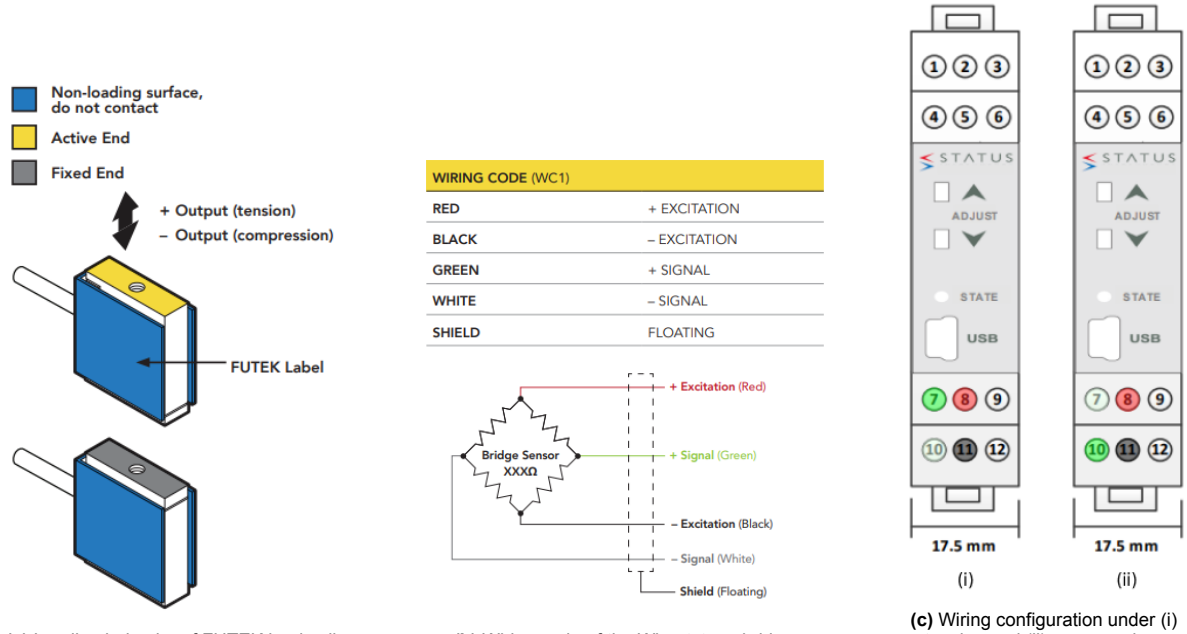

(a) Loading behavior of FUTEK load cell.

(b) Wiring code of the Wheatstone bridge.

(c) Wiring configuration under (i) tension and (ii) compression.

Figure A.6: Information about the FUTEK load cell used to collect the shear force and the normal force during the shear experiments.

A.4.2. Calibrating the load cells

Only one load cell at the time can be calibrated, therefore, the steps underneath should be executed for both load cells separately. The load cell that is not getting calibrated should be locked.

1. Switch the micro-USB wire from the actuator driver to the load cell conditioner corresponding to the load cell that is going to get calibrated.
2. Open USB SpeedLink and click the ‘Quick Connect’ button.
3. Load the calibration files twice: calibration_SLC.xml and calibration_NLC.xml for the shear and normal load cell respectively. *
4. Check whether the values for the load cells correspond to the values shown in figures A.7a and A.7b, for the shear and normal load cell respectively.
5. Send the values to the device by clicking the ’Send to device’ button twice.
6. Close USB SpeedLink.
7. Switch the micro-USB wire back to the actuator driver in order to be able to start testing.

* Each load cell contains a data sheet with the corresponding calibration values delivered by the manufacturer. In principle, these values should be used to calibrate the load cell. It is important to keep

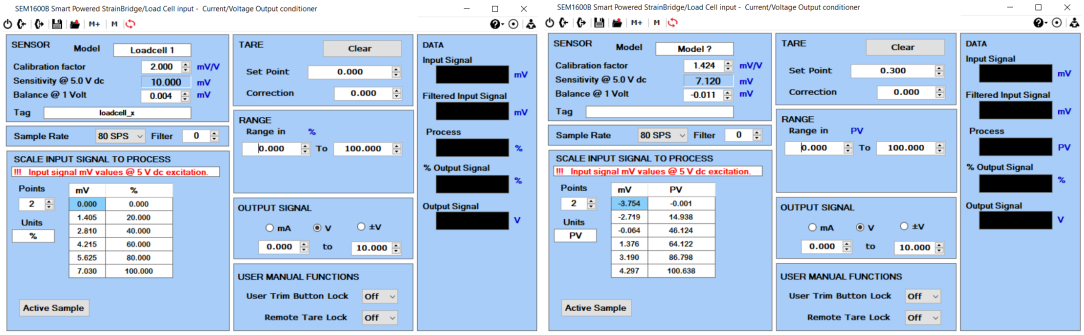

(a) Calibration values for the SLC. **(b)** Calibration values for the NLC.

Figure A.7: Screenshots of USB Speedlink showing the setup for both load cells.

in mind that the given values should be multiplied by 5 before being substituted in USB SpeedLink as the values given on the datasheet are the calibration values at 1 Volt excitation, and the calibration is performed at 5 Volt excitation. However, as the delivered values did not lead to sufficient calibration for the normal load cell, new calibration values were found. How this calibration was performed is described in the 'Load cell recalibration' section. The values shown in figure A.7 are thus the calibration values after the load cell has been recalibrated.

A.4.3. Validating the calibration

The calibration check principle remains consistent for both load cells in the shear test setup. However, the procedure for conducting this check varies slightly. Any distinctions will be indicated by referring to either the shear load cell (*SLC*) or the normal load cell (*NLC*) in the subsequent steps.

1. *SLC:* Get the weigh attachment and screw into position on the actuator holder (Fig. A.8a).
   NLC: Place the small scale underneath the top plate. Try to position it as such that the load cell is centered on the scale as much as possible (Fig. A.8b).
2. *SLC:* Take the calibrated weights from the shelf.
3. Make sure the micro-USB wire is plugged into the actuator driver.
4. Open the LabVIEW file: shear_experiment.exe
5. Change the maximum value of the load cell to 0.5N.
6. Click run.
7. Tare the load cell by pressing the tare button.
8. Check that the load cell actually measures 0N (when no weight is attached). If not, tare the load cell again.
9. *SLC:* Hang weights off the load cell by placing the wire attached to the weight around the micrometer displacer.
   NLC: Use the micrometer displacer to apply pressure on top of the scale.
10. Check whether the load cell gives the expected values. Do this for multiple weights/pressures.

Weight (g)	Output (N)
0	0
5	0.05
10	0.1
20	0.2
50	0.5

Table A.1: Required load cell readout

11. If the calibration did not work, repeat the steps again. If the calibration still did not succeed afterward, recalibrate the load cell.

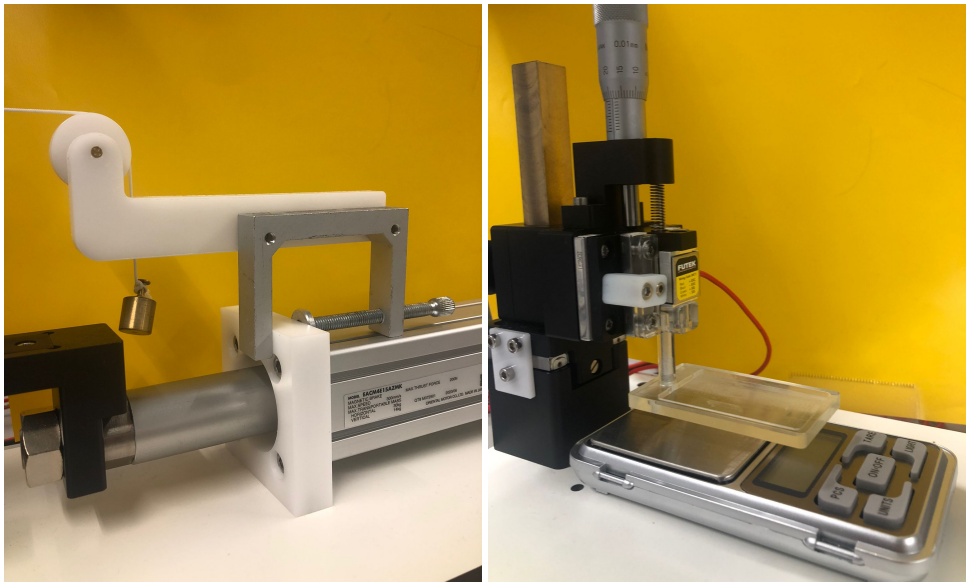

(a) (b)

Figure A.8: The calibration setups for calibration of the (a) shear load cell and the (b) normal load cell.

A.4.4. Load cell recalibration

When the load cell readout is too divergent from what it is supposed to be, the load cell should get recalibrated. The recalibration should be done whilst the load cell is located inside the test setup, as the dead weight on the load cell will influence the calibration values.

In order to calibrate the load cell, the setup used to check the calibration is required, as well as a multimeter. The following steps are general for the recalibration of both the shear and normal load cell. The difference between the two is the way the weight is applied on the load cell, which is similar to the way in which this is done when the calibration is validated (Section A.4.3).

1. Switch the micro-USB wire from the actuator driver to the load cell conditioner corresponding to the load cell that is going to get recalibrated.
2. Open USB SpeedLink and click the ‘Quick Connect’ button.
3. Change the ‘Calibration factor’ to the ’Output Value’ from the datasheet delivered with the load cell.
4. Change the ‘Balance @ 1 Volt’ value to the ’Zero Balance’ from the datasheet delivered with the load cell.
5. Check that the ‘Sample rate’, ‘Range’, ‘Output Signal’, and ‘User Manual Functions’ correspond to the values in figure A.7.
6. Make sure that there are six points in the ‘Scale input signal to process’ box.
7. Set the multimeter to 10V and stick the black and red probe into contacts 5 and 6 of the load cell conditioner, respectively.
8. In the table shown in USB SpeedLink, select the first box in the ’mV’ column at PV = 0.000.
9. Tare the load cell.
10. Click the ’Active Sample’ button and accept the data.
11. Note down the ‘Process’ value given in the ‘Data’ box.
12. In the table, select the second ‘mV’ box at PV = 0.000.
13. Tare the load cell.
14. Place a weight on the load cell.
15. Click the ’Active Sample’ button and accept the data.
16. Note down the ‘Process’ value given in the ‘Data’ box.
17. Repeat steps 13 to 16 four more times by increasing the weight each repetition, until it reaches 50g.

18. Send the values to the device by clicking the ’Send to device’ button twice.
19. Check whether the calibration worked. The calibration is sufficient when it measures within a 5% accuracy. If not, repeat the procedure.

B

Preliminary experiments

B.1. Thrombus creation with heparin infused blood

For the friction experiments, the jugular vein and blood was taken from pigs that were sacrificed for another study. The experimental protocol for these pigs included the administration of heparin throughout the day. Heparin is an anti-coagulant that prevents a clot from forming, making the regular thrombus creation protocol unsuitable. Therefore, a solution was sought to counter the effect of heparin on thrombus coagulation, allowing for the creation of thrombi using the same pig from which the jugular vein was retrieved.

In clinical settings, protamine is commonly administered to counter the anti-coagulating effects of heparin. The dosage of protamine that is administered is dependent on the amount of heparin present in the blood. Despite the administration of approximately 25000-30000 IU of heparin to the pigs throughout the day, the actual residual heparin at the time of blood retrieval remains unknown. As an overload of protamine addition may reintroduce anticoagulation effects, it is important that the right ratios are found for the blood used from this particular pig study [56].

To establish the appropriate ratios for thrombus creation with heparin-infused blood, an experiment consisting of two distinct steps was conducted. The initial step aimed to understand the onset of blood coagulation upon the introduction of protamine. Subsequently, the second step focused on establishing the final protamine ratio for effective thrombus formation. The methodology and findings from these experiments are elaborated on in the subsequent sections.

B.1.1. Coagulation test 1

Methodology

1. Five vials with thrombotic solution were created according to the regular thrombus formation protocol, with a total volume of 800µL.
   (a) Whole blood: 776µL
   (b) $CaCl_2$: 16µL
   (c) Thrombin: 8µL
2. Protamine is added to the samples below the level of the liquid. The solution is mixed by pipetting multiple times. The amount of protamine added to each individual sample can be found in table B.1.
3. After a total of 5, 10 and 15 minutes, the thrombotic solution was observed. These time points were chosen as regular blood clot tests are commonly performed after 5-15 minutes of protamine administration.
4. After 15 minutes, an additional 20µL of protamine was added to all vials (except for the control group). The final volumes of added protamine can be found in table B.1.

	Control	Sample 1	Sample 2	Sample 3	Sample 4
Added protamine - round 1	0µL	5µL	20µL	35µL	50µL
Added protamine - round 2	0µL	20µL	20µL	20µL	20µL
Total added protamine	0µL	25µL	40µL	55µL	70µL

Table B.1: Volumes used for experimental step 1 in order to determine the amount of protamine required to neutralize heparin

Results

As clot coagulation did not occur in the first 15 minutes of the experiment, the decision was made to add more protamine to the sample vials. After a total time period of 20 minutes, slight clot formation could be observed in sample 1. The same response was observed in sample 2 after a total of 40 minutes.

B.1.2. Coagulation test 2

Methodology

Taking into consideration the outcomes of the first step, a second coagulation test was conducted. In this test, five thrombi were generated in 3mL syringes. Given that the samples in this experimental step would undergo incubation for one hour, influencing the coagulation, a few volumes (around 25µL) of protamine were chosen to be added to the thrombotic solution.

1. Five vials with thrombotic solution were created according to the regular thrombus formation protocol, with a total volume of 900µL.
   (a) Whole blood: 873µL
   (b) $CaCl_2$: 18µL
   (c) Thrombin: 9µL
2. Protamine is added to the samples below the level of the liquid. The solution is mixed by pipetting multiple times. The amount of protamine added to each individual sample can be found in table B.2.
3. The total volumes were pipetted into 3mL syringes.
4. The filled syringes were placed in the incubator for 1 hour.
5. After removal from the incubator, the samples were removed from the syringes.

	Control	Sample 1	Sample 2	Sample 3	Sample 4
Added protamine	0µL	15µL	25µL	35µL	45µL

Table B.2: Volumes used for experimental step 2 in order to determine the amount of protamine required to neutralize heparin

Results

When removing the samples from the syringes it was found that only sample 1 formed a thrombus. No (complete) coagulation took place for the other samples.

B.1.3. Conclusion

The second coagulation experiment found that the addition of 1.67% of the total thrombus volume in protamine effectively neutralized the impact of heparin. This protocol was repeated for two more samples from blood of a different donor. Once more, the sample generation proved to be successful with this method. Consequently, for the thrombus formation using blood from pigs involved in this study, the addition of 1.67% of the total volume in protamine is deemed effective.

Sample	Gelatin granules (g)	Demineralized water (µL)	Total volume (µL)
3% gelatin	0.036	1164	1200
5% gelatin	0.060	1140	1200
8% gelatin	0.096	1104	1200

Table B.3: Volumes used to create gelatin samples of different concentrations

Gelatin concentration	Shear Modulus (kPa) (SD)	Young's Modulus (kPa) (SD)
3% gelatin	0.443 (0.258)	1.329 (0.774)
5% gelatin	2.424 (0.609)	7.272 (1.826)
8% gelatin	4.149 (0.585)	1.245 (1.754)

Table B.4: Mean Shear and Young's modulus determined for different gelatin concentrations

B.2. Shear experiments with gelatin samples

In order to validate the working principle of the shear test setup, experiments with gelatin samples were performed. This was done by creating gelatin samples with different concentrations (3, 5 and 8%). The experiments were performed according to the same protocol as how the thrombus samples are tested, with an exception in the normal force application step. The normal force of approximately 0.2N was applied in one step. This was adjusted for the experiments performed with thrombi due to the observed stress-relaxation behavior during compression.

The gelatin samples were created using the same mold employed for thrombus creation, including the Velcro connection to the bottom plate. Each sample had a total volume of 1200µL and was created with gelatin granules and demineralized water. Table B.3 outlines the specific volumes utilized. After the deminerialized water was added to the gelatin granules it was shaken gently and set aside for five minutes. Consequently, the solution was stirred and heated until fully transparent. The heated solution was poured into the molds and stored in a refrigerator at 4°C for 24 hours.

For each gelatin concentration a total of 10 samples were tested. Of these 10 samples, samples 1 till 6 were created on one day, and the remainder 4 samples were created on a second experimental day. In figure B.1 the shear and normal force response is found for all samples tested within the shear test setup. For the 8% gelatin samples it can be seen that the shear force of four samples is cut of at 0.5N. This is due to the limit of the load cell being reached, requiring the experiment to be stopped in order to avoid damaging the load cell.

The Young's modulus of gelatin increases with an increasing gelatin concentration. Furthermore, gelatin is generally assumed to be incompressible (ν=0.5) [57]. The relation between the Young's modulus (E), shear modulus (G) and Poisson's ratio (ν) is defined by equation B.1.

$$E = 2G(1 + \nu) \tag{B.1}$$

Consequently, an elevation in Young's modulus due to an increased gelatin concentration should theoretically result in a higher shear modulus. This relation is also observed when analyzing the acquired data. The shear modulus was calculated within strain region 0.2 to 0.3 for all samples of which the experiment could be completed. This region was chosen such that the results could be compared under the same strain deformation. The boxplot in figure B.2 shows that an increased gelatin concentration indeed leads to higher shear moduli. Using equation B.1, the mean Young's modulus for all gelatin concentrations is calculated, depicted in table B.4. The found values correspond with what is found in literature [58], validating the working principle of the shear test setup.

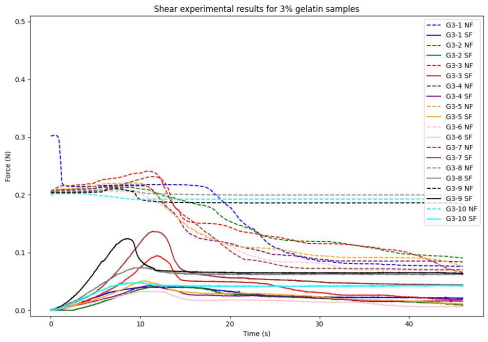

(a) 3% gelatin

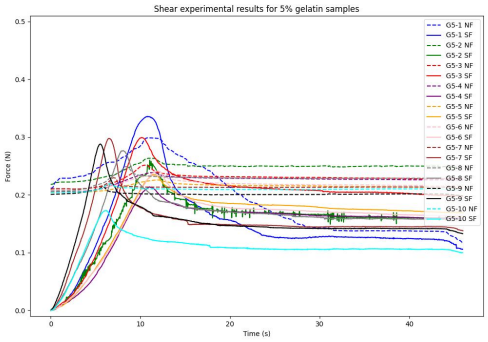

(b) 5% gelatin

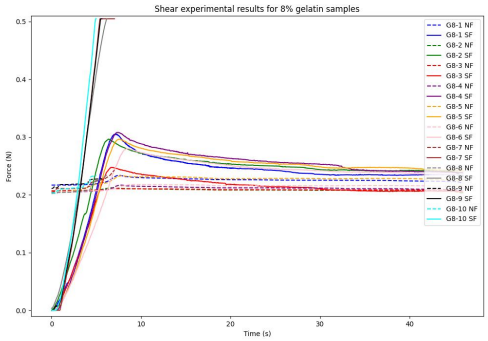

(c) 8% gelatin

Figure B.1: Raw data from shear experiments performed on gelatin samples.

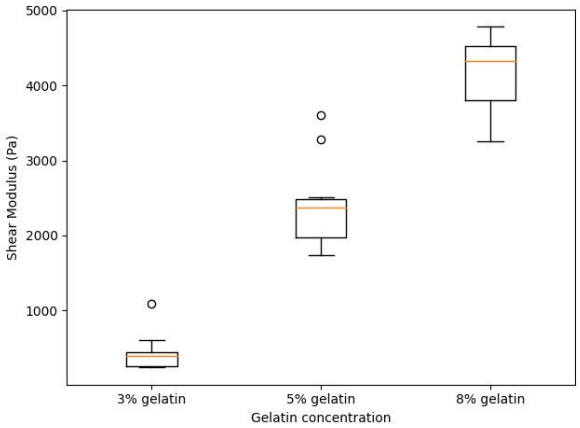

Figure B.2: Boxplot showing the shear modulus determined at 20-30% strain for different concentrations of gelatin samples.

B.3. Shear experiments with RBC thrombi

The final shear experiments with RBC samples have been executed by fixating the sample between the bottom and top plate, whereas the FBR samples were only fixated to the bottom plate. This difference in protocol originated from initial shear experiments executed with RBC samples. In figure B.3 the shear and normal response of the RBC samples can be found, employing the same protocol utilized for the FBR samples. It occurred that the RBC sample immediately slipped along the top plate in 21 out of 28 cases. The early slippage might be caused by the moisture that is released from the RBC samples under compression, acting as a lubricant between the RBC sample and the top plate.

In order to be able to measure the shear response, the protocol for RBC samples was adjusted. In the revised protocol, tissue glue (histoacryl) is applied to the top plate, after which contact with the sample is formed. This causes only the top layer of the sample to harden out, attaching it to the top plate. During the shear experiment this connection will eventually break, leaving some residue on the top plate. The amount of residue indicates whether an experiment was performed successfully or not. In figure B.4 the residue after a failed and successful experiment is shown. In the unsuccessful experiment, the histoacryl penetrated the sample too much, causing the sample to break during the shear experiment. In contrast, in a successful experiment, only a thin layer of glue will be left on the top plate.

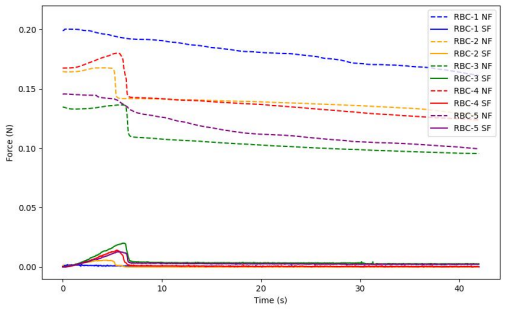

(a) Preliminary shear experiment 1

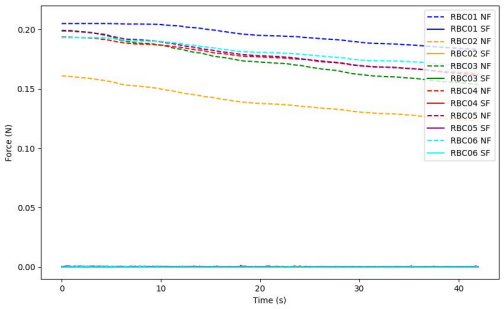

(b) Preliminary shear experiment 2

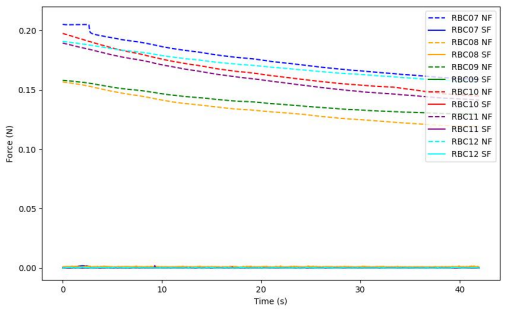

(c) Preliminary shear experiment 3

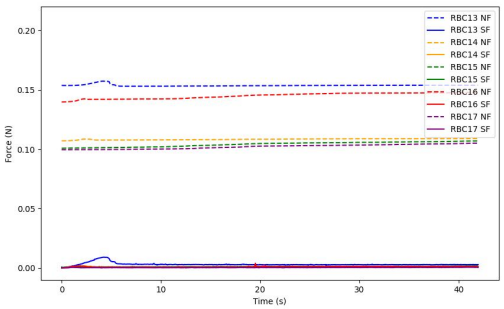

(d) Preliminary shear experiment 4

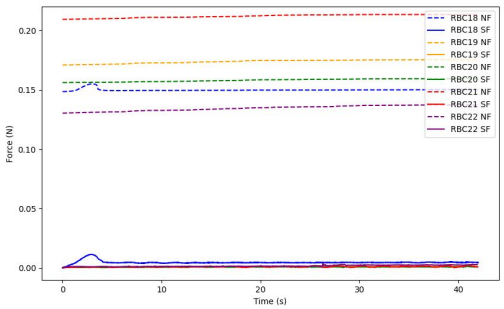

(e) Preliminary shear experiment 5

Figure B.3: The diagrams above portray the raw data of the initial shear experiments with RBC samples. The normal force is indicated with a dotted line, whereas the shear force is shown with a continuous line. Each diagram portrays the results of the samples created from the blood from one healthy human donor.

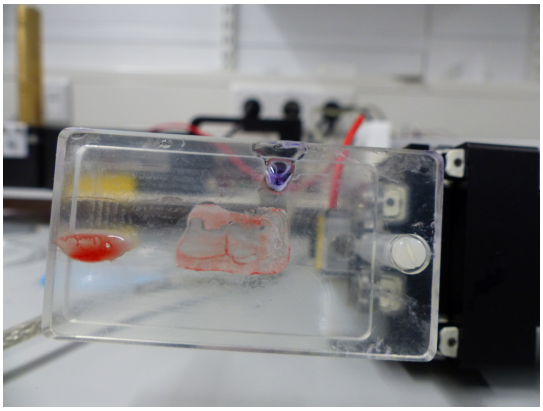

(a) Residue after a successful experiment.

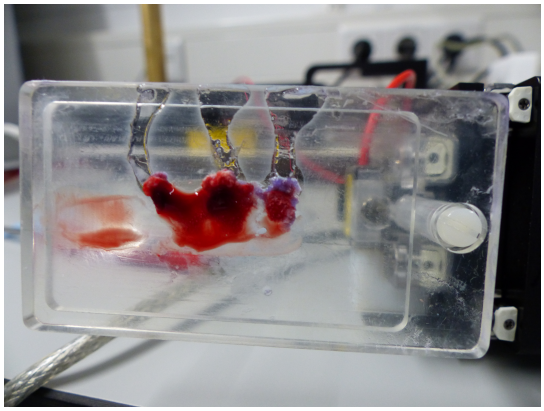

(b) Residue after a failed experiment.

Figure B.4: Tissue glue and thrombus residue left on the top plate after a shear experiment has been completed.

C

Final experiments

C.1. Raw data plots of all final RBC and FBR shear experiments

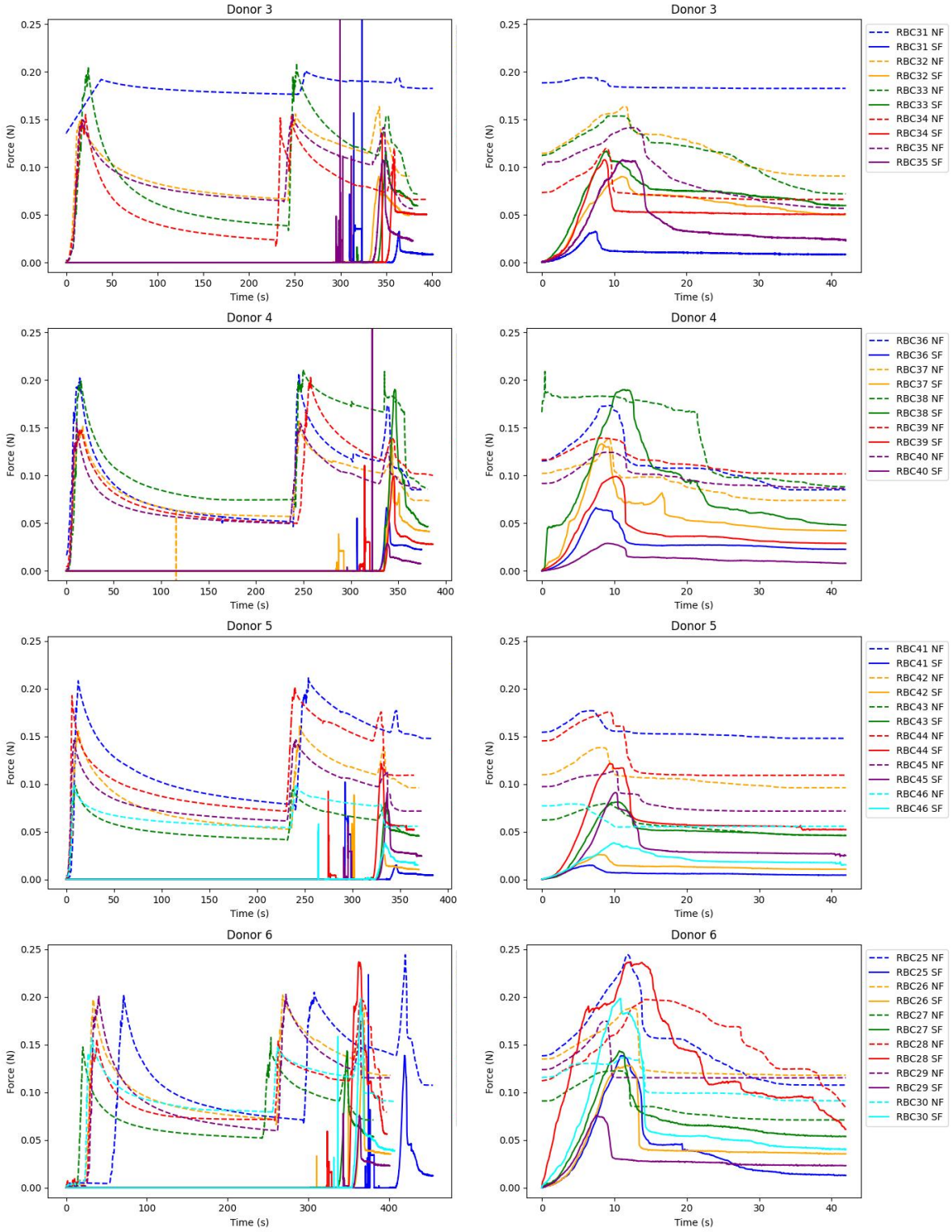

Figure C.1: The plots within the left column show the force over time for the entire experimental run for the RBC samples, including both the normal force application and the shearing part of the experiment. The right column zooms in on the experimental data from the shear part of the experiment.

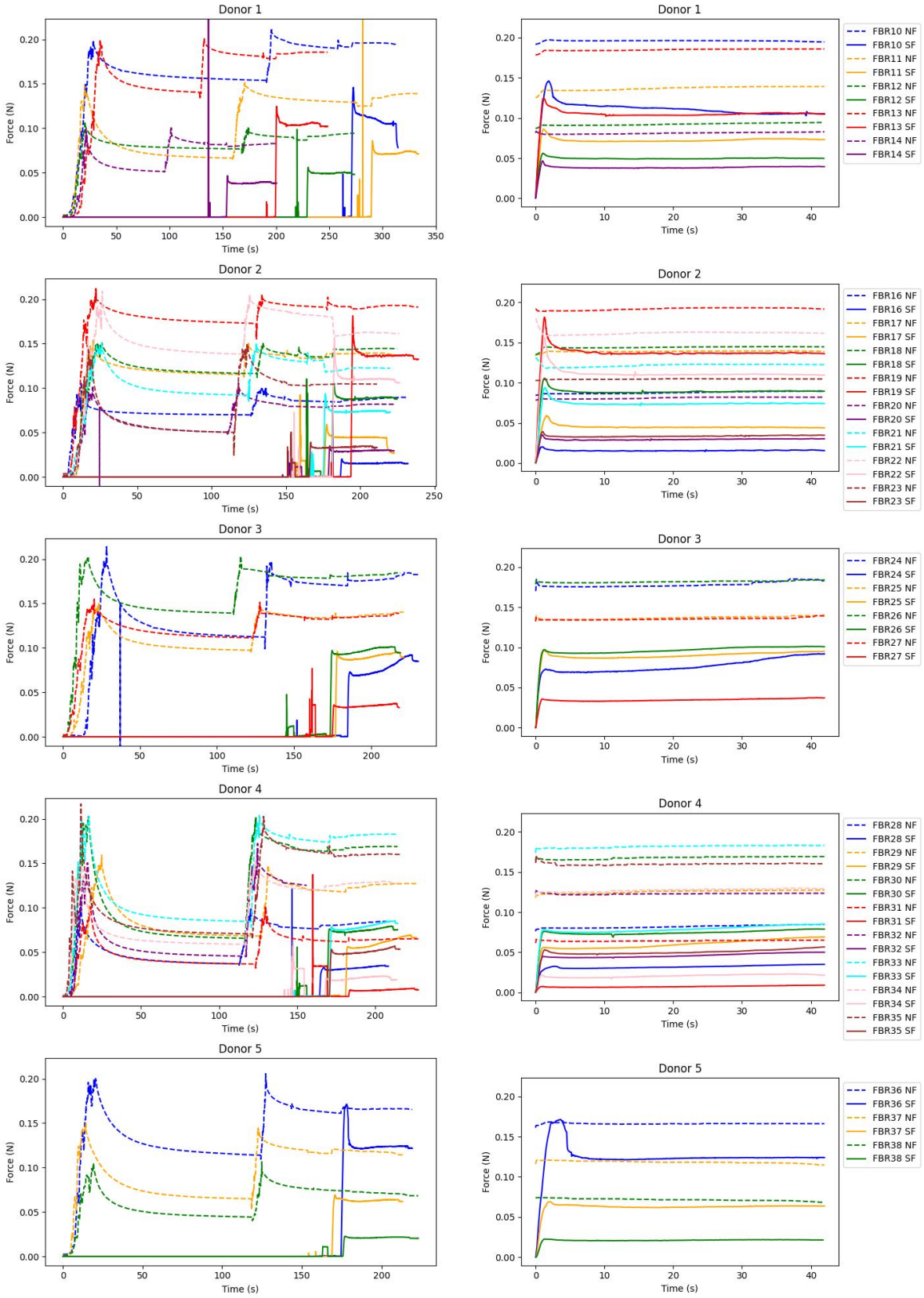

Figure C.2: The plots within the left column show the force over time for the entire experimental run for the FBR samples, including both the normal force application and the shearing part of the experiment. The right column zooms in on the experimental data from the shear part of the experiment.

C.2. Determination of high- and low-strain periods from shear experimental data

C.2.1. FBR samples

Figure C.4a shows that the shear stress strain behavior of the FBR thrombi is non-linear, meaning that no singular shear modulus can be determined. Therefore, the shear modulus is determined during periods of low- and high-strain. Within these smaller regions a linear stress, strain response is observed. The periods of low- and high-strain are quantified as a certain percentile region from the maximum strain. This method was chosen due to the normal force variable that was applied during the shear experiments. A higher normal force will result in more friction and consequently a higher strain. This theory was confirmed by the experimental data. In figure C.3 the mean normal force is set out against the maximum shear strain per sample, showing a significant positive correlation (r=0.3808, p=0.0456). The mean normal force is calculated within the shearing period, and the maximum strain is defined at the moment the maximum shear force is reached.

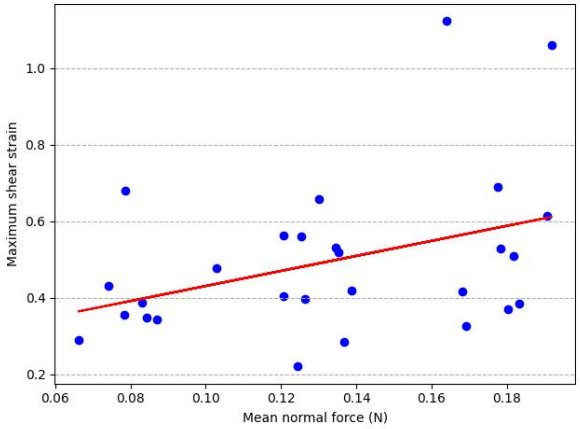

Figure C.3: Maximum shear strain plotted against the mean normal force for the FBR samples (r=0.3808, p=0.0456).

Due to the strain being dependent on the amount of normal force applied, the high- and low-strain is determined by looking at a certain percentage of the maximum strain. In figure C.4 the shear stress strain curve of a randomly chosen FBR sample is given, in which the red and blue parts show the low and high strain regions respectively. The low-strain period is taken from 5-15% of the maximum strain in order to avoid the toe off region within the stress-strain curves, that occurs within the first 5% maximum strain. The region of 30-40% maximum strain is chosen for the high-strain period. This range is chosen to ensure that the high-strain shear modulus is calculated before reaching the plateau region, leading towards slippage. The plateau is observed when the shear force exhibits a diminishing rate of increase, leading to the curve flattening. This plateau phenomenon is commonly initiated for most samples between approximately 50% to 70% of the maximum strain.

Multiple FBR samples were excluded for high- and/or low-strain analysis due to the data containing too much noise, too little data was available in the chosen strain regions or the plateau occurred within the chosen region. As a result, the low-strain shear modulus was not calculated for four FBR samples, and the high-strain shear modulus was not determined for three samples. Hence, some of the white spaces in table C.1 containing the calculated high- and low-strain shear modulus for the FBR samples.

C.2.2. RBC samples

The shear stress strain behavior of the RBC samples in non-linear as well. However, as the normal force does not correlate with the maximum strain in these experiments, a different approach is taken in order to determine the low- and high-strain regions. For the RBC samples, no correlation is found due to the tissue glue connection between the sample and the top plate.

The low- and high-strain regions are set at certain strain values in order to make the results for the RBC samples comparable. For the low-strain region, 0.1 till 0.2 strain was chosen in order to avoid the toe off region, occurring before 10% strain. The high-strain region was set at 1.5 till 1.6 strain to

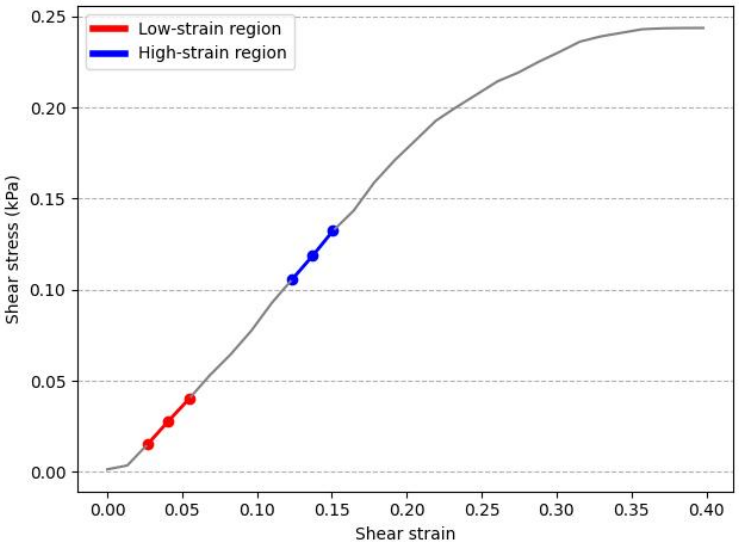

(a) The complete shear stress strain curve.

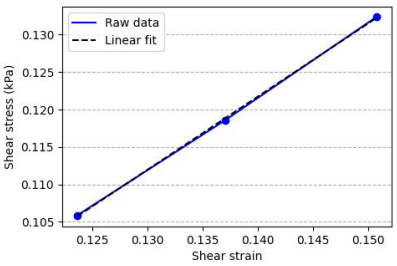

(b) The linear high-strain region (30-40% of maximum strain).

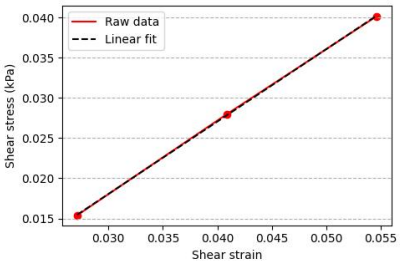

(c) The linear low-strain region (5-15% of maximum strain).

Figure C.4: (a) The shear stress strain curve of FBR32, including zoomed plots of the (b) high- and (c) low-strain regions.

Sample	Low-strain Shear Modulus (kPa)	High-strain Shear Modulus (kPa)
FBR10	1.684	1.264
FBR11	1.620	1.223
FBR12	1.649	1.377
FBR13	2.257	1.977
FBR14	1.073	1.029
FBR16	0.977	0.745
FBR17	0.797	0.577
FBR18	2.549	1.689
FBR19	3.580	2.225
FBR20	-	-
FBR21	-	-
FBR22	1.946	1.651
FBR23	0.756	1.035
FBR24	3.265	1.495
FBR25	2.520	2.195
FBR26	3.744	2.078
FBR27	1.447	1.241
FBR28	0.813	-
FBR29	1.389	1.270
FBR30	1.949	1.315
FBR31	-	0.255
FBR32	0.901	0.977
FBR33	1.525	1.752
FBR34	-	0.539
FBR35	1.219	1.618
FBR36	1.916	1.452
FBR37	1.129	1.091
FBR38	0.410	0.675

Table C.1: The low- and high-strain shear modulus for all FBR samples

Sample	Low-strain Shear Modulus (kPa)	High-strain Shear Modulus (kPa)
RBC25	0.061	0.484
RBC26	0.038	0.619
RBC27	0.097	0.545
RBC29	0.060	0.350
RBC30	0.166	0.788
RBC31	0.028	-
RBC32	0.053	0.250
RBC33	0.085	0.316
RBC34	0.082	0.446
RBC35	0.041	0.427
RBC36	0.059	-
RBC37	0.262	-
RBC39	0.066	0.348
RBC40	0.027	0.117
RBC41	0.043	-
RBC42	0.042	-
RBC43	0.031	0.179
RBC44	0.058	0.264
RBC45	0.030	0.448
RBC46	0.062	0.142

Table C.2: The low- and high-strain shear modulus for all RBC samples

determine the high-strain shear modulus. In table C.2 all calculated high- and low-strain shear moduli for the RBC samples can be found. Due to noisy data, or the high-strain region being out of the scope of the strain of the sample, five samples had to be excluded from the high-strain shear modulus analysis.

C.3. Exclusion criterion period of kinetic friction

In the shear force over time plots, the horizontal region is denoted as the period of kinetic friction. However, not all sample responses exhibit a clear horizontal region, leading to the establishment of exclusion criteria. Due to the load cells measuring within an accuracy of 5%, the exclusion criteria is set to a 5% offset as well. This offset is determined by calculating the mean shear force and plotting a linear fit through the raw data within the period of kinetic friction. The maximum deviation between the extreme values of the linear fit and the mean is calculated as a percentage.

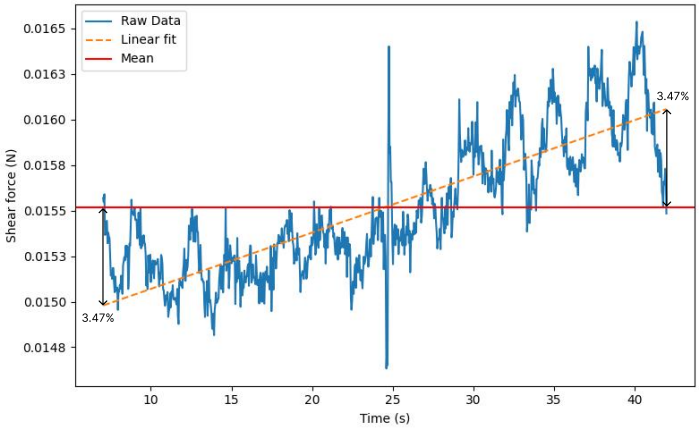

Figure C.5: Plot showing how the maximum deviation was established to determine which samples should be excluded when determining the kinetic coefficient of friction. This plot shows the maximum deviation of sample FBR16, which can be included with a maximum deviation of 3.47%.

In tables C.3 and C.4 the deviation from the mean shear force is given for all samples. Additionally, it is indicated whether a sample can be included or should be excluded, depending on whether the deviation is less than 5% or not. The normal force measurements of the samples included were all within a 5% offset, and therefore did not influence the exclusion of samples to calculate the kinetic coefficient of friction.

Sample	Deviation (%)	Exclude
FBR10	5.72	YES
FBR11	2.77	NO
FBR12	0.99	NO
FBR13	1.24	NO
FBR14	3.13	NO
FBR16	3.47	NO
FBR17	0.44	NO
FBR18	1.38	NO
FBR19	0.12	NO
FBR20	3.23	NO
FBR21	1.13	NO
FBR22	0.05	NO
FBR23	3.36	NO
FBR24	16.46	YES
FBR25	5.33	YES
FBR26	5.16	YES
FBR27	6.36	YES
FBR28	8.05	YES
FBR29	13.13	YES
FBR30	4.91	NO
FBR31	18.18	YES
FBR32	8.46	YES
FBR33	7.22	YES
FBR34	11.79	YES
FBR35	8.10	YES
FBR36	1.12	NO
FBR37	1.12	NO
FBR38	2.71	NO

Table C.3: Exclusion table for FBR samples for the kinetic coefficient of friction

Sample	Deviation (%)	Exclude
RBC25	75.25	YES
RBC26	4.99	NO
RBC27	14.18	YES
RBC29	10.03	YES
RBC30	19.08	YES
RBC31	13.10	YES
RBC32	19.18	YES
RBC33	13.07	YES
RBC34	2.30	NO
RBC35	21.01	YES
RBC36	10.84	YES
RBC37	16.89	YES
RBC39	15.13	YES
RBC40	26.14	YES
RBC41	18.15	YES
RBC42	14.42	YES
RBC43	6.56	YES
RBC44	5.24	YES
RBC45	5.49	YES
RBC46	13.75	YES

Table C.4: Exclusion table for RBC samples for the kinetic coefficient of friction

D

Python code

D.1. Friction experiments

Python code use to analyze the experimental data following from the friction experiments. The resulting DataFrame is utilized to create different plots.

```
import pandas as pd
import matplotlib.pyplot as plt
import numpy as np
import math

df = pd.read_excel('Data␣friction.xlsx', sheet_name='final')
df = df.set_index('Information')
df = df.transpose()

# Determine the % of clot contraction

df['Weight␣mould␣volume␣(g)'] = df['Weight␣of␣full␣mould␣(g)'] - df['Weight␣of␣empty␣mould␣(g)']
df['%␣Clot␣contraction'] = (df['Weight␣mould␣volume␣(g)']-df['Weight␣of␣clot␣(g)'])/df['Weight␣mould␣volume␣(g)'] * 100

# Determine sample acceleration

df['Acceleration␣(m/s^2)'] = 2*df['Distance␣travelled␣(m)'] / df['Time␣passed␣(s)']**2

# Determine the coefficients of friction in case the angle of inclination is smaller than 90 degrees

move = df['Angle␣of␣inclination␣(degrees)'] < 90
df.loc[move, 'Angle␣of␣inclination␣(radians)'] = df.loc[move, 'Angle␣of␣inclination␣(degrees)'].apply(lambda x: math.radians(x))
df.loc[move, 'Static␣coefficient␣of␣friction'] = np.tan(df.loc[move, 'Angle␣of␣inclination␣(radians)'])
df.loc[move, 'Kinetic␣coefficient␣of␣friction'] = ((df.loc[move, 'Gravity␣(m/s^2)'] * np.sin(df.loc[move, 'Angle␣of␣inclination␣(radians)']) - df.loc[move, 'Acceleration␣(m/s^2)']) / (df.loc[move, 'Gravity␣(m/s^2)'] * np.cos(df.loc[move, 'Angle␣of␣inclination␣(radians)'])))

# Substitute NaN values in case the angle of inclination was 90 degrees

df.loc[~move, ['Angle␣of␣inclination␣(radians)', 'Static␣coefficient␣of␣friction', 'Kinetic␣coefficient␣of␣friction']] = np.nan

df
```

D.2. Shear experiments

Python code used to analyze the shear experimental data. The code below portrays the code used for the FBR samples, but is also usable for the RBC samples. The resulting DataFrame is utilized to create different plots.

```
import pandas as pd
import matplotlib.pyplot as plt
import numpy as np

def measured_data(filename):

    # Open the data file with sample specific characteristics

    dg = pd.read_csv(filename, sep='\t', index_col=False)
    prefix = filename[:3]
    start_index = 1
    row_names = {i: f'{prefix}{str(i+start_index).zfill(2)}' for i in range(len(dg))}
    dg = dg.rename(index=row_names)

    # Calculate the % of clot contraction

    dg['Sample + Velcro weight (g)'] = dg['Plate + sample (g)'] - dg['Plate (g)']
    dg['Velcro (g)'] = dg['Empty mould Velcro (g)'] - dg['Empty mould (g)']
    dg['Sample weight (g)'] = dg['Sample + Velcro weight (g)'] - dg['Velcro (g)']
    dg['Mould volume (g)'] = dg['Full mould (g)'] - dg['Empty mould Velcro (g)']
    dg['% Contraction'] = (dg['Mould volume (g)'] - dg['Sample weight (g)'])/dg['Mould volume
        (g)']*100

    return dg

def process_txt_file(filename, dg):

    # Read the raw data file and structure it
    df = pd.read_csv(filename, sep='\t', header=None)
    df[['Date', 'Timestamp']] = df[0].str.split(' ', expand=True)
    df['Shear force (N)'] = df[1]
    df['Status'] = df[2]
    df['Normal force (N)'] = df[3]
    df = df.drop(columns=[0, 1, 2, 3])
    df['Timestamp'] = pd.to_datetime(df['Timestamp'], format='%H:%M:%S.%f')
    df['Time (s)'] = (df['Timestamp'] - df['Timestamp'].min()).dt.total_seconds()

    # Create dataframe of the shear part of the experiment; Status = 1
    df_status = df[df['Status']==1]
    df_status = df_status.reset_index(drop=True)
    df_status['Time (s)'] = df_status['Time (s)'] - df_status['Time (s)'].min()

    name = filename[:5]

    # Determine the maximum shear force and corresponding normal force
    max_shear_idx = df_status['Shear force (N)'].idxmax()
    seconds_max_shear = df_status.loc[max_shear_idx, 'Time (s)']
    shear_force_max = df_status.loc[max_shear_idx, 'Shear force (N)']
    normal_force_max = df_status.loc[max_shear_idx, 'Normal force (N)']
    dg.loc[name, 'Max normal force (N)'] = normal_force_max
    dg.loc[name, 'Max shear force (N)'] = shear_force_max

    # Determine the shear stress and strain values
    actuator_speed = 0.5 #mm/s
    for i in dg:
        df_status['Shear stress (kPa)'] = df_status['Shear force (N)'] / dg.loc[name,'Top
            area (mm^2)'] * 1e3
        df_status['Displacement (mm)'] = df_status['Time (s)'] * actuator_speed
        df_status['Shear strain'] = df_status['Displacement (mm)'] / dg.loc[name,'Compressed
            height (mm)']

    # Determine moment of max shear stress
    df_status_filt = df_status[df_status['Time (s)'] <= 5]
    max_shear_stress = df_status_filt['Shear stress (kPa)'].idxmax()
    shear_strain_max_stress = df_status_filt.loc[max_shear_stress, 'Shear strain']
```

```
    dg.loc[name, 'Mean normal force (N)'] = df_status_filt['Normal force (N)'].mean()
    dg.loc[name, 'Max shear strain'] = shear_strain_max_stress


    # Create figure with low and high strain regions (stress-strain curve)

        # Complete stress strain curve
    df_full = df_status_filt[df_status_filt['Shear strain'] <= shear_strain_max_stress]
    df_full = df_full[df_full['Shear strain']>= 0]
    epsilon_full = df_full['Shear strain']
    sigma_full = df_full['Shear stress (kPa)']

        # Low-strain region
    df_low = df_status_filt[df_status_filt['Shear strain'] <= shear_strain_max_stress *0.15]
    df_low = df_low[df_low['Shear strain']>= shear_strain_max_stress * 0.05]
    slope_low, intercept_low = np.polyfit(df_low['Shear strain'],df_low['Shear stress (kPa)'
        ], 1)
    dg.loc[name, 'Low-strain Shear Modulus (kPa)'] = slope_low
    epsilon_low = df_low['Shear strain']
    sigma_low = df_low['Shear stress (kPa)']

        # High-strain region
    df_high = df_status_filt[df_status_filt['Shear strain'] <= shear_strain_max_stress*0.4]
    df_high = df_high[df_high['Shear strain'] >= shear_strain_max_stress *0.3]
    slope_high, intercept_high = np.polyfit(df_high['Shear strain'],df_high['Shear stress (
        kPa)'], 1)
    dg.loc[name, 'High-strain Shear Modulus (kPa)'] =  slope_high
    epsilon_high = df_high['Shear strain']
    sigma_high = df_high['Shear stress (kPa)']

        # Creating the plot
    plt.plot(epsilon_full, sigma_full, color='gray')
    plt.plot(epsilon_low, sigma_low, label='Low-strain region',color='red',linewidth=2)
    plt.scatter(epsilon_low, sigma_low, color='red')
    plt.plot(epsilon_high, sigma_high, label='High-strain region',color='blue',linewidth=2)
    plt.scatter(epsilon_high, sigma_high, color='blue')
    plt.xlabel('Shear strain')
    plt.ylabel('Shear stress (kPa)')
    plt.title(f'{name}')
    legend = plt.legend()
    for line in legend.get_lines():
        line.set_linewidth(4)
    plt.grid(linestyle='--',axis='y')
    plt.tight_layout()
    plt.show()


    # Determine the static coefficient of friction
    dg.loc[name, 'Static coefficient of friction'] = shear_force_max / normal_force_max


    # Determine the kinetic coefficient of friction
    df_status = df_status[df_status['Time (s)'] >= 7]
    df_status['k_cof_new'] = df_status['Shear force (N)'] / df_status['Normal force (N)']
    dg.loc[name, 'Kinetic coefficient of friction'] = df_status['k_cof_new'].mean()

        # Determine whether the samples can be included

    # Create linear fit through the raw shear force data
    coefficients = np.polyfit(df_status['Time (s)'], df_status['Shear force (N)'], 1)
    linear_line = np.polyval(coefficients, df_status['Time (s)'])
    mean_value = df_status['Shear force (N)'].mean()

    # Determine min & max points of linear fit & deviation percentage
    max_lin_value = max(linear_line)
    min_lin_value = min(linear_line)
    percentage_deviation_lin_max = (max_lin_value - mean_value) / mean_value * 100
    percentage_deviation_lin_min = (min_lin_value - mean_value) / mean_value * 100
    dg.loc[name, 'Deviation pos (%)'] = percentage_deviation_lin_max
    dg.loc[name, 'Deviation neg (%)'] = percentage_deviation_lin_min

```

```
132     # If the deviation is smaller or equal to 5, the sample can be included
133     if percentage_deviation_lin_max <= 5 and percentage_deviation_lin_min <= 5:
134         dg.loc[name, 'Exclude␣(Y/N)'] = 'NO'
135     else:
136         dg.loc[name, 'Exclude␣(Y/N)'] = 'YES'
137 
138 
139     return df_status
140 
141 
142     dFBR = measured_data('FBR␣combined.txt')
143 
144 row_names_FBR = ['FBR10','FBR11','FBR12','FBR13','FBR14','FBR16','FBR17','FBR18','FBR19','
        FBR20','FBR21','FBR22','FBR23','FBR24','FBR25','FBR26','FBR27','FBR28','FBR29','FBR30','
        FBR31','FBR32','FBR33','FBR34','FBR35','FBR36','FBR37','FBR38']
145 dFBR['Row_names_FBR'] = row_names_FBR
146 dFBR.set_index('Row_names_FBR', inplace=True)
147 
148 df_status_list_FBR = []
149 
150 file_names_FBR = ['FBR10.txt','FBR11.txt','FBR12.txt','FBR13.txt','FBR14.txt','FBR16.txt','
        FBR17.txt','FBR18.txt','FBR19.txt','FBR20.txt','FBR21.txt','FBR22.txt','FBR23.txt','FBR24
        .txt','FBR25.txt','FBR26.txt','FBR27.txt','FBR28.txt','FBR29.txt','FBR30.txt','FBR31.txt'
        ,'FBR32.txt','FBR33.txt','FBR34.txt','FBR35.txt','FBR36.txt','FBR37.txt','FBR38.txt']
151 
152 for file_name in file_names_FBR:
153     df_status_list_FBR.append(process_txt_file(file_name, dFBR))
154 
155 dFBR
```